A Touch of Lumen Morphogenesis in *Caenorhabditis elegans*: Anchor Cell Invasion Guides Epithelial Invagination

---

Dissertation

zur Erlangung der naturwissenschaftlichen Doktorwürde

(Dr. sc. nat.)

vorgelegt der

Mathematisch-naturwissenschaftlichen Fakultät

der

Universität Zürich

von

Qiutan Yang

aus China

Promotionskomitee

Prof. Dr. Alex Hajnal (Vorsitz)

Prof. Dr. Anne Spang

Prof. Dr. Stefan Luschnig

Prof. Dr. Yves Barral

Zürich, 2016

君子之学
唯求其是
知行合一
心即是理

献给我挚爱的妈妈，爸爸和外婆。

Zusammenfassung

Die Bildung rohrförmiger Strukturen ist ein grundlegendes Phänomen in der Organ-Entwicklung. Die Korrekte Bestimmung der Zellschicksal, ist in der Regel Voraussetzung für die Röhrchenbildung. Diese wurde ausgiebig untersucht. Der darauffolgende Prozess ist die Morphogenese eines Lumens, der viele Zellverhalten, wie beispielsweise die Veränderung der Zellform, die Zellmigration, Bildung von Zell-Verbindungs und Zellfusionen beinhalten kann. Das Verständnis der Lumenmorphogenese, die in der Tierwelt konserviert ist, kann für die Behandlung von menschlichen Krankheiten, insbesondere für die regenerative Medizin im Bezug auf die Herstellung funktioneller röhrenförmiger Organe wichtig sein. Die molekularen Mechanismen, die der Lumenmorphogenese zu Grunde liegen, sind bis heute weitgehend unbekannt, gewinnen aber immer mehr Aufmerksamkeit.

In dieser Arbeit untersuchte ich die Entwicklung des rohrförmigen Vulva des *C. elegans* Hermaphroditen als Modell, um die Lumenmorphogenese besser zu verstehen. Im ersten Projekt wurde die Invagination des Vulvaepithels, welches die Lumenbildung initiiert, genauer untersucht. Durch Beobachtung der Form der Ankerzelle und des Actomyosin-Netzwerks in den Vulvazellen, konnten die zellulären Prozesse während der Vulvainvagination im Detail beschrieben werden. Die Veranderungen der Zellformen während der Vulvalumenbildung erfolgen in einer definierten Reihenfolge: Apikale Konstriktion der VulF Zellen, VulE Zellteilung, VulF laterale Konstriktion und Teilung der VulF Zellen. Wir beobachteten eine neue Art der Membrankonstriktion, die sogenannte “laterale VulF Konstriktion”, die auf den lateralen Membranen der beiden VulF Zellen geschieht und durch die invasive Ankerzelle induziert wird. Außerdem fanden wir, dass die VulF laterale Konstriktion durch die Actomyosin-Kontraktion angetrieben wird. Zusätzlich hat ein RNAi-Screen gezeigt, dass die BAR-Domänenproteine TOCA-1 und TOCA-2, welche Membrankrümmung detektierend die kleine GTPase RHO-1, CDC-42 und MRCK-1 benötigt werden für die ankerzellabhängige Rekrutierung von Myosin. So konnten wir zeugen, dass Zellinvasion zu direkterem Kontakt der Ankerzelle mit den VulF Zellen führt, und so die Actomyosin induzierte, laterale Membrankonstriktion induziert. Während dieses Prozesses werden die BAR-domänen Proteine TOCA-1 und TOCA-2 zur AC/VulF Kontaktstelle rekrutiert, wo der sie CDC-42/MRCK-1 Signalung aktivieren, um die Actomyosin Kontraktion zu induzieren.

In einem zweiten Projekt wurde ein systematischer Screen durchgeführt, um Gene zu

finden， welche die Vulva-Morphogenese steuern. Für diesen Screen benutzten wir eine RNAi-Bibliothek die 694 ausgewählte Gene enthält, deren RNAi- Knockdown nach Literaturangaben einen „protruding vulva“ (Pvl) Phänotypen verursachte. Anhand hochauflösender Mikroskopieaufnahmen der Zell-Verbindungen wurden die 93 Kandidatengene aufgrund ihrer morphogenetischen Defekte in fünf Gruppen eingeteilt. Zwei Gruppen von Genen, die gewebespezifische Defekte während der Vulva-Toroid-Bildung zeigten, wurden für die weitere Untersuchung ausgewählt. Die erste Gruppe besteht aus den Chaperon-Proteinen PFD-1, PFD-6 und CCT-2. PFD-1 und PFD-6 tragen zur Reifung von Mikrotubuli bei, indem sie Tubulin-Proteine dem CCT-2-Komplex übergeben. Wir beobachteten, dass PFD-1 RNAi behandelte Tiere einen spezifischen Defekt in der Bildung der primären Toroide aufzeigten, während PFD-6 RNAi behandelte Tiere Defekte in der Bildung der sekundären Toroide aufzeigten. CCT-2 RNAi behandelte Tiere wiesen Defekte in der Bildung sowohl der primären als auch der sekundären Toroide auf. Unsere Daten deuten darauf hin, dass eine gewebespezifische Regulierung von Mikrotubuli für die Toroid-Bildung während der Vulva-Morphogenese erforderlich ist. Die zweite Gruppe von Proteinen, die in unserem Screen isoliert wurde, umfasst die Septin-Proteine UNC-59 und UNC-61. Septine bilden filamentöse Strukturen in Zellen. Sowohl RNAi-Experimente als auch Mutantenanalyse der Septin-Gene *unc-59* und *unc-61* zeigten Defekte in der Bildung der primären Toroide. Der erste detektierbare Defekt der untersuchten Septin-Mutanten war die abnorme Zellteilung der VulE Zellen. Eine genauere Untersuchung unter Verwendung eines YFP:: alpha-Tubulin Reporters, einem Marker für die Mikrotubuli, hat gezeigt, dass sich die Zellachse der VulE Zellen verändert in Septin Mutantene und zwar von einer T-Teilung (transversal entlang der L/R Achse) hin zu einer O- Teilung (mit einer Teilungsachse 0 ~ 90 ° entlang der L/R Achse).

Zusammenfassend habe ich mit meiner Arbeit zum besseren Verständnis der Lumen-Morphogenese beigetragen, in dem ich unter anderem gezeigt habe dass die Invasion der Ankerzelle zwischen die VulF Zellen Voraussetzung ist für die Invasion des Vulva-Epithels. Zur systematischen Suche von Regulatoren der Vulva-Morphogenese wurden in einem genetischen Screen Kandidatengene gefunden, die uns helfen können, beser zu verstehen, wie Signalwege zeitlich und räumlich die morphogenetischen Ereignisse in der Organentwicklung koordinieren.

Summary

The formation of tubular structures is a fundamental phenomenon in development. The tissue patterning that specifies the fates of cells is a perquisite for proper tube formation. The following process of tube morphogenesis includes multiple cellular behaviors such as cell shape changes, cell migration, junction formation, and cell fusion. Understanding lumen morphogenesis, which is a conserved process during animal development can be important for the treatment of human diseases, especially in the regenerative medicine for the engineering of functional tubular organs. To date, the molecular mechanisms that underly lumen morphogenesis are largely unknown but they attract more and more attention.

In my thesis, I used the seminal model of the vulval tube in *C. elegans* to study lumen morphogenesis. The first project dissected the invagination of the vulval epithelium, the process that initiates the vulval lumen. By analyzing the shape of the Anchor cell (AC), the cytoskeletal structures and the actomyosin network in the vulval cells over time, the cellular behavior during vulval invagination were described in detail. We have found that the vulval cell shape changes during vulval lumen formation follow the order of VulF apical constriction, VulE cell division, VulF lateral constriction and VulF cell division. A novel fashion of membrane constriction, termed as the “VulF lateral constriction”, was observed on the lateral membranes between the two VulF cells, which is induced by the invading AC. In addition, we found that the shrinkage of the VulF lateral membranes is driven by contractile forces generated by the actomyosin network. Finally, an RNAi screen revealed that the membrane-curvature sensing BAR-domain proteins TOCA-1 and TOCA-2, the small GTPase RHO-1, CDC-42 and MRCK-1 are required for the AC-dependent recruitment of non-muscle myosin II (NMY-2). In summary, we found that AC invasion results in direct contact between the AC and VulF cells, which induces the RHO-1/ MRCK-1-activated actomyosin-driven lateral membrane constriction. During this process, the BAR-domain protein TOCA-1 and TOCA-2 are recruited to the AC/VulF contact site, where they activate CDC-42 to promote actomyosin contraction.

In my second project, an RNAi screen searching for genes that are involved in vulval morphogenesis was performed. Thereby, 694 genes that have been reported to cause a protruding vulval (Pvl) phenotype were knocked-down by RNAi effect. Based on the high-resolution microscopy images of the cell junctions, 93 candidates were grouped into five classes according to the morphogenesis defects. Two groups of genes that showed tissue

specific defects during vulval toroid formation were chosen for further studies. The first group of proteins are the chaperone proteins PFD-1, PFD-6 and CCT-2. Although all three proteins have been reported to promote the maturation of microtubules, the *pfd-1, pfd-6* and *cct2* RNAi treated animals showed defects in different vulval toroids, suggesting that a tissue-specific regulation of microtubules is required for proper toroid formation. The second class of proteins identified in our screen are the *septin* genes *unc-59 and unc-61*. Both the RNAi and the mutant analysis of the *septin* genes *unc-59* and *unc-61* revealed defects in the primary toroid formation. The first detected defect of *septin* mutants was the abnormal VulE cell division, in which the cell division plane was altered from a normal T division (transversal along the L/R axis) to an abnormal O division (with a division axis 0~90° along L/R axis).

In summary, this thesis contributes to our understanding of lumen morphogenesis through the study of vulval invagination, a process that requires the touch (invasion) of the AC and involves the novel process of lateral membrane constriction. Furthermore, an RNAi screen searching for the regulators of vulval morphogenesis has provided a large number of promising candidates required for tissue-specific aspects of vulval morphogenesis.

Table of contents

List of figures

List of tables

CHAPTER I. Literature review

1.1. *C. elegans* as a model organism in developmental biology

The roundworm *Caenorhabditis elegans* is a genetic model for the study of developmental biology. It has been chosen as an animal model by Sydney Brenner in the early 70s based on many of its user-friendly features (Brenner, 1974). The worms can be easily cultured on agar plates or in liquid medium, fed with *E. coli* and stored in liquid nitrogen for decades. The life cycle of *C. elegans* is short and under lab condition requires about three days from the single-cell egg to adulthood (Fig. 1.1). After hatching and before the first molting, the larva can switch its development to the tolerant status as entering into the dauer stage that endures tough living conditions for long term up to about four months (Fig. 1.1) (Altun and Hall, 2009).

The body of *C. elegans* is transparent and beneficial for the observation of cells under light microscopes (Sulston et al., 1983). The invariant cell linage and programmed cell death of *C. elegans* has facilitated the study of developmental biology (Sulston et al., 1983). *C. elegans* contains the sample yet complete range of physiological systems including the nervous, the reproductive, the respiratory and the digestive systems, which provide tools to study the conserved mechanisms behind the related human diseases (*C. elegans* Sequencing Consortium, 1998). *C. elegans* has two sexes, males and hermaphrodites. In addition to five pairs of autosomal chromosomes, the hermaphrodite genome has one pair of the X chromosomes (XX). Males which are present in around 0.05% in wild-type population contains only one X chromosome (XO). The hermaphrodite is able to self-fertilizing, which is an advantage for keeping its genetic information over generations (Altun and Hall, 2009).

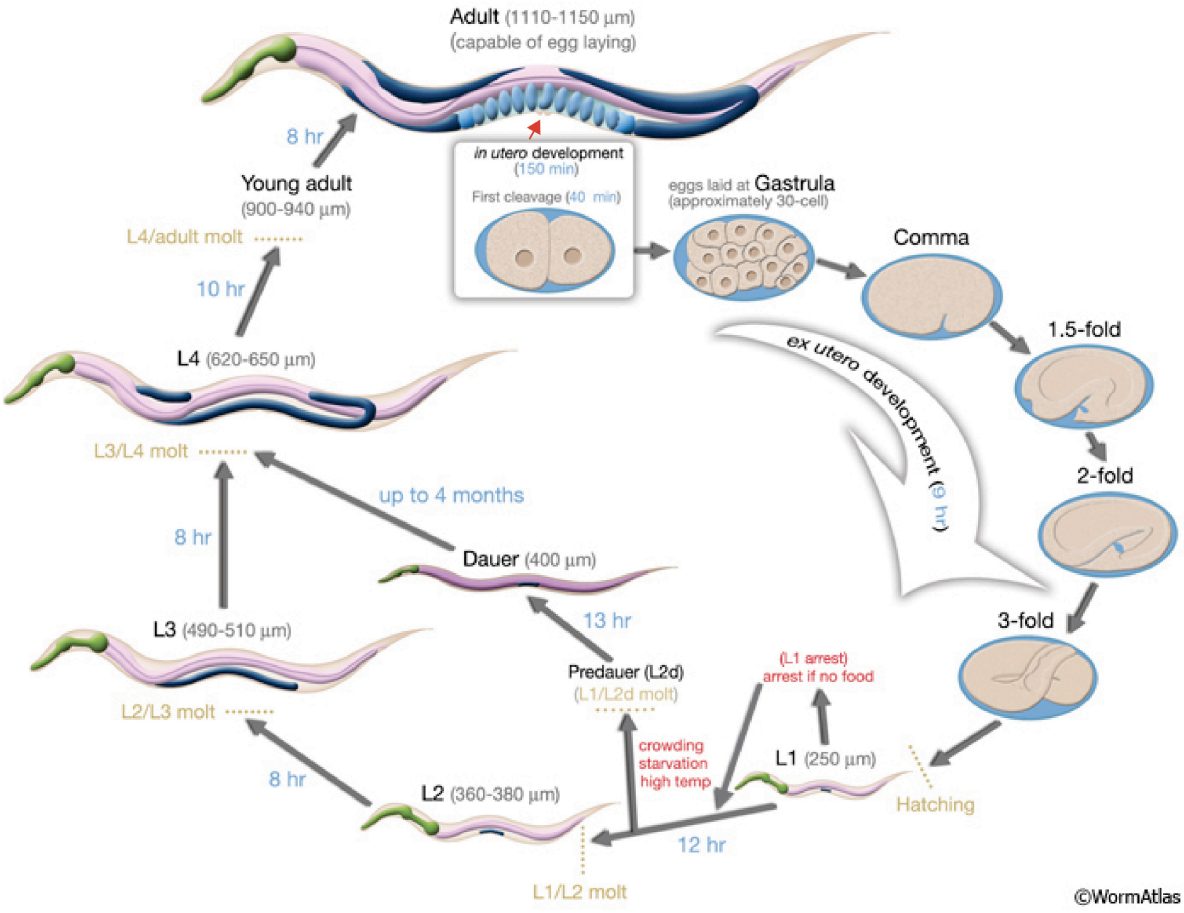

Figure 1.1. The life cycle of cycle of *C. elegans* at 22°C. The L1 larva hatches after nine hours ex-utero development. In condition with adequate food resource, the worm larvae undergo four rounds of molting becoming adult hermaphrodites that produce the next generation. In stress conditions, such as crowding, starvation and high temperature, L1 larva enter into the dauer phase that endures harsh conditions for long term. The red arrow in hermaphrodite indicates the position of the vulva. Picture is adapted from WormAtlas.

1.2. *C. elegans* vulval development

1.2.1. Vulval cell specification

The *C. elegans* vulva is the egg-laying organ that is located on the ventral side of the mid section of the worm body (Fig. 1.1). It has provided a seminal systems for the study of cell patterning and cell fate specification (Sternberg, 2005). Six vulval precursor cells (VPCs) (P3.p to P8.p) have an equal potential to adapt the VPC fate at the late L1 stage under the

regulation of the WNT signal induced transcription factor LIN-39. Other Pn.p cells that lack of LIN-39 fuse with the epidermis (Fig. 1.2 A) (Schmid and Hajnal, 2015).

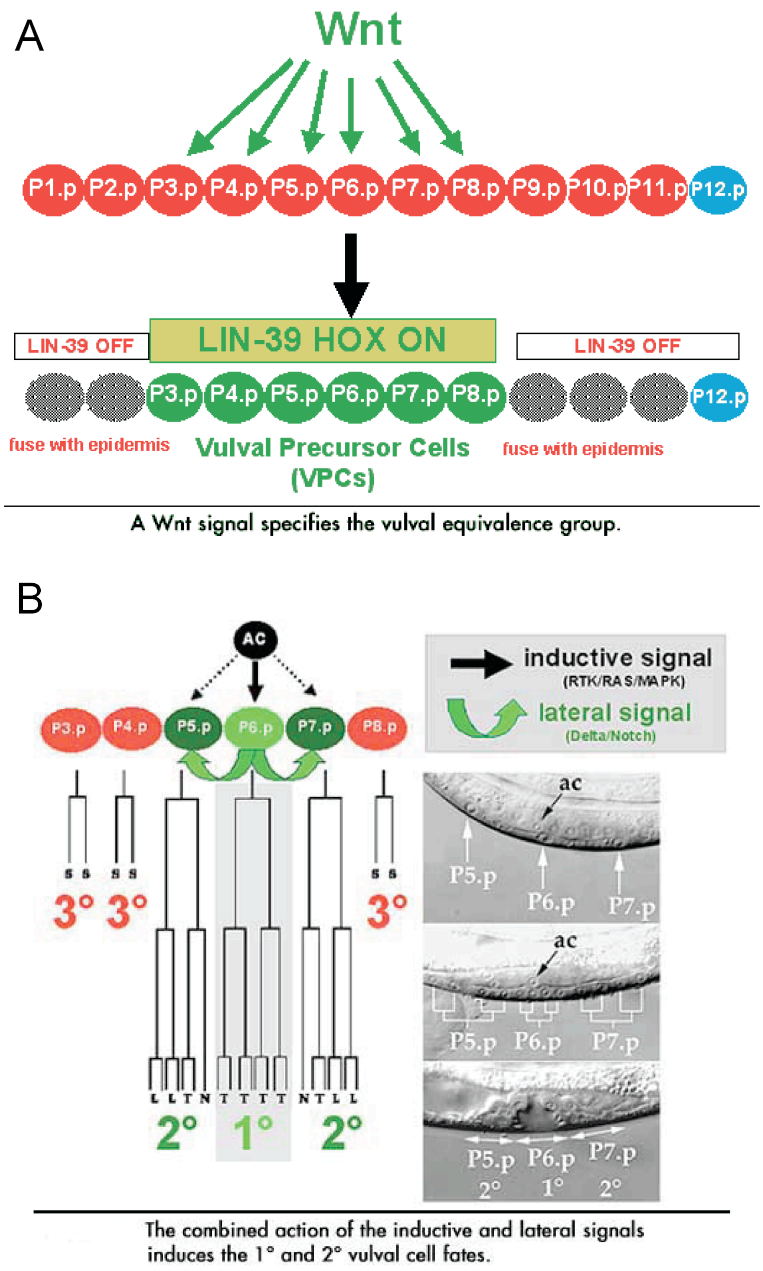

Figure 1.2. The pathways that induce vulval cell fate. (A) the WNT signal specifies the vulval cell linage through activating the Hox gene *lin-39* in the six vulval precursor cells that have the equal potential to differentiate. (B) the patterning of the VPCs by the crosstalk between the inductive RAS/MAPK signal sending from the AC and lateral NOTCH signal. The RAS/MAPK signal specifies the primary cell fate in P6.p while the NOTCH signal, activated by the primary cell, specifies the secondary cell fate in P5.p and P7.p. The P3.p, P4.p and P8.p adapt to the tertiary cell fate that fuse with epidermis after one cell division. The Nomarski pictures show the vulval cells at the one cell stage, the four cell stage and the Christmas tree stage. Pictures are adapted from the Hajnal lab homepage: http://www.imls.uzh.ch/research/Hajnal/Researchgroups/VulvalDevel.html.

The six VPCs adopt to three different cell fates based on the RAS and NOTCH signals. A gonad derived cell, the anchor cell (AC), secretes the EGF ligand LIN-3 towards the vulval epithelium in a gradient manner. Usually, P6.p is located closer to AC compared to other VPCs. Therefore, the EGF receptor LET-23, which is expressed in all the VPCs, is activated mostly in P6.p. The downstream RAS/MAPK pathway of LET-23 determines the primary vulval cell fate of P6.p and drives the expression of NOTCH ligands. The adjacent P5.p and P7.p cells receive the lateral NOTCH signal from P6.p, which inhibits the RAS signal. As a result, P5.p and P7.p with high NOTCH signal and low RAS activation adopt the secondary cell fate (Fig.1.2 B). The primary and secondary vulval cells then undergo three rounds of cell divisions, generating the 22 cells with seven sub-cell fates as the VulA, VulB1, VulB2, VulC, VulD, VulE, VulF. P3.p and P8.p cells, which receive less RAS and NOTCH signal, fuse with the syncytial epidermis after one cell division (Fig. 1.2 B) (Schmid and Hajnal, 2015).

1.2.2. AC invasion

The AC is still required after vulval cell fate induction at L2 stage. It moves towards the primary cells after P6.p has divided into two cells (P6.pa and P6.pp), a stage termed as the two-cell stage (Sherwood and Sternberg, 2003). The AC sends protrusions that secrete the matrix metalloprotease ZMP-1 under the regulation of the transcription factor FOS-1a, breaking the two layers of basal laminae precisely above P6.pa and P6.pp (Fig. 1.3 A and B). The process has been termed as AC invasion due to its similarity with cancer cell invasion. FOS-1a also activates the expression of its downstream target genes *cdh-3* and *him-4,* which encode the Fat-like protocadherin CDH-3 and the fibulin-like matrix component hemicentin HIM-4. ZMP-1, CDH-3 and HIM-4 function together to drive the AC invasion (Fig. 1.3 C) (Sherwood et al., 2005).

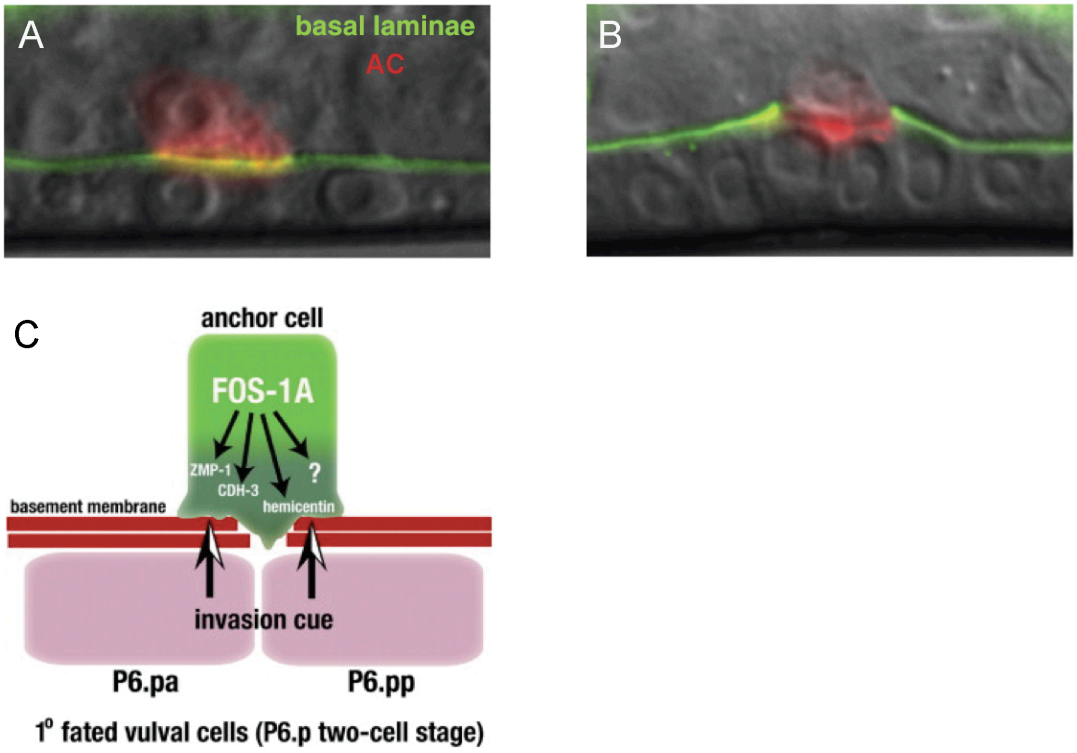

Figure 1.3. The AC invasion. The merged signal of the PIP2::mCherry marked AC and the LAM-1::GFP marked basal lamina before (A) and after (B) invasion. The Gap of GFP signal in (B) indicates the breaching of basal laminae by AC invasion. (C) Model of important molecular that regulate the AC invasive behavior. The invasion cue sent from the neuron cord underneath the VPC induce the polarity and the directional movement of AC. The FOS-1a transcription factor and its downstream targets the ZMP-1, CDH-3 and the hemicentin promote the process of basal laminal breaching. (A) and (B) are adapted from Schmid and Hajnal, 2015. (C) is adapted from Sherwood, 2005.

1.2.3. Vulval morphogenesis

Vulval morphogenesis starts with epithelial invagination during the last round of vulval cell division. Thereby, a liner-array of vulval cells detach from the cuticle, bending dorsally, and generate the beginning lumen of the vulva. As morphogenesis continues, VulE cells circumferentially extend apical membranes to contact their contralateral homologous cells in the midline of the vulva (Fig. 1.4). After VulE toroid are generated, in a proximal to distal order of VulD, VulC, VulB2, VulB1 and VulA, the new toroid forms ventrally to its former one (Gupta et al., 2012). Then, intra-toroidal fusions happen in the order of VulD, VulA, VulC, VulF and VulE toroids. Cell junctions are remained in the midline of VulB1 and VulB2

toroids (Sapir et al., 2007). Following the cell contacts and the cell fusions, the ventral contraction and

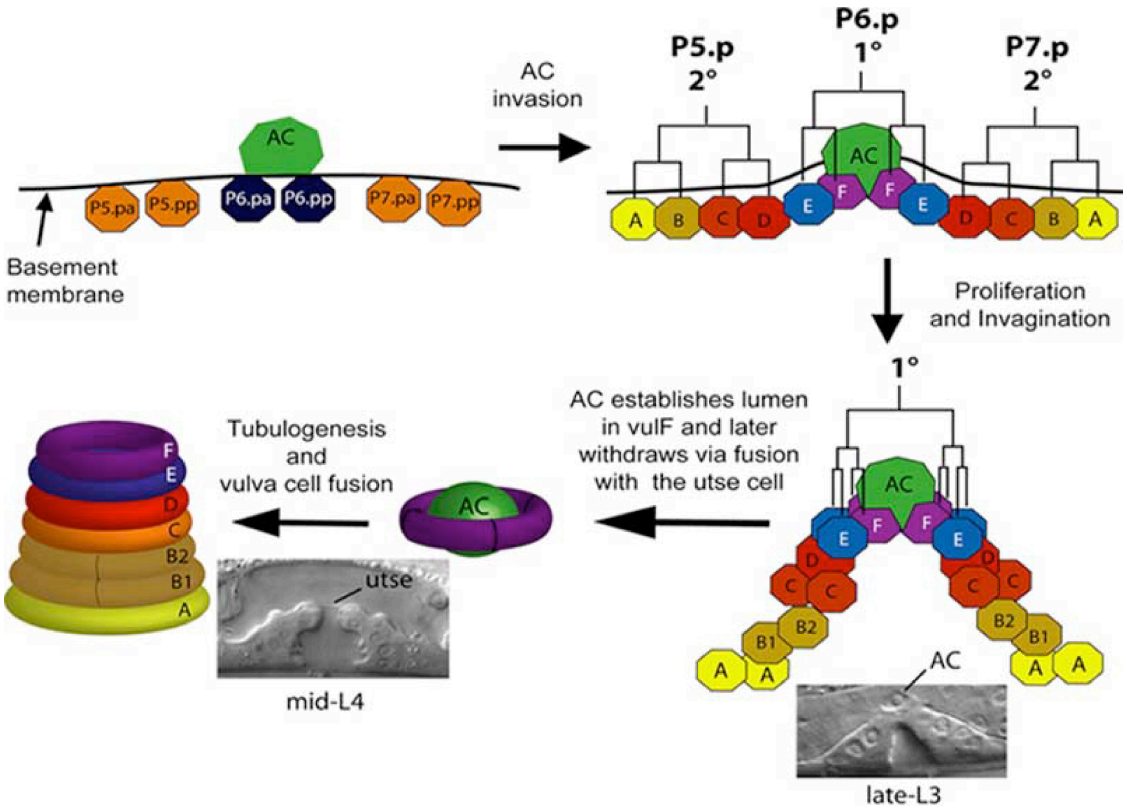

Figure 1.4. Vulval morphogenesis. The vulval morphogenesis takes place after AC invasion and two rounds of cell division that generate 12 liner arrayed vulval cells. During the last round of cell division, the vulval epithelium invaginates, forming the three-dimensional mirror-imaged structure of lumen. In the end, the AC fuse with utse cell, leaving a membrane between the vulval lumen and the utero. After the intro-toroid fusion finished, seven donut-like vulval toroids located one on top of another. Adapted from Gupta, 2012.

the dorsal expansion of vulval lumen shape the “Christmas tree” structure of vulva at mid-L4 stage (Farooqui et al., 2012). Finally, in the last step of eversion, the inside of vulva partially turns outside, forming a functional adult vulva (Sternberg, 2005).

Different proteins have been reported to function during different phases of vulval morphogenesis: 1) During invagination, the SQV (squashed vulva) proteins regulate expression of GAGs (glycosaminoglycans) in vulval cells, which is required for lumen enlargement (Herman et al., 1999). 2) During circumferential extension, the proximal toroid formation has been proposed to drive the migration of the distal vulval cells to the vulval

midline. The SMP-1 (Semaphorin)/PLX-1 (Plexin) pathway, which functions in downstream of the LET-60 (Ras)/LIN-39 (Hox)/VAB-23 (a zinc-finger transcription factor) signal pathway, is involved in the short-ranged migration (Dalpe et al., 2005). Apically expressed SMP-1 interacts with its receptor PLX-1 in distal neighbor vulval cells, regulating cell migration through CED-10 (Rac) and the CED-10 GEF UNC-73. In cells without the activated PLX-1 pathway, MIG-2 is under the regulation of the same GEF UNC-73 and functions redundantly with CED-10 (Kishore and Sundaram, 2002). 3) During vulval lumen shaping, the NOTCH signal controls the ventral acto-myosin contraction through RHO kinase, while the Ras signal regulates the AC-invasion-dependent dorsal expansion (Farooqui et al., 2012). 4) During intra-toroidal fusion, the membrane-associated EMK-family serine/threonine kinase Par-1 regulates the homologous cell contact at vulval midline. The vulva in *par-1* RNAi-treated animal displays the midline-gap between rings while all the early vulval morphogenetic events are normal (Hurd and Kemphues, 2003). The fusogen, protein EFF-1, is required for all the cell fusions happened in vulval development (Mohler et al., 2002). Another fusogen, the AFF-1 protein, is additionally necessary for cell fusions in VulA and VulD toroids formation (Sapir et al., 2007).

1.3. The force-driven cell shape change during morphogenesis

1.3.1. Overview

Tissue remodeling and organ formation can be driven by cumulative cell shape changes or triggered by the individual cellular behavior. The former cases include the cell movement in convergent extension and the apical constriction of the amnioserosa cells in *Drosophila* dorsal closure. The example of single cell shape that triggers tissue remodeling has been found in the mitotic cell rounding that accelerates tissue invagination in *Drosophila* tracheal epithelium (Kondo and Hayashi, 2013). Mechanical forces are required for the cell shape change during morphogenesis (Lecuit and Lenne, 2007). The main groups of proteins that

generate force for cell shape changes are the cortical actin network and the motor protein myosin that slides along the actin filament (F-actin) (Guillot and Lecuit, 2013). The dynamics of cell junctions and the microtubule network are affected by the acto-myosin generated forces and can *vice versa* regulate the force generation (Hoffman et al., 2011). In the following sections, I summarize and review the literatures related to the cellular phenomenas and the molecular mechanisms on one typical cell shape change, the apical constriction that promotes the tissue bending.

1.3.2. Apical constriction: the cell shape change that promotes tissue bending

Tissue bending is one of the key progresses in the formation of many tubular organs. It refers to a sheet of tissue that invaginates or folds, forming a three dimensional structure and setting up the beginning of the lumen (Iruela-Arispe and Beitel, 2013). The major cell shape change during tissue bending is the apical constriction, which refers the shrinkage of the apical domain within a cell. As a cumulative effect, the apical constriction of several cells that contact with each other in the middle of the tissue sheet can lead to the bending of tissue (Fig. 1.5 A) (Sawyer et al., 2010). Apical constriction has been studied in many model systems including the *Drosophila* ventral furrow formation, the *Xenopus* gastrulation, the bud formation in the embryonic chicken lung and the vertebrae neural tube development (Kim et al., 2013).

The prodominant theory of the apical constriction mechanism says that the contractile force is the generated by actomyosin. The contractile network in apical membrane is composed of F-actin that links to junctional proteins and the motor protein non-muscle myosin II (NM II). NM II interacts with the parallel aligned F-actin and translocates along it, generating tension. This energy is provided by the hydrolysis of ATP though the catalytic sites with ATPase activity in the globular head domain of NMII (Bendix et al., 2008). It has been shown that during *C. elegans* gastrulation the phosphorylation activated NM II light

chain is localized at the apical sides of the invaginating cells, associating with the shrinking apical membrane (Fig. 1.5 B).The apical constriction is NM II dependent since the inhibitor of activated NM II blocks the whole process (Lee, 2003).

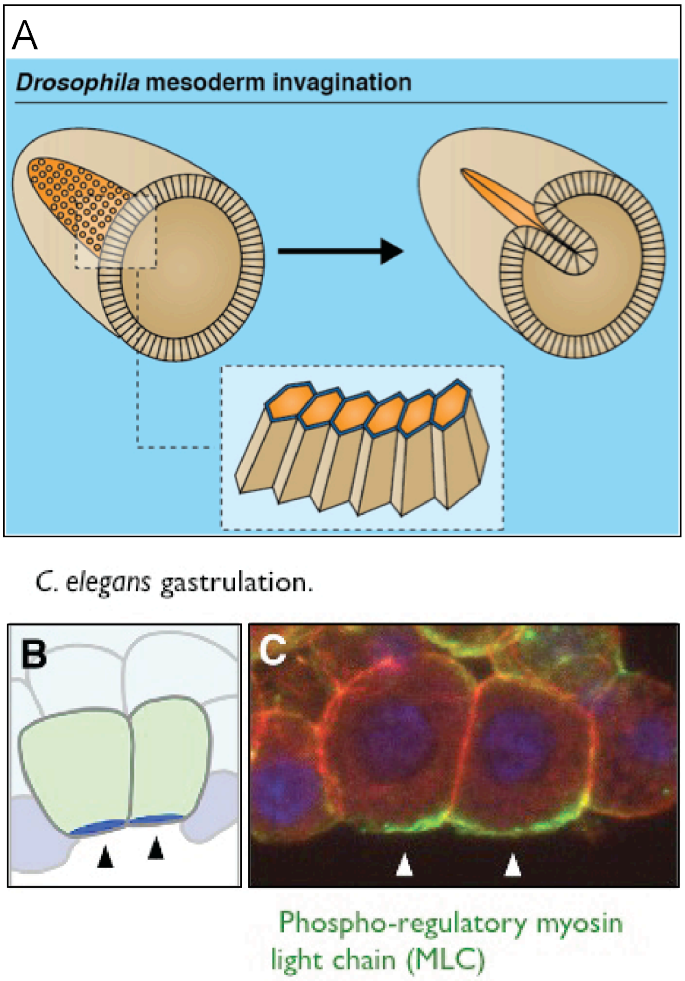

Figure 1.5. The apical constriction in invagination. (A) the example of apical constriction drive tissue bending in *Drosophila* mesoderm invagination. (B) the Phospho-regulatory myosin light chain located in the apical side of the cells that undergo invagination during the *C. elegans* gastrulation. Pictures are modified from Sawyer, 2011.

Time-lapse fluorescence image analysis revealed that activated NM II moves with oscillatory characteristics during actomyosin contraction. Each time after contraction, the actomyosin network needs to be relaxed to allow the next round of contraction. How cell shape changes get fixed after each contraction is well studied. The actin bundles or the cell junctions control the stabilization of cell shape change, performing like the “ratchet” for fixation (Solon et al., 2009).

Besides the actomyosin-generated force-driven apical constriction, other mechanisms have been elucidated in fly tissue bending. For example, the adherens junctions shifting along the apical-basal axis, which is supported by Bazooka/Par-1 during *Drosophila* gastrulation, triggers the apical shrinkage, upon which the epithelium folds without the cortical contractility (Wang et al., 2012). Another example is that the mitotic cell rounding facilitates tissue bending in *Drosophila* tracheal placode (Kondo and Hayashi, 2013). And during *Drosophila* eye development, the morphogenetic furrow is formed through the shortening of the apical-basal length in leading cells, which is regulated by DPP and Hedgehog signaling (Schlichting and Dahmann, 2008).

1.3.3. The regulation of actomyosin networks

The actomyosin generated force drives multiple important cellular behaviors such as membrane constriction, migration, division, and apoptosis. The activity of the actomyosin network is controlled by multiple regulators during development.

The activation of non-muscle Myosin II (NM II) is essential for the regulation of the actomyosin network. The NM II is composed of one pair of heavy chain peptides and two pairs of light chain peptides. Phosphorylation of the heavy and light chains regulates the

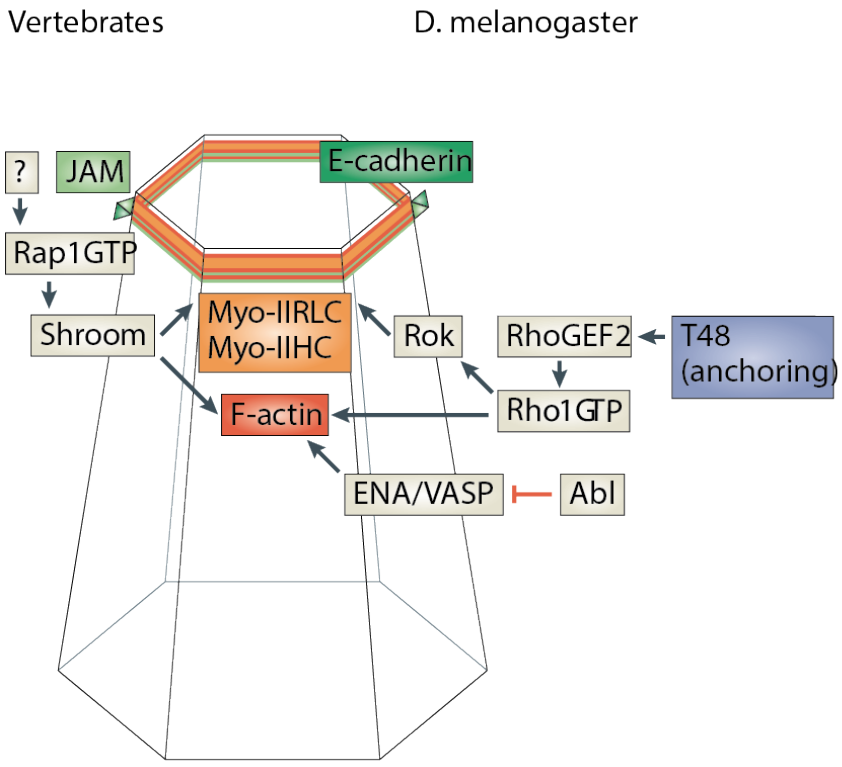

Figure 1.6. The model of apical constriction in vertebrates and *Drosophila*. The actomyosin network (orange) is located along the apical junctional area (green) and interacts with the junctional proteins. The important regulators that were described in Chapter 1.3.3 are demonstrated in the diagram. The black arrows indicate the positive regulation, and the red line indicates the inhibition effect. The Picture is modified from Lecuit, 2007.

activity of NM II (Vicente-Manzanares et al., 2009). Two conserved serines in NM II light chain are phosphorylated by the Rho Kinase. Rho kinase is often activated by the small Rho GTPase Rho-1, which can be activated by RhoGEF and inhabited by RhoGAP. In *Drosophila*, RhoGEF2 localizes to the apical junction area through binding with the apical transmembrane protein T48 and the EB1 that is concentrated at MT plus end towards apical side (Fig. 1.6) (Lecuit and Lenne, 2007). In *C. elegans*, the small GTPase Rho-1 activates LET-502 Rho Kinase, positively regulating the actomyosin-driven tissue morphogenesis (Fig. 1.7 A). In contrast, the UNC-73/Trio Rac/Rho GEF activity controls MIG-2 Mlt Rac that activates MEL-11 myosin phosphatase, which antagonizes the Myosin II activity (Fig. 1.7 A) (Lundquist, 2006). Epistasis studies have shown that the P21-activaed kinase homolog protein PAK-1 functions redundantly with LET-502 in activating

myosin light chain 4 (MLC-4). In addition, the Myotonic dystrophy kinase-related CDC-42-binding kinase homolog protein MRCK positively regulates MLC-4 through inhibiting MEL-11 (Fig. 1.7 A) (Gally et al., 2009). The RhoGAP protein RGA-2 binds to actin and microtubule, inhibiting Rho-1 and the downstream actomyosin activity. RGA-2 is expressed in epidermal cells during embryonic elongation, restricting the activity of actomyosin in seam cells (Fig. 1.7 A) (Diogon et al., 2007). During vulval lumen formation, NOTCH signal

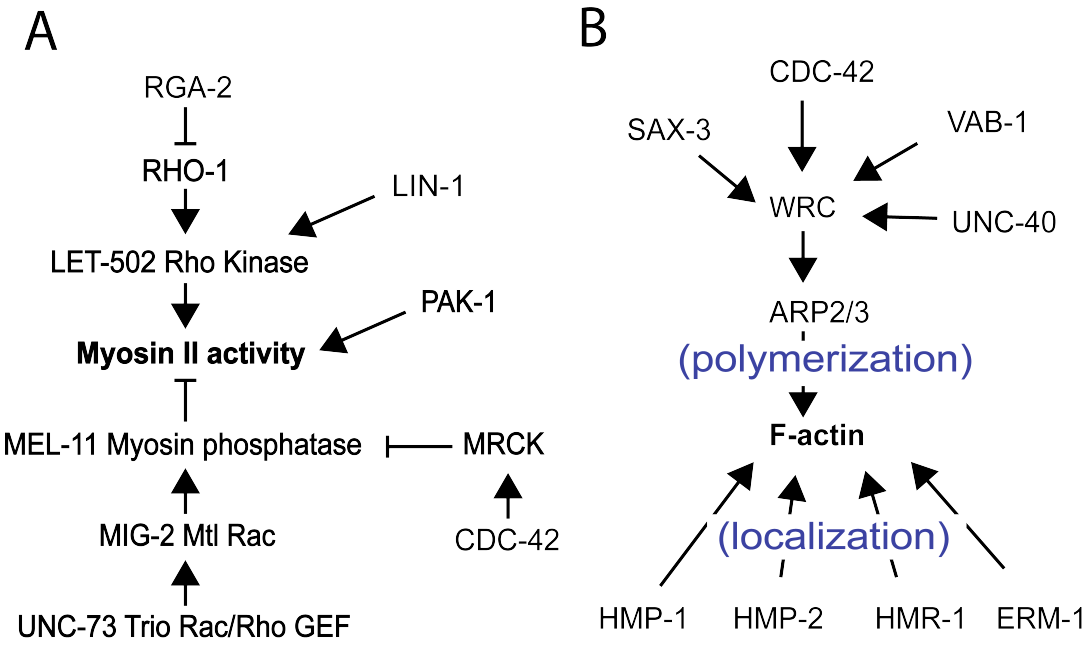

Figure 1.7. The regulation of actomyosin network in *C. elegans*. (A) The main regulators of the Myosin II activity. (B) The main regulators of the F-actin. the blue texts in the brackets indicate the types of regulation that are controlled by the proteins on the starting side of the arrows .

regulates the LET-502 expression in secondary cells through the ETS-family transcription factor LIN-1 (Fig. 1.7 A) (Farooqui et al., 2012).

The polymerization of F-actin is another important process for force generation and underlies the control of multiple proteins. In vertebrate neural tube formation, the PDZ-domain protein Shroom facilitates apical F-actin accumulation through interaction with Actin and Rho Kinase (Hildebrand and Soriano, 1999). During *Drosophila* mesoderm

invagination, the Abelson kinase Abl restricts the polymerization of F-action by inhibiting the actin regulator ENA/VASP, while RhoGEF2 promotes F-actin by mediating the link between apical junctions and actin (Fig. 1.6) (Fox and Peifer, 2006). The WAVE regulatory complex (WRC) regulates the accumulation of F-actin on cell membrane through mediating the actin-nucleating function of the Arp2/3 complex from nematodes to mammals (Fig. 1.7 B) (Rotty et al., 2013). It has been reported that the WRC localizes at different areas of cell membrane via the interaction with different receptors (Chen et al., 2014). In *C. elegans*, the Ephrin receptor VAB-1, the Netrin receptor UNC-40 and the Slit receptor SAX-3 positively regulate WRC (Fig. 1.7 B) (Bernadskaya et al., 2012). The Rho family GTPase CDC-42 modulates Actin branching and nucleating by acts upstream of the WRC (Fig. 1.7 B) (Simske and Hardin, 2001).

Actin bundles are anchored to membrane though the interaction with junctional protein complex and several membrane associating proteins. The circumferential actin bundles often binds to the apical junction (AJ) proteins such as HMP-1/alpha-Catenin, HMP-2/beta-Catenin and HMR-1/E-cadherin. Other proteins for example the cytoskeleton linker ERM-1 (Ezrin, Radixin, Moesin) are associated with AJ or other fibrous organelles also link with F-actin (Fig. 1.7 B) (Ivetic and Ridley, 2004).

1.3.4. Actin-independent forces in morphogenesis

Actin-independent forces have been identified to function during tissue morphogenesis, rising attention to their contributions in balancing the actomyosin contractile force and driving tissue shape change during development of organs (Zhang et al., 2012). One Actin-independent force is the osmotic pressure, which is controlled by the osmotic gradients in cell and is one of the force that antagonizes actomyosin generated tension in mitotic animal cells (Stewart et al., 2012). The osmotic pressure allows mitotic cell rounding in an environment contacting with other cells, which triggers tissue bending in the

Drosophila tracheal invagination (Kondo and Hayashi, 2013). Another example is the force provided by cell matrix proteins during invagination. It has been reported during *Sea Urchin* gastrulation, the hydrophilic proteoglycan secreted by vegetal plate cells swells the apical lamina and drives the bending of vegetal plate (Davidson et al., 1995). A similar situation has been reported in *C. elegans* vulval development, where reals the *sqv* genes that regulate the expression of extracellular matrix proteins during vulval epithelia invagination (Herman et al., 1999). However, how exactly the osmatic force collaborates with other forces is not known and remains to be elucidated (Lane et al., 1993).

1.4. Objectives and rationale of the present study

The *C. elegans* vulva is an ideal system to study tubular organ formation. The molecular mechanisms underlying tissue patterning and cell fate specification have been thoroughly studied, while only limited number of genes have been described during vulval morphogenesis. The details of the pathways or principles behind the vulval morphogenesis remain to be elucidated.

This thesis focuses on describing the cellular behaviors during vulval morphogenesis and in particular, the first event during lumen formation. The principle behind morphogenesis is often not only about the biochemical reactions within the central dogma of molecular biology, the reaction among genes, mRNAs and proteins, but also involves in the biophysical activities that mediate the tension in the three dimensional structure of the whole tissue as well as in the single cell.

In the first project, I studied the first morphogenetic event which has been termed as the vulval invagination. This process is interesting because of the conserved phenomena of epithelial invagination that initiates the tube lumen and the special cell interactions between the AC and the VPCs that resembles the cancer cell invasion induced angiogenesis (Lopes-Bastos et al., 2016). The AC was found to be required for force

generation on the lateral cell membranes between the two VulF cells, which turned out to be the driving force for the constriction of the VulF lateral membranes. This lateral membrane constriction is a novel finding in the field, which stimulated me to dissect the molecular mechanisms behind it. By using the expression pattern of the force generating molecular NMY-2 as the readout, a RNAi- and mutant-based screen was performed to search the regulators that controls the force generation in VulF cells.

In the second project, the screen for genes controlling vulval morphogenesis aimed to complete the searching of the genes exhabiting a protruding vulval phenotype (Pvl) based on the high-resolution pictures of the cytoskeleton structure. Phenotypes of candidate genes were grouped into five different vulval morphogenesis defects. The selection of candidates for further experiments was decided based on their phenotypes and their known gene function. One of the candidate genes (*unc-59)* that demonstrated a primary-toroid morphogenesis defect in mutant analysis was chosen for further study.

The specific aims of this thesis were to:

Describe the vulval invagination and the requirement of AC during this process (Chapter 2);

Dissect the mechanism of force generation in vulval cells during vulval invagination (Chapter 2);

Perform a screen of the genes in the Pvl library to identifiy regulators of vulval morphogenesis (Chapter 3);

Analyze the phenotypes of *septin* mutant animals identified in the morphogenesis screen in toroid formation (Chapter 4).

1.5 References

Altun, Z.F. and Hall, D.H. 2009. Introduction. In *WormAtlas*.

Bendix P.M., Koenderink, G.H., Cuvelier, D., Dogic, Z., Koeleman, B.N., Brieher, W.M., Field, C.M., Mahadevan, L., Weitz, D.A., 2008. A Quantitative Analysis of Contractility in Active Cytoskeletal Protein Networks. Biophysical Journal 94, 3126–3136. doi:10.1529/biophysj.107.117960

Bernadskaya, Y.Y., Wallace, A., Nguyen, J., Mohler, W.A., Soto, M.C., 2012. UNC-40/DCC, SAX-3/Robo, and VAB-1/Eph Polarize F-Actin during Embryonic Morphogenesis by Regulating the WAVE/SCAR Actin Nucleation Complex. PLoS Genet 8, e1002863. doi: 10.1371/journal.pgen.1002863.s003

Brenner, S., 1974. The genetics of *Caenorhabditis elegans.* Genetics 77, 71–94.

C. elegans Sequencing Consortium, 1998. Genome sequence of the nematode *C. elegans*: a platform for investigating biology. Science 282, 2012–2018.

Chen, X.J., Squarr, A.J., Stephan, R., Chen, B., Higgins, T.E., Barry, D.J., Martin, M.C., Rosen, M.K., Bogdan, S., Way, M., 2014. Ena/VASP Proteins Cooperate with the WAVE Complex to Regulate the Actin Cytoskeleton. Developmental Cell 30, 569–584. doi: 10.1016/j.devcel.2014.08.001

Dalpe, G., Brown, L., Culotti, J.G., 2005. Vulva morphogenesis involves attraction of plexin 1-expressing primordial vulva cells to semaphorin 1a sequentially expressed at the vulva midline. Development 132, 1387–1400. doi:10.1242/dev.01694

Davidson, L.A., Koehl, M.A., Keller, R., Oster, G.F., 1995. How do sea urchins invaginate? Using biomechanics to distinguish between mechanisms of primary invagination 1–14.

Diogon, M., Wissler, F., Quintin, S., Nagamatsu, Y., Sookhareea, S., Landmann, F., Hutter, H., Vitale, N., Labouesse, M., 2007. The RhoGAP RGA-2 and LET-502/ROCK achieve a balance of actomyosin-dependent forces in *C. elegans* epidermis to control morphogenesis. Development 134, 2469–2479. doi:10.1242/dev.005074

Farooqui, S., Pellegrino, M.W., Rimann, I., Morf, M.K., Muller, L., Frohli, E., Hajnal, A., 2012. Coordinated lumen contraction and expansion during vulval tube morphogenesis in *Caenorhabditis elegans.* Developmental Cell 23, 494–506. doi:10.1016/j.devcel. 2012.06.019

Fox, D.T., Peifer, M., 2006. Abelson kinase (Abl) and RhoGEF2 regulate actin organization during cell constriction in *Drosophila*. Development 134, 567–578. doi:10.1242/dev.02748

Gally, C., Wissler, F., Zahreddine, H., Quintin, S., Landmann, F., Labouesse, M., 2009. Myosin II regulation during *C. elegans* embryonic elongation: LET-502/ROCK, MRCK-1 and PAK-1, three kinases with different roles. Development 136, 3109–3119. doi:10.1242/ dev.039412

Guillot, C., Lecuit, T., 2013. Adhesion Disengagement Uncouples Intrinsic and Extrinsic Forces to Drive Cytokinesis in Epithelial Tissues. Developmental Cell 24, 227–241. doi: 10.1016/j.devcel.2013.01.010

Gupta, B.P., Hanna-Rose, W., Sternberg, P.W., 2012. Morphogenesis of the vulva and the vulval-uterine connection. WormBook 1–20. doi:10.1895/wormbook.1.152.1

Herman, T., Hartwieg, E., Horvitz, H.R., 1999. sqv mutants of *Caenorhabditis elegans* are defective in vulval epithelial invagination. Proc Natl Acad Sci U S A 96, 968–973.

Hildebrand, J.D., Soriano, P., 1999. Shroom, a PDZ domain-containing actin-binding protein, is required for neural tube morphogenesis in mice. Cell 99, 485–497.

Hoffman, B.D., Grashoff, C., Schwartz, M.A., 2011. Dynamic molecular processes mediate cellular mechanotransduction. Nature 475, 316–323. doi:10.1038/nature10316

Hurd, D.D., Kemphues, K.J., 2003. PAR-1 is required for morphogenesis of the Caenorhabditis elegans vulva. Developmental Biology 253, 54–65.

Iruela-Arispe, M.L., Beitel, G.J., 2013. Tubulogenesis. Development 140, 2851–2855. doi: 10.1242/dev.070680

Ivetic, A., Ridley, A.J., 2004. Ezrin/radixin/moesin proteins and Rho GTPase signalling in leucocytes. Immunology 112, 165–176.

Kim, H.Y., Varner, V.D., Nelson, C.M., 2013. Apical constriction initiates new bud formation during monopodial branching of the embryonic chicken lung. Development 140, 3146–3155. doi:10.1242/dev.093682

Kishore, R.S., Sundaram, M.V., 2002. ced-10 Rac and mig-2 Function Redundantly and Act with unc-73 Trio to Control the Orientation of Vulval Cell Divisions and Migrations in *Caenorhabditis elegans*. Developmental Biology 241, 339–348. doi:10.1006/dbio. 2001.0513

Kondo, T., Hayashi, S., 2013. Mitotic cell rounding accelerates epithelial invagination. Nature 494, 125–129. doi:10.1038/nature11792

Lane, M.C., Koehl, M.A., Wilt, F., Keller, R., 1993. A role for regulated secretion of apical extracellular matrix during epithelial invagination in the sea urchin. Development 117, 1049–1060.

Lecuit, T., Lenne, P.-F., 2007. Cell surface mechanics and the control of cell shape, tissue patterns and morphogenesis. Nat Rev Mol Cell Biol 8, 633–644. doi:10.1038/nrm2222

Lee, J.Y., 2003. Mechanisms of cell positioning during *C. elegans* gastrulation. Development 130, 307–320. doi:10.1242/dev.00211

Lopes-Bastos, B.M., Jiang, W.G., Cai, J., 2016. Tumour-Endothelial Cell Communications: Important and Indispensable Mediators of Tumour Angiogenesis. Anticancer Res. 36, 1119–1126.

Lundquist, E., 2006. Small GTPases. WormBook. doi:10.1895/wormbook.1.67.1

Mohler, W.A., Shemer, G., del Campo, J.J., Valansi, C., Opoku-Serebuoh, E., Scranton, V., Assaf, N., White, J.G., Podbilewicz, B., 2002. The type I membrane protein EFF-1 is essential for developmental cell fusion. Developmental Cell 2, 355–362.

Rotty, J.D., Wu, C., Bear, J.E., 2013. New insights into the regulation and cellular functions of the ARP2/3 complex. Nat Rev Mol Cell Biol 14, 7–12. doi:10.1038/nrm3492

Sapir, A., Choi, J., Leikina, E., Avinoam, O., Valansi, C., Chernomordik, L.V., Newman, A.P., Podbilewicz, B., 2007. AFF-1, a FOS-1-regulated fusogen, mediates fusion of the anchor cell in C. elegans. Developmental Cell 12, 683–698. doi:10.1016/j.devcel. 2007.03.003

Schlichting, K., Dahmann, C., 2008. Hedgehog and Dpp signaling induce cadherin Cad86C expression in the morphogenetic furrow during Drosophila eye development. Mechanisms of Development 125, 712–728. doi:10.1016/j.mod.2008.04.005

Schmid, T., Hajnal, A., 2015. ScienceDirectSignal transduction during *C. elegans* vulval development: a NeverEnding story. Current Opinion in Genetics & Development 32, 1–9. doi:10.1016/j.gde.2015.01.006

Sherwood, D.R., Butler, J.A., Kramer, J.M., Sternberg, P.W., 2005. FOS-1 promotes basement-membrane removal during anchor-cell invasion in *C. elegans*. Cell 121, 951–962. doi:10.1016/j.cell.2005.03.031

Sherwood, D.R., Sternberg, P.W., 2003. Anchor Cell Invasion into the Vulval Epithelium in *C. elegans*. Developmental Cell 5, 21–31. doi:10.1016/S1534-5807(03)00168-0

Simske, J.S., Hardin, J., 2001. Getting into shape: epidermal morphogenesis in *Caenorhabditis elegans* embryos. Bioessays 23, 12–23. doi: 10.1002/1521-1878(200101)23:1<12::AID-BIES1003>3.0.CO;2-R

Solon, J., Kaya-Copur, A., Colombelli, J., Brunner, D., 2009. Pulsed Forces Timed by a Ratchet-like Mechanism Drive Directed Tissue Movement during Dorsal Closure. Cell 137, 1331–1342. doi:10.1016/j.cell.2009.03.050

Sternberg, P.W., 2005. Vulval development. WormBook 1–28. doi:10.1895/wormbook.1.6.1

Stewart, M.P., Helenius, J., Toyoda, Y., Ramanathan, S.P., Muller, D.J., Hyman, A.A., 2012. Hydrostatic pressure and the actomyosin cortex drive mitotic cell rounding. Nature 469, 226–230. doi:10.1038/nature09642

Sulston, J.E., Schierenberg, E., White, J.G., Thomson, J.N., 1983. The embryonic cell lineage of the nematode Caenorhabditis elegans. Developmental Biology 100, 64–119.

Vicente-Manzanares, M., Ma, X., Adelstein, R.S., Horwitz, A.R., 2009. Non-muscle myosin II takes centre stage in cell adhesion and migration. Nat Rev Mol Cell Biol 10, 778–790. doi:10.1038/nrm2786

Wang, Y.-C., Khan, Z., Kaschube, M., Wieschaus, E.F., 2012. Differential positioning of adherens junctions is associated with initiation of epithelial folding. Nature 484, 390–393. doi:10.1038/nature10938

Zhang, H., Landmann, F., Zahreddine, H., Rodriguez, D., Koch, M., Labouesse, M., 2012. A tension-induced mechanotransduction pathway promotes epithelial morphogenesis. Nature 470, 99–103. doi:10.1038/nature09765

The invading anchor cell induces lateral membrane constriction during vulval lumen morphogenesis in *C. elegans*

Qiutan Yang[1,2], Daniel Roiz[1,2], Louisa Mereu[1,2], Alex Hajnal[1,3]

[1]University of Zurich, Institute of Molecular Life Sciences, Winterthurerstrasse 190 CH-8057 Zurich, Switzerland.

[2]Zurich PhD Program in Molecular Life Sciences

[3]corresponding author: alex.hajnal@imls.uzh.ch

Keywords: *Caenorhabditis elegans*; morphogenesis; lumen formation; actomyosin; Bin–Amphiphysin–Rvs domain; cell invasion.

running title: Cell invasion during lumen morphogenesis

27.10.2016

Summary

During epithelial morphogenesis, linear arrays of cells are converted into three dimensional tubular structures, which are the basic building blocks of epithelial organs. Tube morphogenesis depends on actomyosin generated intracellular forces that induce tissue invagination and lumen formation. However, in many cases the extrinsic signals regulating actomyosin contraction are not known.

We have investigated the mechanisms controlling lumen morphogenesis in the *C. elegans* vulva, a tubular organ formed by 22 epithelial cells. The first discernible event initiating lumen formation is the constriction of the apical membranes of the inner-most pair of primary VulF cells. Unlike other cases of epithelial invagination, the VulF cells then constrict their lateral membranes along the apico-basal axis to extend the lumen dorsally. Lateral but not apical VulF constriction requires the prior invasion of the anchor cell (AC) into the vulval epithelium. The invading AC extends actin-rich protrusions towards the apical VulF junctions, resulting in the formation of a new AC-VulF interface. The recruitment of the Bin-Amphiphysin-Rvs (BAR) domain protein TOCA-1 to the AC-VulF contact sites induces the accumulation of the force-generating non-muscle myosin. Through this mechanism, the AC reorients the contractile forces in the VulF cells, causing a switch from apical to lateral membrane constriction and the dorsal extension of the lumen. Invasive cells may need to induce similar shape changes in adjacent cells to penetrate their target tissues.

Introduction

Tubes are the basic building blocks of most epithelial organs (Andrew and Ewald, 2010). A key step during the morphogenesis of tubular organs is the invagination of the tissue, which converts a monolayer of epithelial cells into a three-dimensional structure. The constriction of the apical cell surface is a crucial process that initiates the bending of the invaginating epithelium. Apical constriction has been extensively studied, most notably during gastrulation, vertebrate neurulation, dorsal closure in *Drosophila* and branching morphogenesis of various tubular organs (Sawyer et al., 2010). In all of these examples, apical constriction is the result of contractile forces generated by the actomyosin network on the apical cortex of the cells. These cell shape changes can either be controlled by cell intrinsic factors and by extracellular cues such as diffusible growth factor signals. In particular, during gastrulation cell intrinsic transcription factors that determine the regional cell fates induce apical constriction in the invaginating epithelium, while fibroblast and vascular endothelial growth factors (FGF and VEGF) released from neighboring cells induce apical constriction during branching morphogenesis of tubular organs (Helker et al., 2013). In all of these cases, apical constriction is induced through intracellular signaling pathways that control actomyosin contractility, via a CDC42 or Rho-dependent kinase that phosphorylates and thereby activates the non-muscle myosin light chain regulatory subunit (Heisenberg and Bellaiche, 2013). The sub-cellular localization and orientation of the actomyosin network plays a pivotal role in determining the directivity and distribution of the intracellular forces between the different cortical domains. Hence, the localized activation of the various actomyosin regulators determines the type of shape changes a cell will undergo.

In this study, we investigated the cell shape changes occurring during lumen morphogenesis in the *C. elegans* vulva, the egg-laying organ of the hermaphrodite. The vulva is a tubular organ that passes the fertilized eggs from the uterus to the outside. Thanks to the small number of only 22 cells that form the vulval tube and to the ability to observe the process in real time, vulval development is an excellent model to study epithelial morphogenesis at single cell resolution (Schindler and Sherwood, 2012). Vulval invagination and lumen formation begins in L3 larvae, after the three proximal vulval precursor cells (VPCs), P5.p, P6.p and P7.p, have each divided twice to generate 12 vulval cells (Fig. 1A). At this stage, the gonadal anchor cell (AC), which is located dorsally to the vulval cells, has breached the two basal laminae separating the gonad from the vulva (Sherwood and Sternberg, 2003). Thereafter, the AC invades the vulval epithelium and establishes direct cell-cell contacts with the two inner-most primary (1°) VulF cells.

The VulF cells then begin to move dorsally and initiate the formation of the vulval lumen (Fig. 1A). The remaining vulval cells (VulE through VulA) follow the VulF cells while undergoing the last round of cell divisions. After these cell rearrangements, the vulval tube is built by a stack of seven toroids that are each generated by the homotypic fusion between vulval cells of the same subfate (Pellegrino et al., 2011; Schindler and Sherwood, 2012). Whereas the molecular pathways controlling vulval fate specification and AC invasion are well studied, the events that initiate the formation of the vulval lumen have not yet been characterized. In particular, it is unknown what type of cell-cell interactions and signaling pathways control the cell shape changes that are required for wild-type lumen morphogenesis.

We have used live-imaging combined with cell ablation experiments and cortical tension measurements to dissect the temporal sequence of events occurring during vulval lumen morphogenesis. In contrast to other known models of lumen formation, vulval lumen morphogenesis involves a sequence of apical and lateral membrane constrictions of the VulF cells, which extend the lumen dorsally. The invading AC plays a central role in orchestrating the vulval cell shape changes. The newly forming AC-VulF interface reorganizes the cortical actomyosin network in the VulF cells and induces the constriction of the VulF cells along their lateral membranes after apical constriction has been completed. For this purpose, the F-BAR (Bin-Amphiphysin-Rvs) domain protein TOCA-1 (Bai and Grant, 2015) is recruited to the newly forming AC-VulF contact sites. TOCA-1 and its paralog TOCA-2 then capture the non-muscle myosin NMY-2 to reorient the contractile forces in the VulF cells along the dorso-ventral axis. In this manner, the temporal sequence of cell autonomous apical and AC-induced lateral membrane constriction shapes the vulval lumen.

Results

Sequential apical and lateral constriction of the VulF cells during vulval lumen morphogenesis

The formation of the vulval lumen begins after the second round of vulval cell divisions in mid L3 larvae (Pn.pxx stage). First, the apical membranes of two inner descendants of P6.p (the VulF cells P6.pap and P6.ppa) detach from the cuticle and the cells move dorsally (Fig. 1A,B). As the vulval lumen gradually expands, the vulval cells undergo their last round of cell divisions to generate 22 cells with seven different subfates (the 1° VulF and VulE cells and the 2° VulD through VulA cells) that form the vulval tube (Schindler and Sherwood, 2012; Sharma-Kishore et al., 1999).

We characterized the cell shape changes during the early phases of vulval lumen morphogenesis by performing 3D time-lapse microscopy of mid to late L3 larvae. For this purpose, we first observed larvae expressing the CED-10::GFP reporter, which labels the basolateral plasma membranes (Lundquist et al., 2001). Before the emergence of a lumen, the apical VulF membranes began to constrict, resulting in a gradual shortening of the distance between the apical ends of their lateral membranes (40 minute time point in Fig. 1B-B'', suppl. Movie s1 and suppl. Fig. s1A for quantification). The VulE and the 2° cells, on the other hand, did not display signs of apical constriction at this stage. Around the time when the apical constriction of VulF had reached its maximum, the VulE cells underwent their last round of transversal (along the left/right axis) divisions (100 minute time point in Fig. 1B-B''), making space for VulD to move towards the vulval midline and establish direct contact with VulF (140 minute time point in Fig. 1B-B'',C'). After the VulE divisions, the apical VulF membranes relaxed partially, while the lateral membranes between the two VulF cells started to constrict until their apical ends reached the basal apex of the VulF cells, a process we termed lateral constriction (200 minute time point in Fig. 1B-B'', suppl. Movie s1 and suppl. Fig. s1B for quantification). After the lateral constriction had been completed, the VulF cells underwent their last round of divisions. This temporal sequence of apical and lateral VulF membrane constrictions separated by the VulE divisions resulted in the formation of a characteristic pointed vulval lumen that extends to the AC-VulF contact sites (last time point in Fig. 1B-B'').

The invading AC extends dynamic protrusions towards the apical VulF junctions

Prior to vulval lumen formation, the gonadal AC breaches the two basal laminae that separate the vulval epithelium from the uterus and invades the vulval tissue (Sherwood and Sternberg, 2003). We investigated the morphology of the AC during vulval lumen

formation after basal laminae breaching had occurred. For this purpose, we observed lumen formation in animals carrying the P_{cdh-3}*>mCherry::PLCδ^{PH}* reporter, which labels the phosphatidylinositol-4,5-bisphosphate (PIP_2) containing actin-rich AC plasma membranes, along with the apical junction (AJ) marker P_{ajm-1}*>ajm-1::gfp* (Ziel et al., 2009). As the VulF cells underwent apical constriction, the AC extended circumferential actin-rich protrusions directed at the AJs between the two VulF cells (suppl. Movie s2, Fig. 1C-C''). After VulE division and during lateral VulF constriction, the AC protrusions gradually retracted dorsally (compare third and fifth panels in Fig. 1C'') until the VulF AJs were bent dorsally forming an arch underneath the AC body (fifth panel in Fig. 3C, see 3D reconstruction in suppl. Movie s3). As a result of these cell shape changes, a junction between the AC and the VulF cells was formed (arrowhead in the fifth panel of Fig. 1C'').

The extension of dynamic AC protrusions towards the VulF AJs suggested an active role of the AC in inducing the vulval cell shape changes during lumen formation. The AC protrusions may, for example, guide the apical VulF junctions to move dorsally during lateral membrane constriction.

The AC induces lateral VulF constriction

To test if the AC regulates the shape changes of the vulval cells, we examined the requirement for direct contact formation between VulF and the AC. For this purpose, we observed the *fos-1(ar105)* mutant, in which the AC does not breach the basal laminae and the AC protrusions can not reach the AJs of the VulF cells (Sherwood et al., 2005). *fos-1(ar105)* mutants did not exhibit any signs of lateral VulF constriction, while apical constriction was not significantly affected (Fig. 2A,B and suppl. Fig. s1 for quantification). To distinguish if the absence of basal laminae breaching or the lack of cell-cell contact *per se* caused the loss of lateral VulF constriction, we ablated the AC at the mid-Pn.pxx stage, after the basal laminae had been breached but before the onset of lumen formation. Similar to *fos-1(ar105)* mutants, the post invasion AC ablations resulted in the absence of lateral VulF constriction, while apical constriction did occur (Fig. 2C and suppl. Fig. s1 for quantification). In both, AC ablated animals and *fos-1(ar105)* mutants, we noticed a slight delay in vulval lumen formation. For example, in the AC ablated animal shown in Fig. 2C no lumen was detectable at the 230 minutes time point, even though both VulF cells had initiated their last round of divisions.

We conclude that AC invasion, which permits the formation of direct AC-VulF contact, is

required to induce lateral VulF membrane constriction. Apical VulF constriction, on the other hand, does not depend on direct contact with the AC and hence appears to be an intrinsic property of the 1° VulF cell fate. In the absence of lateral VulF constriction, a vulval lumen does form, though at a slower rate and the lumen is not extended dorsally to reach the AC.

Accumulation of the actomyosin network at the AC-VulF contact sites

Contractile forces generated by the actomyosin network induce epithelial cell shape changes in many developmental processes, including apical constriction during *C. elegans* gastrulation (Nance et al., 2005; Sawyer et al., 2010). We thus examined the subcellular localization of the actomyosin network during vulval lumen formation. To visualize actin filaments (F-actin), we used the P_{dlg-1}*>LifeAct::gfp* reporter (Farooqui et al., 2012). During apical and lateral VulF constriction, most of the F-actin signal in the 1° cells was detected on the basolateral cortex and adjacent to the AJs (Fig. 3 A). 3D image reconstructions of the VulF cells undergoing apical constriction revealed a ring-shaped pattern of apical F-actin staining along the AJs (Fig. 3A'). Interestingly, F-actin on the lateral VulF cortex before and during lateral constriction also exhibited a ring-shaped, though more patchy distribution (Fig. 3B',E).

To observe myosin localization, we performed 3D time-lapse recordings of an endogenous reporter for non-muscle myosin II (NMY-2::GFP) along with the P_{cdh-3}*>mCherry::PLCδ*^{PH} AC marker (Fig. 4A, suppl. movie s6) (Dickinson et al., 2013; Ziel et al., 2009). Prior to lumen formation, NMY-2::GFP was predominantly localized near the AJs between the vulval cells. However, during lateral constriction the NMY-2::GFP signal was enriched on the basal side of the VulF cells at the contact sites with the AC (arrowheads in Fig. 4A,C',G). Similar to the cells undergoing apical constriction during gastrulation in the embryo (Nance et al., 2005), NMY-2::GFP exhibited a dynamic pattern with distinct punctae moving along the VulF membranes (suppl. movie s6). We performed particle tracking on mid-sagittal sections taken at one-second time intervals to estimate the speed of the of NMY-2::GFP punctae in the VulF cells (suppl. Fig. s2). This analysis revealed that the movement of NMY-2::GFP punctae, which had reached the AC-VulF contact sites, was significantly slower compared to punctae on the lateral VulF membranes at a distance form the AC (Fig. 4B).

Taken together, the subcellular distribution of the F-actin network and the dynamic movement of NMY-2 in the VulF cells undergoing lateral constriction suggested that

contractile forces are generated not only on the apical cortex but also at the contact sites between the AC and the VulF cells.

Apical mislocalization of the actomyosin network and lumen morphogenesis defects

To further test the relative contributions of the basolateral and apical actomyosin pools, we examined *erm-1* mutants (Göbel et al., 2004; Van Fürden et al., 2004). *erm-1* encodes a member of the Ezrin/Radixin/Moesin (ERM) protein family that is required for basolateral F-actin localization in the vulval cells (Haag et al., 2014). *erm-1(tm677)* null mutants exhibited a reduction in basolateral and a concomitant increase in apical F-actin staining in all vulval cells at the Pn.pxx stage (Fig. 3C, quantified in E). In particular, no ring-shaped F-actin staining could be observed on the lateral VulF cortex of *erm-1(tm677)* mutants (Fig. 3D'). We next examined if the apical mislocalization of F-actin in *erm-1(lf)* mutants affected NMY-2 distribution. Since the *erm-1* and *nmy-2* genes are located in close proximity on LGI, we used *erm-1* RNAi to observe if reducing *erm-1* expression altered NMY-2::GFP localization. RNAi knock-down of *erm-1* caused a strong reduction in the NMY-2::GFP signal at the AC-VulF contact sites in the affected animals (52% affected, n=71) (Fig. 4D-D'',G). Moreover, time-lapse microscopy using a CED-10::GFP reporter revealed a characteristic lumen morphogenesis defect in *erm-1(tm677)* mutants. Instead of extending the lumen dorsally, the lumen in *erm-1(tm677)* mutants had a bulged shape and did not reach the AC contact sites (Fig. 2D,D' and suppl. movies s4, s5). Lateral VulF constriction was absent in *erm-1(tm677)* mutants, while apical VulF constriction was increased when compared to wild-type larvae (suppl. Fig. s1 for quantification).

These results indicated that the apical mislocalization of the actomyosin network in the VulF cells leads to the loss of lateral VulF constriction and an abnormal lumen morphogenesis. We thus propose that a balance between apical and basolateral actomyosin-driven membrane constrictions is necessary to shape the vulval lumen.

Cortical tension measurements on the lateral and apical VulF cortex

The results presented so far suggested that a contractile force on the lateral VulF cortex is an important factor in determining the shape of the vulval lumen. To directly test this hypothesis, we measured the cortical tension in the different compartments of the VulF cells during apical and lateral constriction by performing laser nanosurgery experiments

with a pulsed two-photon infrared laser (see materials and methods) (Mayer et al., 2010 and Vuong and Labouesse, personal communication). During lateral VulF constriction in wild-type animals, we observed a rapid recoil after cutting across the middle section of the lateral VulF cortex (Fig. 5A,B and suppl. Movie s8). By contrast, a significantly smaller recoil was observed in *erm-1(tm677)* mutants at the same developmental stage, indicating a reduced actomyosin-generated tension on the lateral cortex (Fig. 5A,B and suppl. movie s9). We also measured the cortical tension generated during apical constriction before the onset of lumen formation (Fig. 5C,D). This experiment revealed a slight increase in the apical membrane tension in *erm-1(tm677)* mutants compared to wild-type larvae at the same stage, which might reflect the increased F-actin concentration on the apical VulF cortex in *erm-1(tm677)* mutants.

In conclusion, the cortical tension measurements in wild-type and *erm-1(tm677)* mutant larvae support the notion that the basolateral actomyosin network generates a contractile force to cause lateral VulF constriction.

The invading AC reorients the actomyosin network in the VulF cells

We next examined the localization of the actomyosin network in mutants defective in AC invasion. In *fos-1(ar105)* mutants, the NMY-2::GFP signal at the VulF-AC contact sites was reduced and distributed in irregular patches along the basal VulF and VulE cortex (Fig. 4E,G). Also, the ring-shaped F-actin staining on the lateral VulF membrane was perturbed (suppl. Fig. s3B,D). To test if the polarity of the AC is required for the reorganization of the actomyosin network in the VulF cells, we examined *unc-6(ev600)* loss-of-function mutants. *unc-6* encodes a Netrin homolog that functions as a guidance signal from the ventral nerve cord neurons by polarizing the invading AC towards the ventral side (Ziel et al., 2009). In the absence of the UNC-6 Netrin guidance signal, no actin-rich protrusions towards the VulF cells are produced and the AC is often misplaced (suppl. movie s7). Similar to *fos-1* mutants, the accumulation of NMY-2::GFP at the AC-VulF contact sites and the ring-shaped F-actin staining were lost in *unc-6(ev400)* mutants (Fig. 4F,G and suppl. Fig. s3C,D), indicating that the formation of AC protrusions is necessary to reorganize the actomyosin network in the VulF cells. Furthermore, tracking of the NMY-2::GFP punctae in *unc-6(ev600)* mutants indicated that the mobility of NMY-2 punctae at the basal apex of the VulF membranes remains high if no contact is made with the AC (Fig. 4B, suppl. movie s7 and suppl. Fig. s2).

Thus, the formation of direct contact sites between the AC and the VulF cells reorganizes

the actomyosin network on the lateral VulF membranes, resulting in a switch from apical to lateral VulF membrane constriction.

Recruitment of the F-BAR domain protein TOCA-1 during lateral VulF constriction

We noticed that prior to lateral membrane constriction the invading AC deformed the lateral membranes of the VulF cells at their basal apex (arrow in Figure 3A, compare the cell shapes in Figure 2A' versus B',C'). We thus hypothesized that the membrane deformation of the VulF cells caused by the invading AC constitutes a signal that induces the reorganization of the actomyosin network during lateral membrane constriction. Proteins containing an N-terminal Bar (Bin-Amphiphysin-Rvs) domain bind to curved plasma membranes and activate Rho family small GTPases to remodel the F-actin network at sites, where cells experience mechanical deformations (McMahon and Boucrot, 2015). We thus examined *C. elegans* genes known to encode BAR domain proteins for a possible involvement in vulval lumen morphogenesis. We performed RNAi knock-down in larvae and used, where available, mutant alleles to score lumen shape and NMY-2::GFP recruitment. The genes examined are listed in suppl. Table s1.

Through this targeted screen, we identified *toca-1* (Transducer of Cdc42 dependent actin assembly-1) and its paralog *toca-2* as regulators of lumen morphogenesis and NMY-2::GFP localization (suppl. Table s1). The *toca* genes encode two highly similar and functionally redundant F-BAR domain proteins that control actin dynamics and membrane trafficking through a CDC42/PAR-6/WAVE pathway (Bai and Grant, 2015). In *toca-1(tm3334); toca-2(ng11)* double mutants, the AC was able to breach the basal laminae and establish direct contact with the VulF cells, yet the lumen was abnormally shaped due to a lack of dorsal lumen extension (Fig. 6A-F). Moreover, the recruitment of NMY-2::GFP to the AC-VulF contact sites was strongly reduced (Fig. 6G-I).

Next, we tested the role of small GTPases and their downstream effectors to define the signaling pathways that induce actomyosin contraction in the VulF cells. The expression of a dominant-negative mutant of *rho-1* under control of a heat-shock-inducible promoter (Canevascini et al., 2005) or RNAi knock-down of *cdc-42* caused a reduction of NMY-2::GFP accumulation at the AC-VulF interface (suppl. Fig. s4). The MRCK-1 kinase acts downstream of the CDC-42 GTPases and promotes actomyosin contraction during embryonic elongation by phosphorylating the myosin light chain phosphatase MEL-11 (Gally et al., 2009; Nance et al., 2005). Accordingly, NMY-2::GFP recruitment was perturbed in *mrck-1* RNAi-treated larvae (suppl. Fig. s4). By contrast, RNAi against the

Rho-dependent kinase *let-502* had no effect on NMY-2::GFP localization, even though the later contraction of the vulval lumen was perturbed (suppl. Table s1) (Farooqui et al., 2012). Finally, we generated the endogenous *gfp::toca-1(zh110)* reporter via CRISPR/ CAS9 mediated recombination (Dickinson et al., 2015) to observe TOCA-1 localization in the VulF cells. GFP::TOCA-1 was expressed in both the AC and the VulF cells, where it was enriched at the AC-VulF contact sites and near the apical VulF junctions, similar to the NMY-2::GFP pattern described above (Fig. 6J-K'). Displacement of the AC in *unc-6(ev400)* mutants resulted in the loss of the GFP::TOCA-1 signal at the AC-VulF contact sites, indicating that TOCA-1 recruitment requires physical contact between the AC and VulF cells (Fig. 6L-M').

In summary, our results indicate that the F-BAR domain proteins TOCA-1 and TOCA-2 are used to sense the mechanical deformation of the VulF cells caused by the invading AC. The recruitment of the TOCA proteins to the AC-VulF contact sites then promotes the actomyosin-driven constriction of the lateral VulF membranes via RHO-1 and the CDC-42 GTPase/ MRCK-1 pathway.

Discussion

Vulval morphogenesis in *C. elegans* serves as a powerful model to study how a linear array of epidermal cells forms a three-dimensional tubular organ (Schindler and Sherwood, 2012). Thanks to the relatively small number of 22 cells and recent improvements in 4D live-imaging of *C. elegans* larvae (Farooqui et al., 2012), it is possible to observe vulval morphogenesis at high spatial and temporal resolution. In this study, we have characterized the first phase of morphogenesis by observing the events that initiate the formation of the vulval lumen. We show that the invasion of the AC into the vulval epithelium controls the cell shape changes of the 1° VulF cells during lumen morphogenesis.

Sequential apical and lateral constrictions extend the lumen dorsally

Apical membrane constriction driven by actomyosin contractions initiates cell invagination in many morphogenetic processes, notably during gastrulation, neurulation and branching morphogenesis of tubular organs such as the vasculature (Sawyer et al., 2010). Apical constriction leads to cell lengthening and tissue bending, thereby initiating lumen formation. Also during vulval lumen formation, the first discernible cell shape change is the apical constriction of the two inner-most 1° VulF cells (Fig. 7A,B). In contrast to the above mentioned examples, apical VulF constriction is followed by the constriction of the lateral

VulF membranes (Fig. 7C,D). As a result of these shape changes, the vulval lumen extends dorsally towards the AC and, after the AC has fused with the utse syncytium, the vulval and uterine lumina are connected to each other. To our knowledge, vulval lumen formation is so far the only example where not only apical but also lateral constriction of the invaginating cells has been observed. Several experiments show that the lateral VulF constriction does not simply reflect a repositioning or basal sliding of the apical junctions (Wang et al., 2012), but rather involves an actomyosin-generated force driving the contraction of the lateral cortex: (1) A relatively high tension is detectable on the lateral VulF membranes during lateral VulF constriction. (2) The basolateral actomyosin network is required to create this cortical tension. (3) F-actin is organized in a ring-shaped pattern on the lateral VulF membranes, which is characteristic of contractile membranes. (4) Lateral but not apical VulF constriction requires the formation of direct contact between the VulF cells and the AC in order to recruit the non-muscle myosin NMY-2 to the new contact site.

Furthermore, the transversal division of the VulE cells, which preceded the initiation of lateral VulF constriction in all our recordings, appears to coordinate the temporal sequence of apical and lateral constrictions. It is possible that the division of VulE releases tensions formed through the apical junctions between the VulF and VulE cells, thus permitting lateral VulF constriction to begin. A similar role for cell divisions in accelerating epithelial invagination has previously been proposed for tracheal placode invagination in the *Drosophila* embryo (Kondo and Hayashi, 2013). In all wild-type larvae observed, the final transversal division of VulF occurred only after the completion of lateral VulF constriction. Therefore, the coordination of vulval cell shape changes with cell divisions may establish a temporal sequence for the different morphogenetic events during lumen formation.

AC invasion induces lateral VulF constriction

The AC plays a unique role that distinguishes vulval lumen formation from other cases of tube morphogenesis. By breaching the basal laminae between the vulval cells and uterus, the AC establishes direct contact with the two VulF cells (Sherwood and Sternberg, 2003). It has previously been reported that the AC is required for the morphogenesis of the dorsal lumen during vulval tube formation (Estes and Hanna-Rose, 2009). Our study establishes a new role for the AC at an early step of vulval morphogenesis, during the initiation of lumen formation. The circumferential cell protrusions the AC extends towards the apical VulF junctions may serve as physical guides that direct the VulF cells dorsally. The loss of

lateral constriction in AC ablated animals and in *fos-1* mutants indicates that the AC not only serves as guidepost but also plays an active role in inducing VulF constriction. This notion is supported by the finding that physical contact between the AC and VulF cells alters the distribution of the actomyosin network in the VulF cells. The direct contact formed between the AC and VulF cells induces the recruitment of F-actin, NMY-2 and possibly also other force generators to the lateral VulF membranes, thereby reorienting the contractile forces within VulF (Fig.7 C'). This mechanism involves the accumulation of the the F-BAR domain protein TOCA-1 at the AC-VulF contact sites, where the basal VulF membranes are deformed by the invading AC. Since TOCA-1 is expressed in both the AC and VulF cells, the recruitment probably occurs in both cells. Like many other F-BAR domain proteins, TOCA-1 and its functionally redundant paralog TOCA-2 contain a C-terminal SH3 domain that recruits components of the WAVE complex to regulate F-actin dynamics. During *C. elegans* embryonic morphogenesis and endocytosis in oocytes, TOCA-1 and TOCA-2 activate the CDC-42 pathway and regulate WAVE and WSP-dependent actin dynamics (Bai and Grant, 2015). During vulval morphogenesis, the TOCA proteins stabilize the actomyosin network at the contact AC-VulF sites via the CDC-42/MRCK-1 pathway (Fig.7 E) (Gally et al., 2009). The highly mobile, force-generating myosin complexes are trapped once they have reached the VulF-AC contact sites marked by the TOCA complex, where they may further stabilize F-actin bundles in a positive feedback loop.

Our results provide a good rationale for the developmental role of AC invasion during *C. elegans* vulval development. If the AC has not breached the basal laminae by the mid-L3 stage, vulval lumen formation proceeds, though at a slower speed and without lateral VulF constriction. In the absence of lateral VulF constriction, the vulval lumen does not extend dorsally and cannot be connected to the uterine lumen.

There exist striking similarities between AC invasion and the invasion of metastatic tumor cells, both at the molecular and morphological level (Sherwood et al., 2005). In analogy, invasive cells do not only need to change their own shape, but they also induce cell shape changes in the tissues they invade (Blazejczyk et al., 2015). The conserved F-BAR domain proteins could play an important role in the target tissues to sense the mechanical cues generated by invading cells (McMahon and Boucrot, 2015). A similar strategy could be used by metastatic tumor cells, as they move through the adjacent normal tissue, and to penetrate the endothelial cell layer during intravasation (Chiang et al., 2016).

Materials and Methods

General methods and strains used

C. elegans strains were maintained at 20°C on standard nematode growth plates as described (Brenner, 1974). The wild-type strain was *C. elegans* Bristol, variety N2.

Strains used were as follows: LGI: *erm-1(tm677), hT2[bli-4(e937) let(q782) qIs48] (I;III)*, *nmy-2(cp13[nmy-2::gfp]) (I)* (Dickinson et al., 2013)*, unc-57(e406)(I), wve-1(ok3308), hT2[bli-4(e937) let(q782) qIs48] (I;III),* LGII: *rrf-3(pk1426),* LGIII:*, gbi-1(ok640)(III), ina-1(gm39)(III), toca-2(ng11)* (Giuliani et al., 2009) *(III), pat-3(st564)(III),* LGIV: *srgp-1(ok300)(IV), wsp-1(gm324)(IV),* LGV: *rde-1(ne219), fos-1(ar105), nT1[qIs51, let-XX(m435)](IV;V),* LGX: *dyn-1(ky51)(X), toca-1(tm3334)* (Giuliani et al., 2009)*, gfp::toca-1(zh110)* (this study). Extrachromosomal and integrated arrays: *zhIs396[P_{dlg-1}>lifeact::gfp::unc-54 3'utr, P_{lin-48}>gfp]* (Farooqui et al., 2012)*, qyIs50[P_{cdh-3}>mCherry::moeABD]*, *qyIs23[P_{cdh-3}>mCherry::plc∂PH]* (Ziel et al., 2009)*, swIs79[ajm-1::gfp, P_{scm-1}::gfp, unc-119(+)]* (Diogon et al., 2007)*, qyEx19[ced-10::gfp, unc-119(+)], qyIs102[P_{fos-1a}::rde-1;myo2::yfp; unc-119]*, *zhEx167[hs::rho-1(dom.neg), sur-5::gfp]* (Canevascini et al., 2005)*, zhEx418[P_{lin-31}::rde-1;myo-2::mcherry].*

Generation of an endogenous gfp::toca-1 reporter

The endogenous *gfp::toca-1(zh110)* insertion was generated using the modified CRISPR/ CAS9 protocol described by (Dickinson et al., 2015). The oligonucleotides used to generate the sgRNA, the homology arms and for sequencing are listed in suppl. table 2. The GFP-tag was inserted at the N-terminus. *gfp::toca-1(zh110); toca-2(ng11)* double mutants show a wild-type vulval lumen morphology, indicating that the GFP::TOCA-1 fusion protein is functional.

Microscopy and image analysis

Fluorescent images and four-dimensional (4D) recording were obtained using an Olympus BX61 wide-field microscope equipped with a X-light spinning disc confocal system using a 60x Plan Apo lens and a Hamamatsu Orca CCD camera. For the wild-type, the *erm-1* mutant and the AC ablation, we recorded five and for the *fos-1* mutant three larvae each. The graph in suppl. Fig. s1 shows the mean values ± standard deviations measured in the recordings. For 3D reconstructions, z-stacks with a step size of 0.5 µm were recorded with an Olympus FV1000 confocal microscope. For 4D recordings of vulval invagination,

animals were mounted on 5% agarose pads containing 0.5 mM tetramisole. Images were recorded with an an X-light spinning disc system at 10 minute time intervals taking 30 to 40 z-stacks with a step size of 0.3 µm per time point. The layers representing the mid sagittal sections are shown in Fig. 3 and suppl. Movies s1 & s2.

Spinning disc images were processed using the Huygens Deconvolution platform (SVI) to increase the signal to noise ratio and analyzed using Fiji (ImageJ (NIH)) or Imaris (Bit-plane) software. Measurements of apical and lateral membrane lengths were conducted on mid-sagittal sections. The boundaries of the apical VulF membranes were defined by the AJs displaying a stronger CED-10::GFP signal. The length of the lateral VulF membranes was measured from the VulF-AC intersection to the boundary of the apical VulF membrane as shown in suppl. Fig. s1. Intensity plots of LifeAct::GFP or NMY-2::GFP along the lateral VulF membranes were generated using a custom script as described (Morf et al., 2013). For each animal, the intensity in yz-axis projections of the lateral VulF membrane regions (outlined with a yellow dashed box in the example shown in the inset) or in xz-projections (blue dashed boxes) were divided into ten equal segments along the dorso-ventral axis. In each segment, the total intensity was measured and normalized to the summed intensities of all segments.

RNAi

RNA interference (RNAi) was performed using the feeding method as described (Kamath et al., 2003). P0 worms were synchronized at the L1 stage, transferred to nematode growth plates containing 3 mM IPTG and 50 ng/ml ampicillin seeded with the desired RNAi bacteria and allowed to grow for 5-7 days at 20°C, after which the surviving F1 progeny was analyzed.

Cell ablations experiments

Worms were mounted on 4% agarose containing 4 mM tetramisole pads for laser ablation using Leica DMLB wide-field microscope equipped with MicroPoint Laser system as described (Farooqui et al., 2012). AC ablations were performed in late L3 larvae at the Pn.pxx stage, in which the AC had breached the basal laminae as scored with Nomarski optics. Ablated worms were rescued from the pads and allowed to recover at 15°C for 2hours before mounting them again for 4D imaging.

Cortical tension measurements by laser nanosurgery

L4 larvae were mounted on 4% agarose pads containing 4 mM tetramisole. We used an Olympus two-photon Fluoview 1000 microscope equipped with a pre-compensated Ti:Sapphire Laser. Cutting of the apical and lateral membranes was performed using a wavelength of 900nm. The input power was set at 2.17± 0.05W, the length of the cutting region (yellow bars in Fig. 4) was set at around 2 µm, and the activation time was calculated by the scan speed of 1.25µs/pixel. Animals were imaged at 0.2 sec intervals with a 60x N.A. 1.1 water immersion lens before and after cutting. For each cut, we measured the maximal recoil distance between the edges of the cut membrane as indicated with the dashed red line in Fig. 4. Since the maximal recoil velocity exceeded the recording speed, we calculated the average recoil velocity as $v_{average}$= maximal recoil distance/duration of recoil (µm/sec).

Acknowledgments

We thank all present and past group members for critical discussion. We are also grateful to T. Vuong and M. Labouesse for help with the cortical tension measurements and to G. Scita for sharing the strains of *toca-1* and *toca-2* mutants the *C. elegans* Genetics Center, S. Mitani (Japan Knockout Consortium), the Gene expression consortium for providing strains, and to Andrew Fire for vectors. This research was supported by the Kanton Zürich and by grants from Swiss National Science Foundation to A.H..

References

Andrew, D.J., Ewald, A.J., 2010. Morphogenesis of epithelial tubes: Insights into tube formation, elongation, and elaboration. Dev Biol 341, 34–55. doi:10.1016/j.ydbio.2009.09.024

Bai, Z., Grant, B.D., 2015. A TOCA/CDC-42/PAR/WAVE functional module required for retrograde endocytic recycling. Proc Natl Acad Sci USA 112, E1443–52. doi:10.1073/pnas.1418651112

Blazejczyk, A., Papiernik, D., Porshneva, K., Sadowska, J., Wietrzyk, J., 2015. Endothelium and cancer metastasis: Perspectives for antimetastatic therapy. Pharmacol Rep 67, 711–718. doi:10.1016/j.pharep.2015.05.014

Brenner, S., 1974. The genetics of Caenorhabditis elegans. Genetics 77, 71–94.

Canevascini, S., Marti, M., Fröhli, E., Hajnal, A., 2005. The Caenorhabditis elegans homologue of the proto-oncogene ect-2 positively regulates RAS signalling during vulval development. EMBO Rep. 6, 1169–1175. doi:10.1038/sj.embor.7400574

Carpenter, A.E., Jones, T.R., Lamprecht, M.R., Clarke, C., Kang, I.H., Friman, O., Guertin, D.A., Chang, J.H., Lindquist, R.A., Moffat, J., Golland, P., Sabatini, D.M., 2006. CellProfiler: image analysis software for identifying and quantifying cell phenotypes. Genome Biol 7, R100. doi:10.1186/gb-2006-7-10-r100

Chiang, S.P.H., Cabrera, R.M., Segall, J.E., 2016. Tumor Cell Intravasation. A Review in the Theme: Cell and Molecular Processes in Cancer Metastasis. Am. J. Physiol., Cell Physiol. ajpcell.00238.2015. doi:10.1152/ajpcell.00238.2015

Dickinson, D.J., Pani, A.M., Heppert, J.K., Higgins, C.D., Goldstein, B., 2015. Streamlined Genome Engineering with a Self-Excising Drug Selection Cassette. Genetics 200, 1035–1049. doi:10.1534/genetics.115.178335

Dickinson, D.J., Ward, J.D., Reiner, D.J., Goldstein, B., 2013. Engineering the Caenorhabditis elegans genome using Cas9-triggered homologous recombination. Nat Meth 10, 1028–1034. doi:10.1038/nmeth.2641

Diogon, M., Wissler, F., Quintin, S., Nagamatsu, Y., Sookhareea, S., Landmann, F., Hutter, H., Vitale, N., Labouesse, M., 2007. The RhoGAP RGA-2 and LET-502/ROCK achieve a balance of actomyosin-dependent forces in C. elegans epidermis to control morphogenesis. 134, 2469–2479. doi:10.1242/dev.005074

Estes, K.A., Hanna-Rose, W., 2009. The anchor cell initiates dorsal lumen formation during C. elegans vulval tubulogenesis. Dev Biol 328, 297–304. doi:10.1016/j.ydbio.2009.01.034

Farooqui, S., Pellegrino, M.W., Rimann, I., Morf, M.K., Müller, L., Fröhli, E., Hajnal, A., 2012. Coordinated Lumen Contraction and Expansion during Vulval Tube Morphogenesis in Caenorhabditis elegans. 23, 494–506. doi:10.1016/j.devcel.2012.06.019

Gally, C., Wissler, F., Zahreddine, H., Quintin, S., Landmann, F., Labouesse, M., 2009. Myosin II regulation during C. elegans embryonic elongation: LET-502/ROCK, MRCK-1 and PAK-1, three kinases with different roles. 136, 3109–3119. doi:10.1242/dev.039412

Giuliani, C., Troglio, F., Bai, Z., Patel, F.B., Zucconi, A., Malabarba, M.G., Disanza, A., Stradal, T.B., Cassata, G., Confalonieri, S., Hardin, J.D., Soto, M.C., Grant, B.D., Scita, G., 2009. Requirements for F-BAR proteins TOCA-1 and TOCA-2 in actin dynamics and membrane trafficking during Caenorhabditis elegans oocyte growth and embryonic epidermal morphogenesis. PLoS Genet 5, e1000675. doi:10.1371/journal.pgen.1000675

Göbel, V., Barrett, P.L., Hall, D.H., Fleming, J.T., 2004. Lumen morphogenesis in C. elegans requires the membrane-cytoskeleton linker erm-1. 6, 865–873.

Haag, A., Gutierrez, P., Bühler, A., Walser, M., Yang, Q., Langouët, M., Kradolfer, D., Fröhli, E., Herrmann, C.J., Hajnal, A., Escobar-Restrepo, J.M., 2014. An In Vivo EGF Receptor Localization Screen in C. elegans Identifies the Ezrin Homolog ERM-1 as a Temporal Regulator of Signaling. PLoS Genet 10, e1004341. doi:10.1371/journal.pgen.1004341.s007

Heisenberg, C.-P., Bellaiche, Y., 2013. Forces in tissue morphogenesis and patterning. Cell 153, 948–962. doi:10.1016/j.cell.2013.05.008

Helker, C.S.M., Schuermann, A., Karpanen, T., Zeuschner, D., Belting, H.G., Affolter, M., Schulte-Merker, S., Herzog, W., 2013. The zebrafish common cardinal veins develop by a novel mechanism: lumen ensheathment 140, 2776–2786. doi:10.1242/dev.091876

Jaqaman, K., Loerke, D., Mettlen, M., Kuwata, H., Grinstein, S., Schmid, S.L., Danuser, G., 2008. Robust single-particle tracking in live-cell time-lapse sequences. Nat Meth 5, 695–702. doi:10.1038/nmeth.1237

Kamath, R.S., Fraser, A.G., Dong, Y., Poulin, G., Durbin, R., Gotta, M., Kanapin, A., Le Bot, N., Moreno, S., Sohrmann, M., Welchman, D.P., Zipperlen, P., Ahringer, J., 2003. Systematic functional analysis of the Caenorhabditis elegans genome using RNAi 421, 231–237. doi:10.1038/nature01278

Kondo, T., Hayashi, S., 2013. Mitotic cell rounding accelerates epithelial invagination. 494, 125–129. doi:10.1038/nature11792

Lundquist, E., Reddien, P., Hartwieg, E., Horvitz, H., Bargmann, C., 2001. Three C. elegans Rac proteins and several alternative Rac regulators control axon guidance, cell migration and apoptotic cell phagocytosis 128, 4475–4488.

Mayer, M., Depken, M., Bois, J.S., Jülicher, F., Grill, S.W., 2010. Anisotropies in cortical tension reveal the physical basis of polarizing cortical flows. 467, 617–621. doi:10.1038/nature09376

McMahon, H.T., Boucrot, E., 2015. Membrane curvature at a glance. J Cell Sci 128, 1065–1070. doi:10.1242/jcs.114454

Morf, M.K., Rimann, I., Alexander, M., Roy, P., Hajnal, A., 2013. The Caenorhabditis elegans homolog of the Opitz syndrome gene, madd-2/Mid1, regulates anchor cell invasion during vulval development. Dev Biol 374, 108–114. doi:10.1016/j.ydbio.2012.11.019

Nance, J., Lee, J.-Y., Goldstein, B., 2005. Gastrulation in C. elegans. WormBook 1–13. doi:10.1895/wormbook.1.23.1

Pellegrino, M.W., Farooqui, S., Fröhli, E., Rehrauer, H., Kaeser-Pebernard, S., Müller, F., Gasser, R.B., Hajnal, A., 2011. LIN-39 and the EGFR/RAS/MAPK pathway regulate C. elegans vulval morphogenesis via the VAB-23 zinc finger protein. 138, 4649–4660. doi:10.1242/dev.071951

Sawyer, J.M., Harrell, J.R., Shemer, G., Sullivan-Brown, J., Roh-Johnson, M., Goldstein, B., 2010. Apical constriction: A cell shape change that can drive morphogenesis. Dev Biol 341, 5–19. doi:10.1016/j.ydbio.2009.09.009

Schindler, A.J., Sherwood, D.R., 2012. Morphogenesis of the Caenorhabditis elegansvulva. Wiley Interdiscip Rev Dev Biol 2, 75–95. doi:10.1002/wdev.87

Sharma-Kishore, R., White, J.G., Southgate, E., Podbilewicz, B., 1999. Formation of the vulva in Caenorhabditis elegans: a paradigm for organogenesis. 126, 691–699.

Sherwood, D.R., Butler, J.A., Kramer, J.M., Sternberg, P.W., 2005. FOS-1 promotes basement-membrane removal during anchor-cell invasion in C. elegans. Cell 121, 951–962. doi:10.1016/j.cell.2005.03.031

Sherwood, D.R., Sternberg, P.W., 2003. Anchor cell invasion into the vulval epithelium in C. elegans. 5, 21–31.

Van Fürden, D., Johnson, K., Segbert, C., Bossinger, O., 2004. The C. elegans ezrin-radixin-moesin protein ERM-1 is necessary for apical junction remodelling and tubulogenesis in the intestine. Dev Biol 272, 262–276. doi:10.1016/j.ydbio.2004.05.012

Wang, Y.-C., Khan, Z., Kaschube, M., Wieschaus, E.F., 2012. Differential positioning of adherens junctions is associated with initiation of epithelial folding 484, 390–393. doi: 10.1038/nature10938

Ziel, J.W., Hagedorn, E.J., Audhya, A., Sherwood, D.R., 2009. UNC-6 (netrin) orients the invasive membrane of the anchor cell in C. elegans. Nat Cell Biol 11, 183–189. doi: 10.1038/ncb1825

Figure legends

Fig. 1. Sequential apical and lateral constriction of VulF during during lumen formation.

(A) Schematic drawing showing the cells with the seven vulval subfates, their positions before and during lumen formation and the directions of the division axes during the last round of cell divisions. (B) Nomarski images and (B') CED-10::GFP expression during vulval invagination in a wild-type larva. See also suppl. movie s1. For each time point, a mid-sagittal section is shown. The asterisks label the AC and the capital letters the VulF, VulE and VulD cells. (B'') Outlines of the vulval cells shown in (B') were generated with cell profiler (Carpenter et al., 2006) using a custom script. The dotted circles at 140 minutes outline the dividing VulE cells, which are out of focus in the plane shown. The dashed green and red arrows indicate the constriction of the apical and lateral VulF membranes, respectively. (C) 3D reconstructions of the AC labelled with the P_{cdh3}*>mCherry::PLCδ*^{PH} reporter in magenta and the apical junctions in the vulval cells labelled with the the AJM-1::GFP reporter in green. Each panel shows an individual larva during the distinct phases of lumen formation and corresponding approximately to the time points shown in (B): Before apical constriction (0 minute in (B)), during apical constriction (40 minutes), maximal apical constriction (130 minutes), VulE division (140 minutes) and completion of lateral constriction (200 minutes). (C') Shows ventral views of the apical junctions and the rearrangement of the cells after VulE division. (C'') are single z-sections showing one of the AC protrusions towards the apical VulF junctions. The arrowheads in (C) and (C'') point at the tips of the front protrusions, the arrows indicate the contralateral protrusions. The scale bars in (B') and (C'') are 5 µm. See also suppl. movies s2 and s3.

Fig. 2. Lateral VulF constriction requires AC invasion and basolateral actomyosin.

(A) Mid-sagittal sections from 4D time-lapse recordings of the CED-10::GFP reporter in the wild-type. (A') Outlines of the vulval cells shown in (A). (B,B') A *fos-1(ar105)* mutant, (C,C') wild-type after AC ablation at the Pn.pxx stage and (D,D') an *erm-1(tm677)* mutant exhibiting reduced basolateral actomyosin localization. The asterisks label the AC and the capital letters the VulF, VulE and VulD cells. The red cross in (C) indicates the position of the ablated AC corpse. The dashed green and red arrows in the cell outlines indicate the constriction of the apical and lateral VulF membranes, respectively. The scale bars in (C) and (D) are 5 µm. For quantification, see suppl. Fig. s1. See also suppl. movies s4 and s5.

Fig. 3. Localization of the F-actin during lumen formation.

(A-B') F-actin localization during vulval invagination in the wild-type detected with the LifeAct::GFP reporter (Farooqui et al., 2012). (A') 3D reconstruction of circular F-actin on the apical membrane of the VulF cells. A ventral view (xz-projection) of the region indicated in (A) with the yellow dashed box is shown. (B') 3D reconstruction of F-actin on the lateral VulF membrane. An anterior-posterior view (yz-projection) of the region indicated with the blue dashed box in (B) is shown. (C-D') Apical mis-localization of F-actin in *erm-1(tm677)* mutants. (C') 3D reconstruction of F-actin on the apical VulF membranes in the region indicated with the yellow dashed box in (C). (D') 3D reconstruction of the lateral VulF membrane in the region indicated with the blue dashed box in (D). The scale bars in all the figures are 5 µm. (E) Intensity plots of LifeAct::GFP along the lateral VulF membranes shown in the inset were generated using a custom script as described by (Morf et al., 2013) (see also materials and methods). The error bars in (E) indicate the standard deviations and the numbers in brackets the numbers of animals analyzed. See supl. Fig. s2 for the same analysis of *fos-1* and *unc-6* mutants.

Fig. 4. Recruitment of dynamic NMY-2 particles to AC-VulF contact sites.

(A) Time-lapse recording of an endogenous NMY-2::GFP reporter in green and the P_{cdh3}*>mCherry::PLCδ*^{PH} reporter in magenta during lateral VulF constriction. Two-channel z-stacks were recorded every 15 seconds and 3D reconstructions of selected time points are shown. See suppl. movie s6 for the complete dataset. For each time point, the left panel shows a lateral (xy) and the right panel an anterior-posterior (zy) projection. The arrowheads point at NMY-2::GFP particles approaching the AC contact site. (B) Box plots showing the normalized diffusion coefficients of NMY-2::GFP particles that were tracked in the different regions of wild-type and *unc-6(ev400)* mutants using the µ-track software (Jaqaman et al., 2008) as detailed in suppl. Fig. s2. The numbers in brackets indicate the number of particles tracked in a total of 11 wild-type and 9 *unc-6(ev400)* recordings. n.s., *, ** and *** indicate $p>0.05$, $p<0.05$, $p<0.01$ and $p<0.001$ in a two-tailed t-test. (C-C'') Localization of NMY-2::GFP in a wild-type larva at the Pn.pxx stage during vulval invagination. The yellow and blue dashed boxes in (C) indicate the regions used for the yz and xz projections shown in (C') and (C''), respectively. The yellow and blue arrow heads point at NMY-2::GFP at the AC-VulF contact site. (D-D'') Localization of NMY-2::GFP in an *erm-1* RNAi-treated larva, (E-E'') a *fos-1(ar105)* mutant and (F-F'') an *unc-6(ev400)* mutant at the Pn.px stage during vulval invagination. Note the loss of NMY-2::GFP accumulation at the AC-VulF contact sites in the xz-projections in (D''), (E'') and (F''). The scale bars in

(A), (F) and (F'') are 5 µm. (G) Intensity plots of NMY-2::GFP along the basal VulF membranes (see inset) were generated from wild-type and the indicated mutants as described by Morf et al. (2013) (see also materials and methods).

Fig. 5. Cortical tension measurements on the apical and lateral VulF membrane.

(A) Membrane recoil on the lateral VulF membrane after laser-cutting in a wild-type (top panels) and an *erm-1(tm677)* mutant larva (bottom panels) during the lateral constriction phase. The CED-10::GFP reporter was used to visualize the cell membranes. For each example, the animals are shown before (0 s) and in the first frame after the cut (0.2 s). The right panels show kymographs obtained from the recordings. The dashed red lines indicate the ventral and dorsal extent of the lateral membranes and the solid yellow lines the cutting regions. The yellow arrow in the kymographs indicates the time point of the cutting. See also suppl. movies s8 and s9 for examples. (B) Box plots showing the average recoil velocities after lateral membrane cutting measured as described in materials and methods. The numbers of animals analyzed are indicated by the numbers in brackets. The p-values obtained in a two-tailed t-test are indicated. (C) Apical VulF membrane recoil after laser-cutting in a wild-type (top panels) and an *erm-1(tm677)* mutant larva (bottom panels) during the apical constriction phase, as described above for (A). The scale bar in (C) is 5µm. (D) Box plots showing the average recoil velocities after apical membrane cutting.

Fig. 6. The TOCA proteins are required for actomyosin driven lateral VulF constriction.

(A-C) Nomarski images showing mid-sagittal sections of wild-type and (D-F) *toca-1(tm3334);toca-2(ng11)* double mutant larvae during vulval lumen formation. (A) and (D) show larvae stage before, (B) and (E) during and (C) and (F) after lateral VulF constriction. The dashed red lines in (C) and (F) indicate the length of the lateral VulF membranes, the arrowheads point at the gaps in the basal laminae formed by the invading AC and the asterisks label the positions of the AC nuclei. (G-G''') Localization of NMY-2::GFP in green and the P_{cdh3}*>mCherry::PLCδ^{PH}* reporter in magenta in *a* wild-type and (H-H''') a *toca-1(tm3334);toca-2(ng11)* double mutant larva at the Pn.px stage during vulval invagination. (G) and (H) are merged images of mCherry::PLCδ^{PH} and NMY-2::GFP and (G') and (H') show mid-sagittal sections of NMY-2::GFP alone. The dashed yellow and blue boxes in (G') and (H') indicate the regions shown in (G'') & (H'') as yz and in (G''') & (H''') as xy projections. The white, yellow and blue arrowheads in (G'') & (H'') point the AC-VulF contact sites in the different views. (I) Intensity plots of NMY-2::GFP along the basal

VulF membranes (see inset) were generated from wild-type and *toca-1(tm3334); toca-2(ng11)* double mutant larvae as described by Morf et al. (2013) (see also materials and methods). (J-K') Localization of the endogenous GFP::TOCA-1 reporter *zh110* in wild-type and (L-M') *unc-6(ev400)* mutants before (J,L) and after (K,M) lumen formation. The dashed blue boxes in the mid-sagittal sections indicate the regions selected for the xz projections shown in (J'-M') and the asterisks label the AC. The inset in (L) shows the displaced AC in the *unc-6(ev400)* mutant in a different focal plane. The scale bars are 5 µm.

Fig. 7. Cell shape changes during the different stages of lumen morphogenesis.
(A) Beginning of apical constriction, (B) completion of apical constriction and division of VulE, (C) beginning of lateral VulF constriction, and (D) lumen extension after complete lateral constriction. (C') The AC-induces the reorientation of the actomyosin network on the lateral VulF membranes via the TOCA protein complex. Cell shapes of the images shown in Fig. 1B' were traced using the cell profiler software package using a custom script (Carpenter et al., 2006). The basolateral membranes are shown in red and the apical membranes in blue. The division planes and directions of cell migrations are indicated with solid and dashed arrows, respectively. (E) Molecular pathway inducing lateral VulF constriction.

Inventory of supplementary material

Supplementary figures

Suppl. Fig. s1. (related to Figs. 1 & 2) Quantification of apical and lateral VulF membrane constriction during lumen morphogenesis.

Suppl. Fig. s2. (related to Fig. 4) Tracking of NMY-2::GFP particles on VulF membranes.

Suppl. Fig. s3. (related to Fig. 5) Quantification of F-actin distribution in the VulF cells of *fos-1(ar105)* and *unc-6(ev600)* mutants.

Suppl. Fig. s4. (related to Fig. 6) Loss of basal NMY-2::GFP recruitment after *mrck-1* RNAi and in dominant-negative *rho-1* mutants.

Supplementary tables

Suppl. Tab. s1. (related to Fig. 6) List of candidate genes screend for defects in vulval lumen morphogenesis and NMY-2::GFP recruitment.

Suppl. Tab. s2. (related to materials and methods) List of oligonucleotide primers used to generate the *gfp::toca-1* strain *zh110*.

Supplementary movies

Suppl. Movie s1. (related to Fig. 1) Cell shape changes during vulval invagination in a wild-type larva.

Suppl. Movie s2. (related to Fig. 1) Dynamic AC protrusions directed towards the AJs between the VulF cells.

Suppl. Movie s3. (related to Fig. 1) 3D reconstruction of the AC protrusions and the AJs in a wild-type larva after the completion of lateral constriction.

Suppl. Movie s4. (related to Fig. 2) Abnormal vulval invagination in an *erm-1(tm677)* mutant.

Suppl. Movie s5. (related to Fig. 2) 3D reconstruction of the AC protrusions and the AJs in an *erm-1(tm677)* mutant failing to undergo lateral VulF constriction.

Suppl. Movie s6. (related to Fig. 4) Movement of NMY-2::GFP particles along the lateral VulF cell membranes in a wild-type larva.

Suppl. Movie s7. (related to Fig. 4) Movement of NMY-2::GFP particles along the lateral VulF cell membranes in an *unc-6(ev600)* mutant larva.

Suppl. Movie s8. (related to Fig. 5) Cortical tension measurement on the lateral VulF membrane in a wild-type larva during lateral constriction.

Suppl. Movie s9. (related to Fig. 5) Cortical tension measurement on the lateral VulF membrane in an *erm-1(tm677)* mutant.

Supplementary figures

suppl. Figure s1

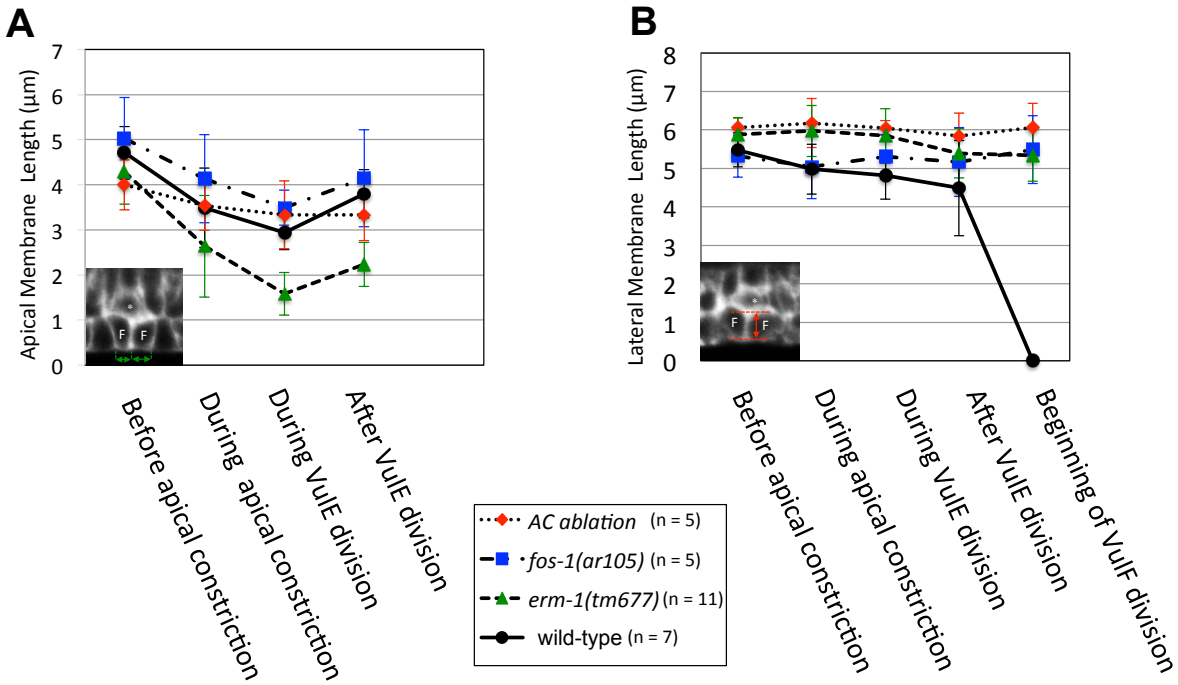

Suppl. Fig. s1. Quantification of apical and lateral VulF membrane constriction during lumen morphogenesis.

(A) Apical cell diameters and (B) lateral membrane lengths were measured at the indicated stages as shown in the insets and described in materials and methods. Error bars indicate the standard deviations and the numbers of animals analyzed are shown in the legend.

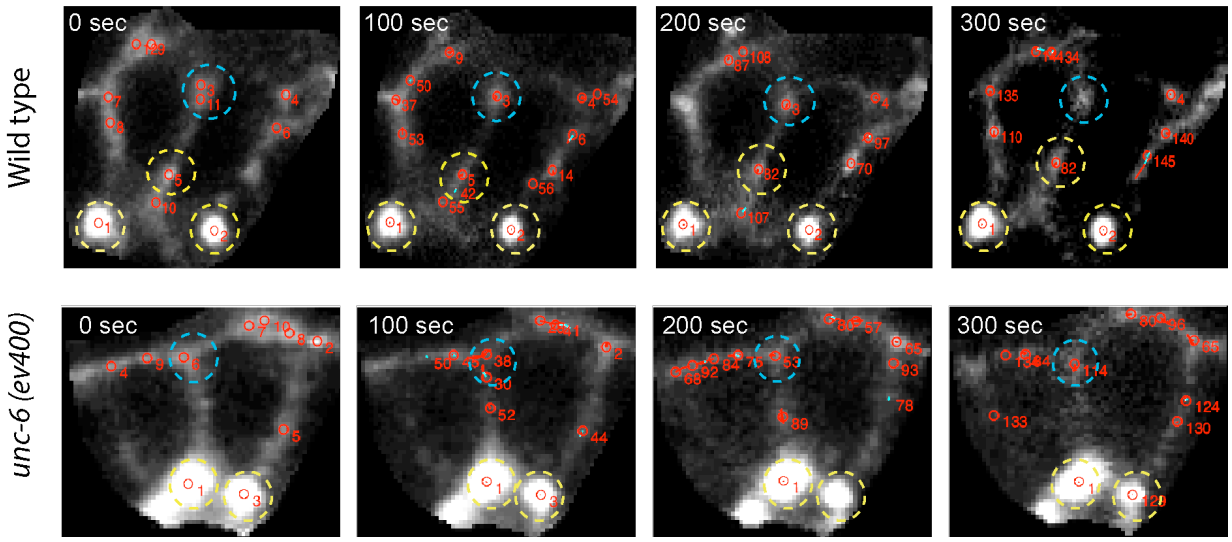

Suppl. Fig. s2. Tracking of NMY-2::GFP particles on VulF membranes of wild-type and *unc-6(ev600)* larvae.

Mid-sagittal confocal sections of the VulF cells during lateral constriction were recorded at a one-second frame rate. NMY-2::GFP punctae were tracked and analyzed using the μ-track software package (Jaqaman et al., 2008). NMY-2::GFP punctae were automatically selected using a Gaussian mixture model and tracked using the motion analysis module. For each tracked particle, the normalized diffusion coefficient was calculated as as a measure of its mobility. Tracked punctae are marked with red circles and numbered. The yellow dashed cycles indicate the apical junctions and the blue dashed cycles the region of the AC/VulF contact sites in wild-type larvae or the basal apex of lateral VulF membranes in *unc-6(ev400)* mutants.

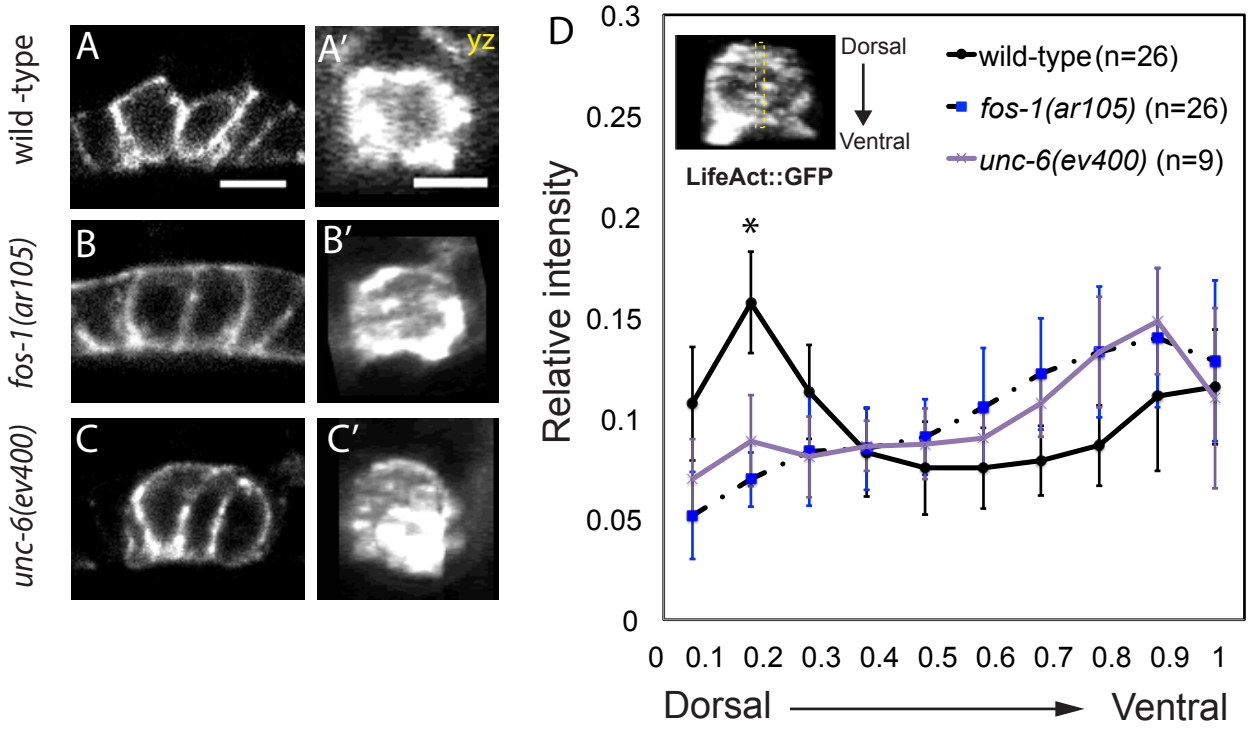

Suppl. Fig. s3. Quantification of F-actin distribution in the VulF cells of *fos-1(ar105)* and *unc-6(ev600)* mutants.

Localization of F-actin in (A,A') a wild-type, (B,B') a *fos-1(ar105)* and (C,C') an *unc-6(ev400)* mutant larva at the Pn.pxx stage. (A',B' and C') show YZ projections of the lateral VulF membranes. (D) Intensity plots of NMY-2::GFP along the lateral VulF lateral membranes as described in the legend to Fig. 3 E and in materials and methods.

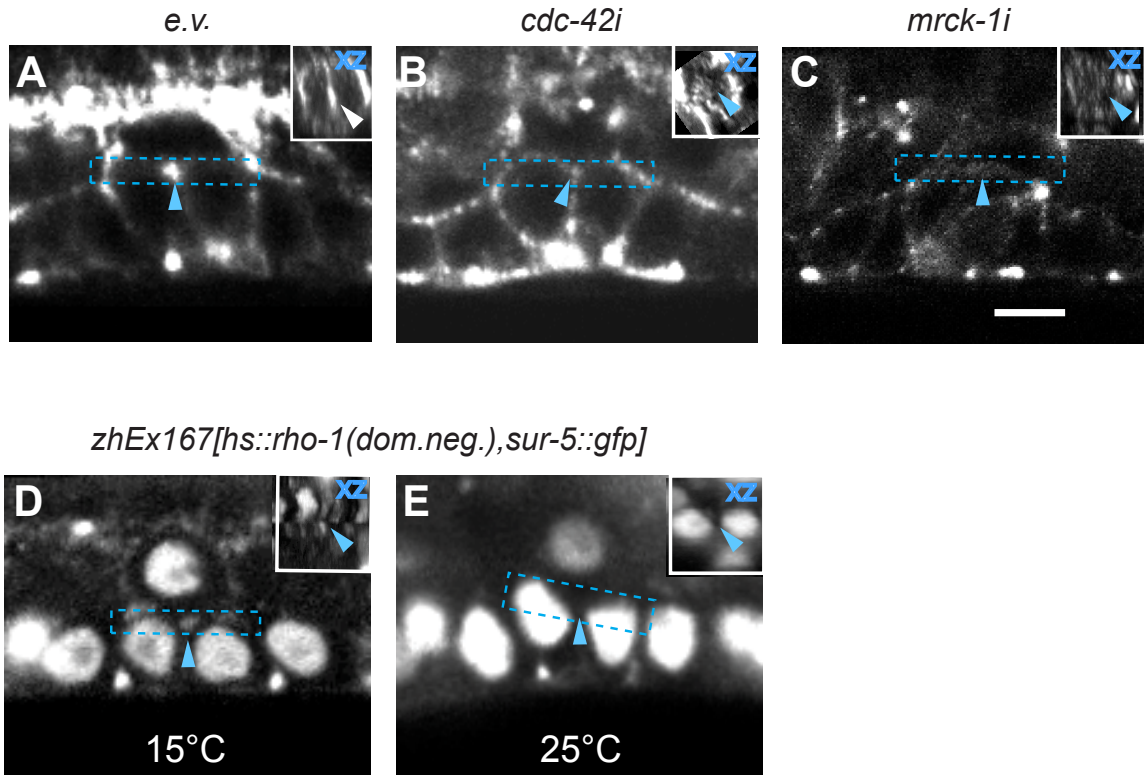

Suppl. Fig. s4. Loss of basal NMY-2::GFP recruitment after *mrck-1* RNAi and in *rho-1* dominant negative mutants.

NMY-2::GFP localization in (A) an empty vector treated control, (B) after *cdc-42* RNAi (58% affected, n=57) and (C) *mrck-1* RNAi (44% affected, n=25). (D) in a *zhEx167[hs::rho-1(dom.neg), sur-5::gfp]* (Canevascini et al., 2005) larva grown at 15°C and (E) a *zhEx167[hs::rho-1(dom.neg), sur-5::gfp]* larva grown at 25°C. In (D) and (E), the nuclei of the vulval and AC are labelled with SUR-5::GFP. The blue arrowheads point at the NMY-2::GFP signal at the VulF-AC contact sites. The insets in the upper-right corners show xz-projections of the basal membrane regions highlighted with the dashed blue boxes.

Gene name	allele or array used	RNAi clone	Brief description	Lumen shape	NMY-2 pattern
sdpn-1	-	F45E1.7	Bar-domain, synaptic dynamin binding protein	N*	N*
unc-57	*e406*	T04D1.3	endophilin A; Bar-domain protein	N	N
srgp-1	*ok300*	F12F6.5	Bar-domain, srGAP proteins	N	N
toca-1	*tm3334*	F09E10.8	Bar-domain, orthologs of human TRIP10, FNBP1L and FNBP1	**D[1]**	**D[1]**
toca-2	*ng11*	K08E3.3			
wve-1	*vc2706*	R06C1.3	WAVE protein for actin dynamic	D	N*
wsp-1	*gm324*	C07G1.4	Regulation of actin dynamic	D	N*
abi-1	*ok640*	B0336.6	Regulation of actin dynamic	N	N*
gex-3	-	F28D1.10	ligand of the small GTPase Rac1	D*	N*
arp-1	-	Y53F4B.22	ACTR1B	D*	N*
glit-1	-	F55D10.3	an ortholog of human TG (thyroglobulin)	N*	N*
par-6	-	T26E3.3	PDZ-domain-containing protein	D*	N*
mrck-1	-	K08B12.5	serine/threonine-protein kinase	**D***	**D***
let-502	-	C10H11.9	Rho-binding Ser/Thr kinase; of non-muscle myosin	D*	N*
dyn-1	*cx51*	C02C6.1	dynamin GTPase	N	N*
cdc-42	-	R07G3.1	Rho GTPase controls polarity of both individual cells	**D***	**D***
rho-1	*zhEx167 [hs::rho-1(d.neg.)]*	n.d.	Rho GTPase Regulation of actin and activation of non-muscle myosin	**D**	**D**

Suppl. Tab. s1. List of candidate genes screened for defects in vulval lumen morphogenesis and NMY-2::GFP recruitment.

N indicates a wild-type vulval lumen and/or NMY-2::GFP localization, D indicates a defect in lumen shape and/or NMY-2::GFP localization.

* Indicates that the phenotypes was detected only in RNAi treated animals.

[1]Only *toca-1; toca-2* double mutants exhibited the phenotypes, while the RNAi clones used simultaneously interfered with *toca-1* and *toca-2*.

Oligo description	Sequence
3xFLAG::toca-1 homology downstream arm for pJW1219	AGGATGACGATGACAAGAGAAATGATAGCTGTAGTTG GGACC
toca-1::plasmid homology downstream arm for pJW1219	aacagctatgaccatgttatATAGTGCGGCGCAAAACCCT
gfp::toca-1 homology upstream arm for pJW1219	CAATTCTTCTCCTTTACTCATTGTTCGCCGCTTCTTCAAAA G
plasmid::toca-1 homology upstream arm for pJW1219	acgacggccagtcgccggcaCCTGGTAACCGTGAACTATAC
sgRNA toca-1 forward	gagatgtcttGAATGAACGACAGTTGCAGTTGTTTAAGAGCTAT GCTGG
sgRNA toca-1 reverse	CTCTTAAACAACTGCAACTGTCGTTCATTCaagacatctcgcaat agg
sgRNA toca-1 forward (long)	cctcctattgcgagatgtcttGAATGAACGACAGTTGCAGTTGTTTAA GAGCTATGCTGG
sgRNA toca-1 reverse (long)	CCAGCATAGCTCTTAAACAACTGCAACTGTCGTTCATTCaa gacatctcgcaataggagg
sgRNA toca-1 for pJW1219 to be used with Q5 mutagenesis kit and primer sgRNA standard	AATGAACGACAGTTGCAGTTGTTTAAGAGCTATGCTGG
toca-1 promoter (outside homology arms of CRISPR)	CTCTTGGGAGCTACTTTTCG
toca-1 (outside homology arms of CRISPR)	CTGTGATCATGCCAGTATCAG

Suppl. Tab. s2. Oligonucleotide primers used to generate the gfp::*toca-1* strain *zh110*.

Figure 1

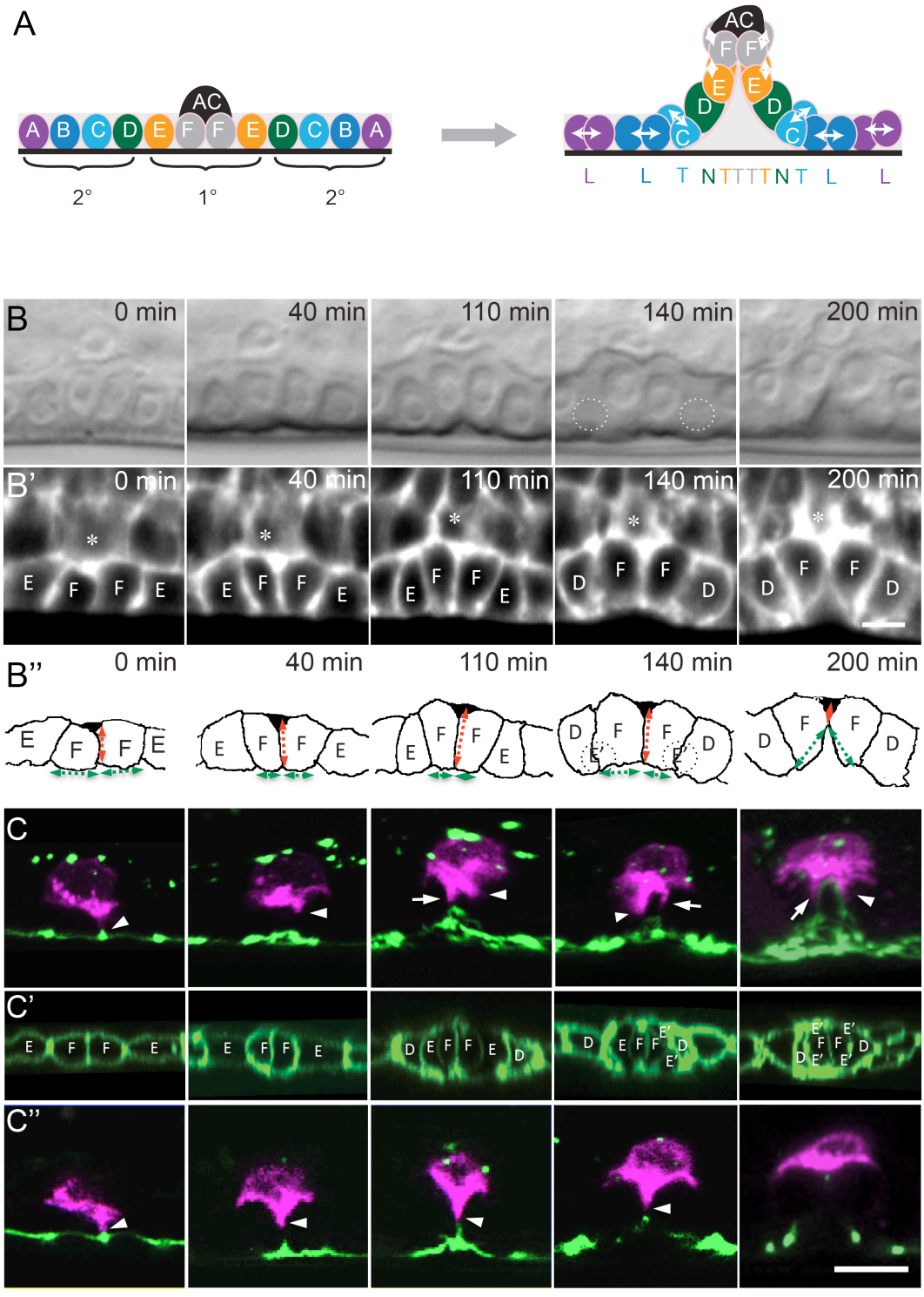
A
AC
A B C D E F F E D C B A
2° 1° 2°
AC
F F
E E
D D
C C
L L T NTTTTNT L L
B 0 min 40 min 110 min 140 min 200 min
B' 0 min 40 min 110 min 140 min 200 min
B'' 0 min 40 min 110 min 140 min 200 min
C
C'
C''

Figure 2

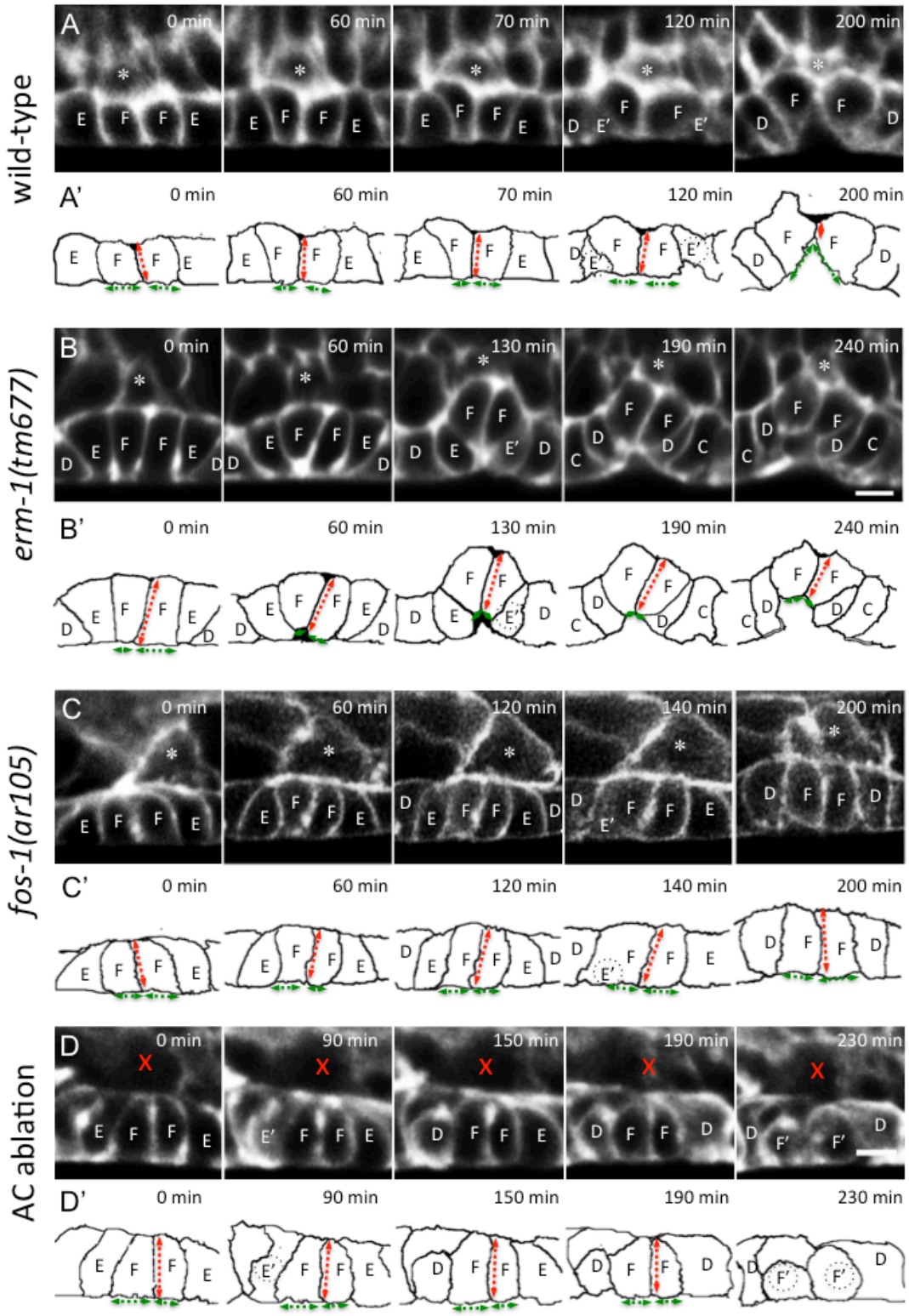
wild-type
A
0 min
60 min
70 min
120 min
200 min
A'
0 min
60 min
70 min
120 min
200 min
erm-1(tm677)
B
0 min
60 min
130 min
190 min
240 min
B'
0 min
60 min
130 min
190 min
240 min
fos-1(ar105)
C
0 min
60 min
120 min
140 min
200 min
C'
0 min
60 min
120 min
140 min
200 min
AC ablation
D
0 min
90 min
150 min
190 min
230 min
D'
0 min
90 min
150 min
190 min
230 min

Figure 3

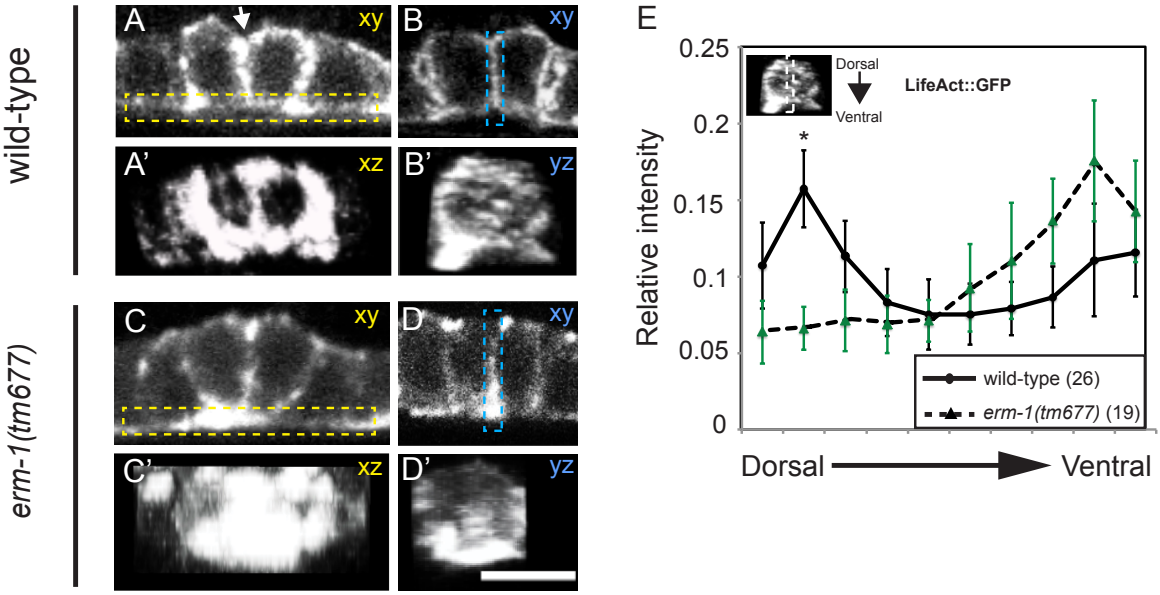
wild-type
erm-1(tm677)
A
xy
B
xy
A'
xz
B'
yz
C
xy
D
xy
C'
xz
D'
yz
E
0.25
0.2
0.15
0.1
0.05
0
Relative intensity
Dorsal
Ventral
LifeAct::GFP
*
wild-type (26)
erm-1(tm677) (19)
Dorsal
Ventral

Figure 4

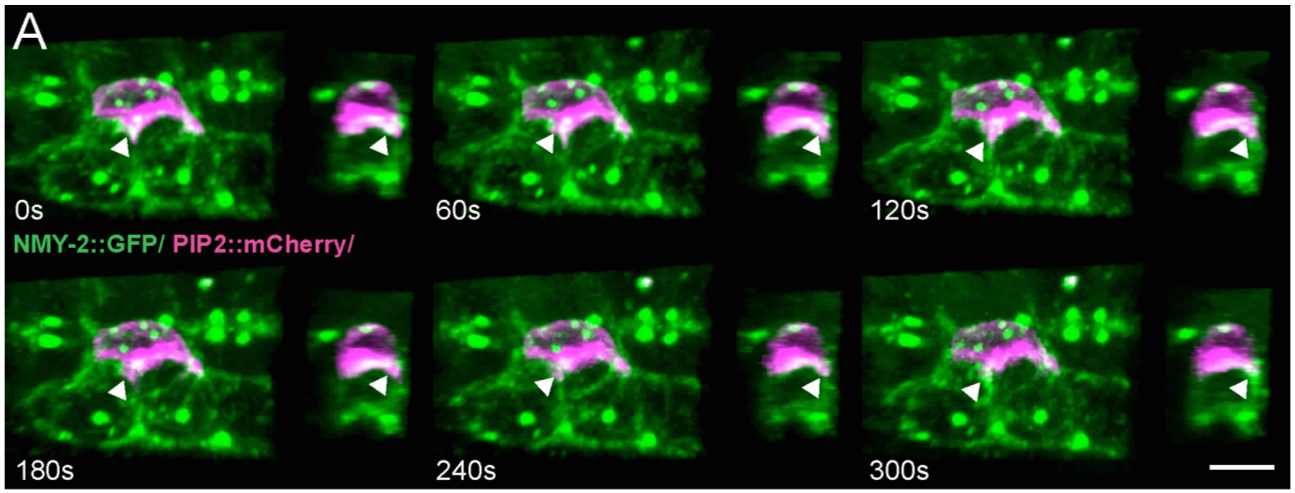
A
0s
60s
120s
NMY-2::GFP/ PIP2::mCherry/
180s
240s
300s

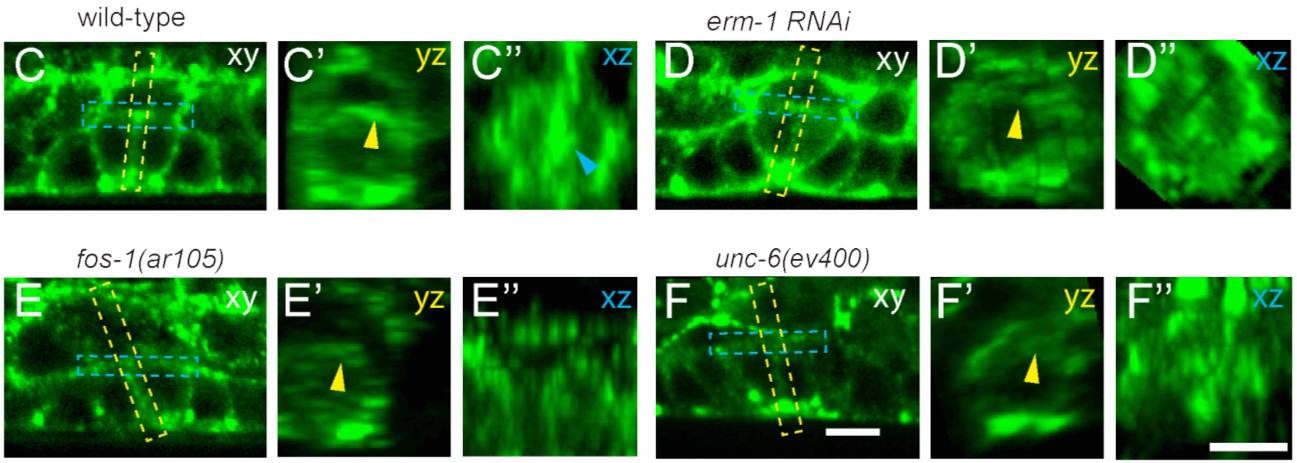
wild-type
C
xy
C'
yz
C''
xz
erm-1 RNAi
D
xy
D'
yz
D''
xz
fos-1(ar105)
E
xy
E'
yz
E''
xz
unc-6(ev400)
F
xy
F'
yz
F''
xz

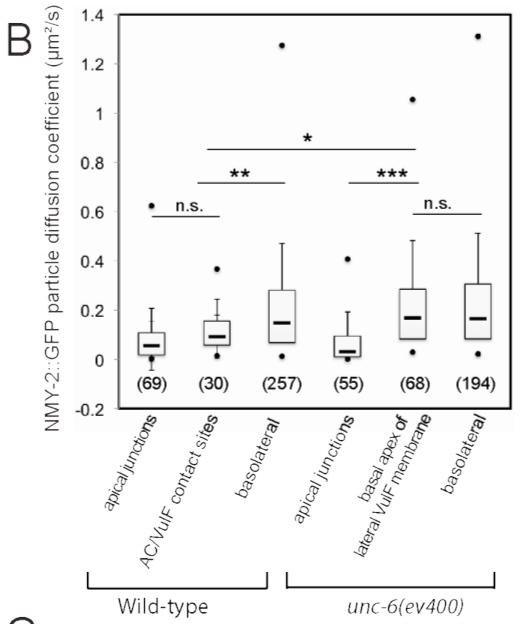
B
NMY-2::GFP particle diffusion coefficient (μm²/s)
1.4
1.2
1
0.8
0.6
0.4
0.2
0
-0.2
n.s.
**
*
***
n.s.
(69)
(30)
(257)
(55)
(68)
(194)
apical junctions
AC/VulF contact sites
basolateral
apical junctions
basal apex of lateral VulF membrane
basolateral
Wild-type
unc-6(ev400)

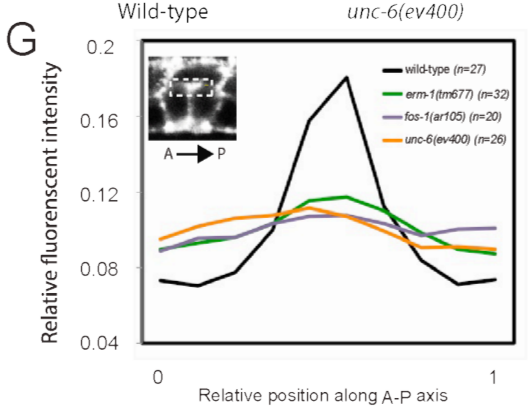
G
Relative fluorenscent intensity
0.2
0.16
0.12
0.08
0.04
A
P
wild-type (n=27)
erm-1(tm677) (n=32)
fos-1(ar105) (n=20)
unc-6(ev400) (n=26)
0
1
Relative position along A-P axis

Figure 5

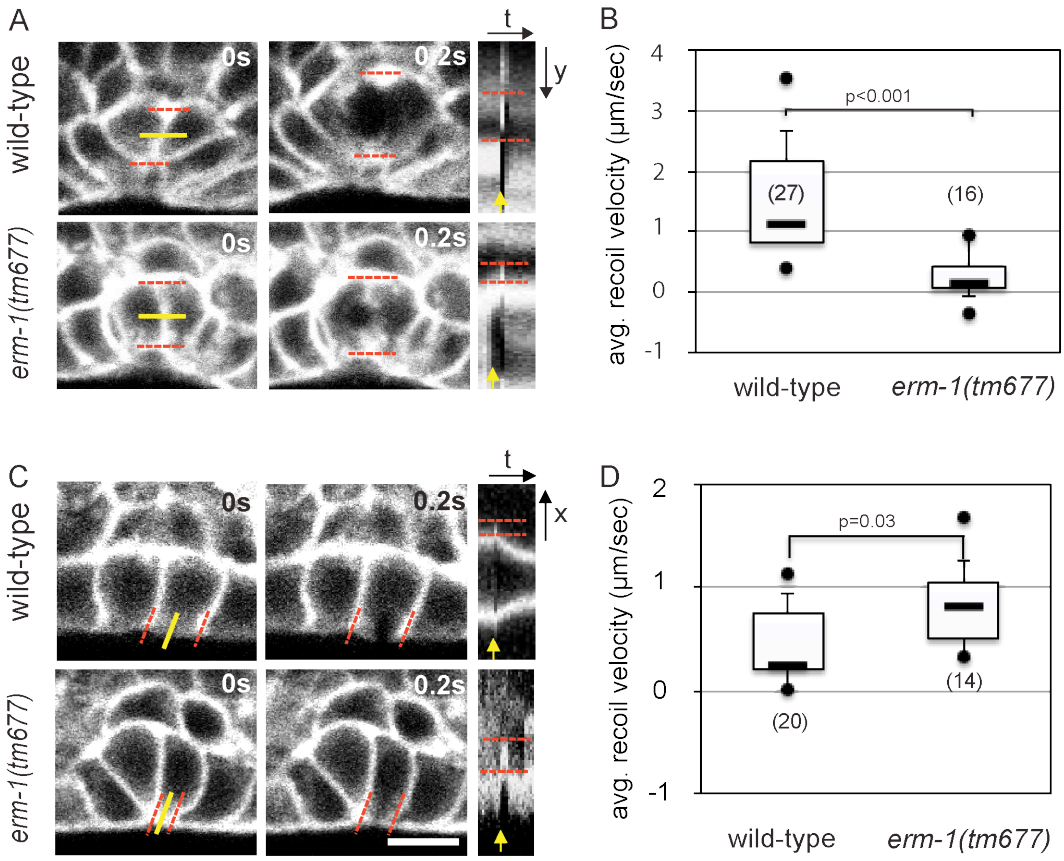
A
wild-type
erm-1(tm677)
0s
0.2s
t
y
B
avg. recoil velocity (µm/sec)
p<0.001
(27)
(16)
wild-type
erm-1(tm677)
C
wild-type
erm-1(tm677)
0s
0.2s
t
x
D
avg. recoil velocity (µm/sec)
p=0.03
(20)
(14)
wild-type
erm-1(tm677)

Figure 6

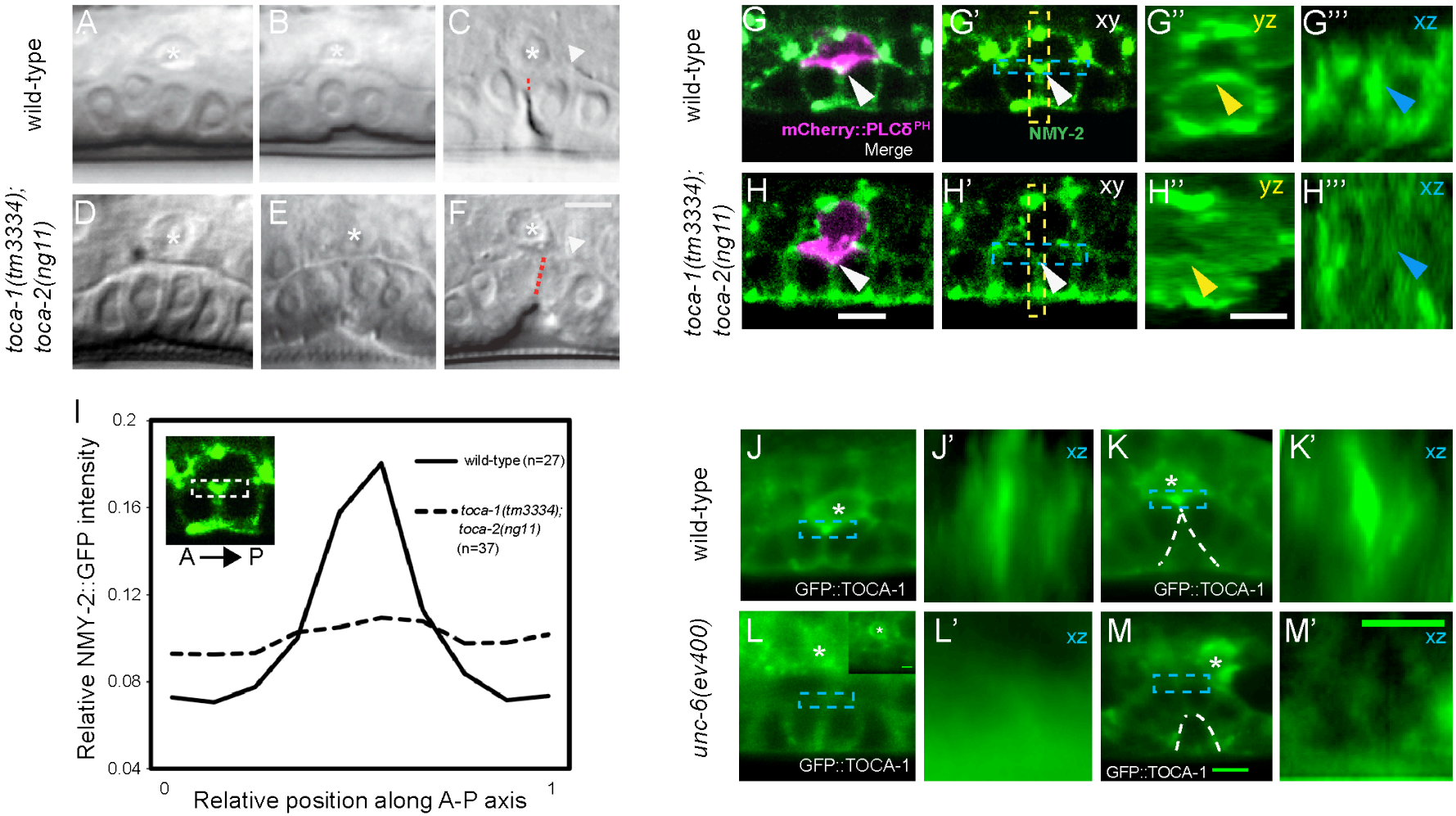
wild-type
toca-1(tm3334); toca-2(ng11)
A
B
C
D
E
F
G
G'
xy
G''
yz
G'''
xz
mCherry::PLCδ PH
Merge
NMY-2
H
H'
H''
H'''
I
Relative NMY-2::GFP intensity
0.2
0.16
0.12
0.08
0.04
0
1
Relative position along A-P axis
A → P
wild-type (n=27)
toca-1(tm3334); toca-2(ng11) (n=37)
J
J'
K
K'
GFP::TOCA-1
unc-6(ev400)
L
L'
M
M'

Figure 7

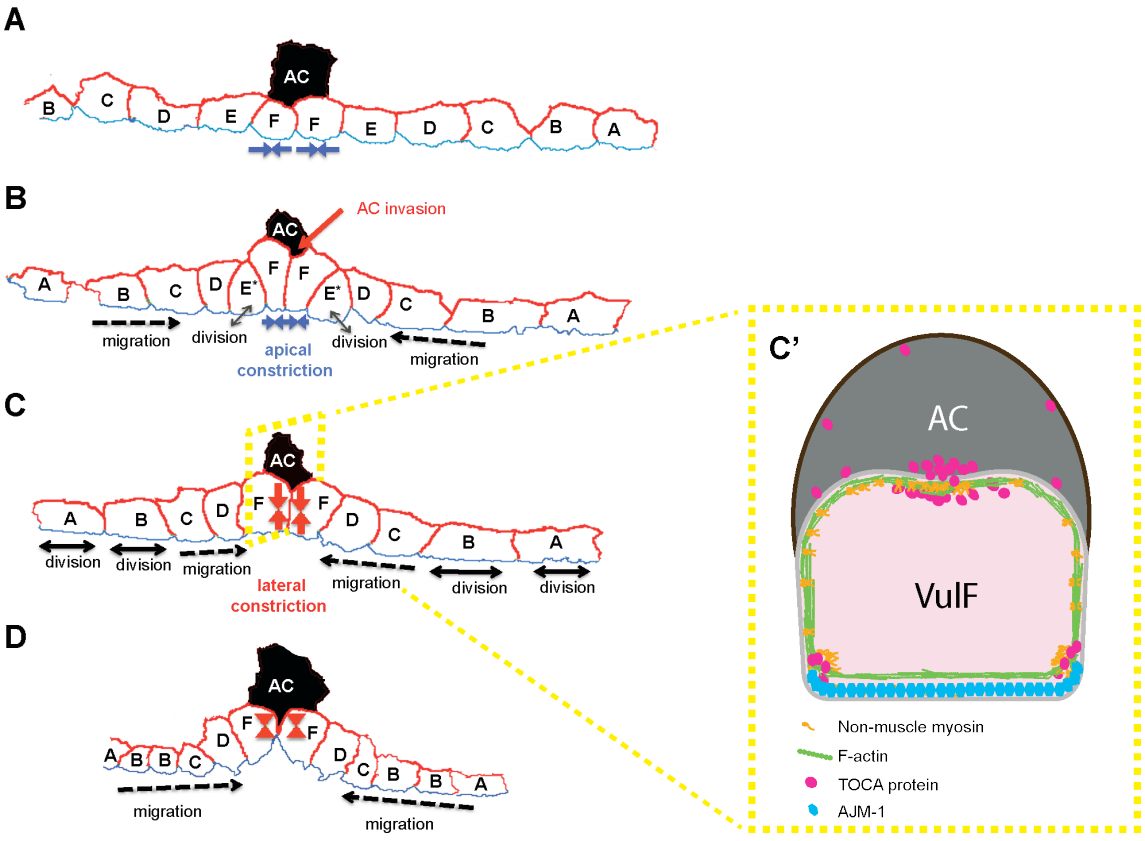
A
AC
B
C
D
E
F
F
E
D
C
B
A
B
AC invasion
AC
migration
division
apical constriction
division
migration
C
division
division
migration
lateral constriction
migration
division
division
D
migration
migration
C'
AC
VulF
Non-muscle myosin
F-actin
TOCA protein
AJM-1

E

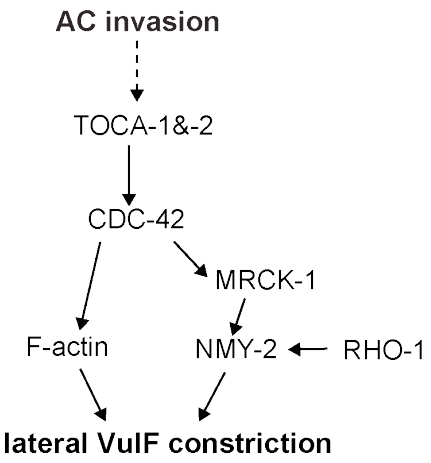
AC invasion
TOCA-1&-2
CDC-42
MRCK-1
F-actin
NMY-2
RHO-1
lateral VulF constriction

CHAPTER III. A screen for genes controlling *C. elegans* vulval morphogenesis

3.1. Introduction

For decades, morphogenetic studies have been essential to link the cell specific signaling to the morphogenetic behavior. Morphogenesis is the process when cells execute their adopted fate and participate in building the organ. To understand the principle behind morphogenesis is the basis to understand organ formation. The *C. elegans* egg-laying organ, the vulva, is an outstanding system to investigate the principles of organogenesis (Sharma-Kishore et al., 1999). Studies of vulval induction have led to a comprehensive molecular model of vulval fate specification, which is based on the concerted action of the conserved EGFR/RAS/MAPK, NOTCH and WNT signaling pathways (Schmid and Hajnal, 2015). However, whereas these signaling networks have been studied extensively in the context of vulval cell fate specification, the molecular mechanisms governing vulval morphogenesis are largely unknown (see Chapter I. for the detailed introduction of vulval morphogenesis).

Several defects of vulval development have been described. The phenotype of a Squashed vulva (Sqv) was identified in a genetic screen for vulval development (Herman et al., 1999). Other vulval defects include the egg-laying defect (Egl, retain developing embryos in the uterus), the protruding vulva (Pvl), multiple vulva (Muv), lack of a vulva (Vul) and defect in the connection of the vulva with the gonad (Cog) (Weinstein and Mendoza, 2013). Among these, the Muv and Vul phenotypes are typical defects that involve abnormal vulval induction. The Egl and Cog phenotypes often relate to the developmental defects of the neighboring tissue such as the gonad, the M cell, the uterine

pi cell and the neurons (Lesa, 2003). The Pvl phenotype can arise from a failure of specific morphogenetic events in any stage during vulval development (Haag et al., 2014).

In order to systematically identify genes required for vulval morphogenesis, I performed an RNA interference (RNAi) screen of all the genes that have been reported to result in a Pvl phenotype upon knockdown (Haag et al., 2014). The morphology of the vulva at the "Christmas tree" stage in mid L4 larvae, which is after the toroids have been formed but before the vulval eversion begins, was scored as the readout. Since most of the genes affecting cell fate specification have been identified previously, we focused on the candidate genes that are not required for cell fate acquisition or the vulval lineage but important at a later stage during cell fate execution (Inoue et al., 2004) .

3.2 Materials and Methods

3.2.1. General methods and strains

C. elegans strains were maintained at 20°C on standard nematode growth plates as described (Brenner, 1974). The wild-type strain was *C. elegans* Bristol, variety N2.

Strains used were as follows: **LGI**: *csnk-1(tm1762)/hT2[bli-4(e937) let(q782) qIs48] (I;III)*, *nmy-2(cp13[nmy-2::gfp+LoxP])(I)* (Dickinson et al., 2013)*, pfd-6(ok2785)/hT2[bli-4(e937) let(q782)qIs48](I;III), src-2(ok819), unc-59(e261), unc-59(e1005),* **LGII**: *cam-1(gm122), cap-2(ok1929)/mln1[mls14 dpy-10(e128)](II),cct-2(ok3438)/mln1[mls14 dpy-10(e128)](II), F10C1.5(ok1394), dpl-1(n2994), rrf-3(pk1426), ntl-2(ok974)/mln1[mls14 dpy-10(e128)](II), trr-1(n3630)/ mln1[mls14 dpy-10(e128)](II),* **LGIII**: *rsa-2(tm3051), sel-8(ok387)/mT1 [dpy-10(e128)](II;III),* **LGIV**: arf-3(tm1877)/*nT1[qIs51](IV;V), C08F8.1(gk526)IV/nT1[qIs51] (IV;V),C43G2.2(ok2731)*, cogc-2(tm3457)/*nT1[qIs51](IV;V), nhr-67(ok631)/nT1[qIs51] (IV;V), npr-3(tm1583),* **LGV***: rde-1(ne219), fos-1(ar105)/nT1[qIs51] (IV;V), rfp-1(ok572)/eT1*

(III,V) LGX: sem-5(cs15). Extrachromosomal and integrated arrays: *swIs79[ajm-1::gfp, P_{scm-1}::gfp, unc-119(+)]* (Diogon et al., 2007).

3.2.2. Microcopy and image analysis

Fluorescent images were obtained using an Olympus BX61 wide-field microscope equipped with an X-light spinning disc confocal system using a 60x Plan Apo lens and a Hamamatsu Orca CCD camera. For 3D reconstructions, z-stacks with a step size of 0.5 µm were recorded with an Olympus FV1000 confocal microscope. The animals were mounted on 5% agarose pads containing 0.5 mM tetramisole. Images were processed using the Huygens Deconvolution platform (SVI) to increase the signal to noise ratio and analyzed using Fiji (ImageJ (NIH)) or Imaris (Bit-plane) software.

3.2.3. RNA interference

RNA interference (RNAi) was performed using the feeding method as described (Kamath et al., 2001). Synchronized L1 worms were transferred to nematode growth plates containing 3 mM IPTG and 50 ng/ml ampicillin seeded with the desired RNAi bacteria and allowed to grow for 5-7 days at 20°C, after which the surviving F1 progeny was analyzed.

3.2.4 GO term and quantification

The GO clustering was analyzed on the website of David bioinformatic resources (version 6.7) (https://david.ncifcrf.gov). The list of gene ID was uploaded, using the identifier of ENSEMBL_GENE_ID and the list type of Gene list. The *C. elegans* genome was automatically chosen as the background list for comparing. After the analysis of Functional Annotation Clustering, an enrichment score more than 1.2 (enrichment score=1.3 is close to P-value=0.05) was chosen as a threshold as demonstrated in Table 3.2.

3.3. Results

3.3.1. Classification of phenotypes

93 out of 467 screened genes demonstrated vulval morphogenetic defects. One third of the RNAi clones in the Pvl library caused a lethal phenotype and therefore, we were not able to observe their vulval phenotypes at L3 or L4 stages. 25 genes with published function in vulval development were found in the screen, which increased the reliability of our screen (Table 3.1).

We classified the phenotypes into five groups based on the morphogenetic structure of the adherens junctions that was marked by the translational reporter AJM-1::GFP (Fig. 3.1) (Koppen et al., 2001). At the “Christmas tree” stage, three finger-like structures are formed in a symmetric fashion on each side of the ventral lumen and represent the acto-myosin contraction that attaches to the secondary toroid junctions (Fig.3.1 A) (Farooqui et al., 2012). The AC fuses with the utse and forms two layers of membrane upon the opened dorsal lumen (Fig.3.1 A) (Rimann and Hajnal, 2007). During this stage, The apical junctions within the VulF, VulB1 and VulB2 toroids do not fuse and remain in the center of the vulva, where the vulval cells from two sides contact with each other (Fig. 3.1 A’). The AJM-1 reporter expression reveals eight junction dots on each side between the seven toroids and the VulF-utse junction (Fig. 3.1 A’’).

The defect of dorsal lumen expansion is defined by a closed or narrowed dorsal lumen, which has been reported to be caused by the failure of AC invasion (Fig.3.1 B-D’’) (Sherwood et al., 2005). 27 RNAi clones showed such a phenotype of dorsal expansion defect.

RNAi knockdown of 38 genes showed defects in toroid matching. Here, cells do not meet in the vulval middle line, but form mismatched toroids or self-toroids (Fig.3.1. E’,F’ and G’).

The number and arrangement of toroidal junction dots are abnormal and asymmetric in the mid sagittal section (Fig.3.1. E'', F'' and G'').

In circumferential extension defects, few secondary cells from one or both sides cannot migrate to the vulval center and therefore do not extend protrusions circumferentially to meet the partner cell from the other side. In some cases, the vulval cells that are more distant invaginate independently and form a smaller lumen next to the main vulval lumen (Fig.3.1. H-J''). 22 RNAi clones caused such a circumferential extension defect.

The phenotype in which the ventral lumen is remarkably wider or irregular while the number and the array of toroidal junctions are normal has been defined as "defects of ventral contraction" (Fig.3.1. K-L'') (Farooqui et al., 2012). The ventral finger-like structures that can be observed in wild-type are not found in the ventral-contraction defective animals (Fig.3.1. A, K and L). 31 RNAi clones showed the phenotypes of ventral contraction defect. A number of these candidate genes directly links to the regulation of acto-myosin contraction.

The discontinuous AJM-1 pattern is associated with the loss of apical junction integrity (Koppen et al., 2001). We term the phenotype caused by 18 RNAi clones with significantly increased AJM-1::GFP aggregates as "the defect of junction formation".

In total, 39 RNAi clones showed multiple phenotypes, which might be due to the linked development of the events mentioned above. For example, knockdown of nine genes caused both toroid matching and circumferential extension defects while 25 RNAi clones led to both abnormal dorsal expansion and disrupted ventral contraction. The abnormal junction frequently comes along with further defects including changes in vulval induction, which is caused by errors in cell fate acquisition but not in cell morphogenesis. Therefore, although some of the RNAi clones showed the junctional formation defect with other types of vulval morphogenesis phenotype such as the dorsal expansion defect, we decided to

group the RNAi clones with several junction formation failures independently (Fig.3.1 M-O'' and Table 3.1).

3.3.2 Enriched GO terms found to control vulval toroid formation.

We have identified 93 RNAi clones that result in vulval morphogenesis defect and can be classified into five groups based on their morphogenetic phenotypes (Table 3.1). By comparing our candidate genes with the *C. elegans* genome as background, several significantly enriched GO clusters have been found. 35 out of 93 genes are involved in tissue morphogenesis and 12 genes are in the regulation of vulval development, validating efficiency of our screen. We found three typical terms related to tissue morphogenesis: the "cell polarity establishment", the "cytoskeleton organization" and the "cell migration". Interestingly, the regulators of actin and the adherens junction proteins that usually are important for morphogenesis were not enriched in the GO cluster in the branch of the cytoskeleton organization or other related GO terms (data not shown). Few groups with slightly lower significance (0.1>P>0.05) regarding enrichment were still selected due to their known function in morphogenesis (Table 3.2.). For example, five genes from the cytoskeleton group are microtubule related cytoskeleton genes and three unfold-protein-binding genes that encode chaperones for microtubule maturation (Table 3.2). In addition, three genes of the Ubiquitin-like protein (Ubl) conjugation pathway have also been indicated in vulval morphogenesis (data not shown).

3.3.3. Verification of candidate genes by mutant analysis

We are interested in genes that are particularly involved in tubular organ morphogenesis. The toroid matching and circumferential extension that resemble the morphogenetic processes during neuron tubule formation and gastrulation are important for the vulval tubule formation and are thus the most interesting phenotypes for us (see more

introduction of toroid matching in Chapter IV). The dorsal expansion defect that is associated with a failure in AC invasion was less considered in this project. The mechanism behind the mutant phenotypes of the dorsal expansion and ventral contraction has been described in a previous study (Farooqui et al., 2012) and was thus not further investigated in this project. The transcriptional factors that often regulate cell fate specification were excluded. In addition, we expect the receptors of signaling pathways, the cytoskeleton proteins and the adherens junction proteins, which contribute to toroids formation.

We term the phenotypes with more than three aspects, or phenotypes with more than 40% penetrance as “strong phenotypes” in vulval morphogenesis. Eventually we chose 26 candidates with the “strong phenotypes”, or with the unique phenotype and interesting protein function. 23 mutant strains of 21 genes were available from the CGC or the Mitani worm strain library and were crossed with AJM-1::GFP or DLG-1::RFP reporters for vulval phenotype dissection (Table 3.3.). Five candidate genes, *uba-2, C18E9.4, ado-2, kbp-1* and *pad-1* were not analyzed due to lack of mutants in the current worm strain libraries.

As shown in table 3.3., most of the mutant strains either exhibited wild-type vulval morphogenesis or the homozygous mutant animals died prior to the “Christmas tree” stage. The tissue specific knock-out of these genes will improve the analysis of their function during vulval morphogenesis. Furthermore, it would be very interesting to investigate the embryonic morphogenesis in those mutants.

3.3.4. Candidate genes controlling microtubule growth during vulval morphogenesis.

One group of candidates indicates the three genes encoding the Chaperone proteins, *pfd-1*, *pfd-6* and the *cct-2*. Prefoldin is a subunit of heteromeric prefoldin complex that chaperones α-tubulin and β-tubulin via direct binding until the delivery of the full-length tubulin proteins to Chaperonin (CCT) is finished (Lundin et al., 2008). In *C. elegans*, Pfd-

mediated tubulin biogenesis is essential for cell division and migration (Lundin et al., 2008). The knockdown of *pfd-1* by RNAi shows a specific defect of primary vulval lumen formation (defects in dorsal expansion and toroid matching) while *pfd-6* RNAi leads to abnormal cell junctions in the secondary lumen (toroid matching) (Fig.3.2. A-C''). The different *pfd-1* and *pfd-6* RNAi results suggest functions of PFD proteins in tissue-specific regulation of microtubule during vulval morphogenesis. The *cct-2* RNAi experiment shows general toroid matching defects (toroid matching, dorsal expansion, ventral contraction) (Fig.3.2. D-D''). However, maternally rescued *pfd-1*, *pfd-6* and *cct-2* animals could not reach the vulval morphogenesis phase at the L3 stage. Nevertheless, since the three proteins (PFD-1, PFD-6 and CCT-2) function in the same chaperone pathway regulating tubulin (Lundin et al., 2008), we speculate that a proper tissue specific control of microtubules is required during vulval morphogenesis. It would be worth analyzing the vulval tissue-specific knock-out phenotypes of these genes.

3.3.5 Septins regulate the toroid formation of the primary lumen but not the secondary lumen.

One of the candidate gene whose mutant phenotype was detected both by RNAi and in mutants was *unc-59* that encodes the Septin protein. The Septin proteins are the fourth type of proteins that form filaments besides actin, tubulin and intermediate filament proteins in eukayotic cells (Beise and Trimble, 2012). Knockout or knockdown of the other filament-structure proteins generate phenotypes that are either lethal or lead to a complete failure of lumen formation. However, in the *unc-59* RNAi treated worms we found the disordered primary vulval toroids without AC invasion defect with a penetrance of 80% (8 out of 10). The specific phenotype in the primary lumen motivates us to analyze the role of *septins* in vulval morphogenesis (see in Chapter 4).

3.4 Discussion and outlook

3.4.1. The advancement and further potentia of our screen

In the screen for genes affecting vulval morphogenesis, we found 93 candidates. Previous RNAi screens in the study of vulval development have been focused on cell patterning rather than morphogenesis (Fernandes and Sternberg, 2007). The result of an EMS to detect defects in vulval developmental suggest that the cell matrix is important. However, the phenotypes of the vulval cell during morphogenesis were not analyzed (Herman et al., 1999).

Our screen is more advanced for the following reasons: 1) We used the Pvl library to pre-selected the genes reported with Pvl phenotype that likely include all the genes essential for vulval morphogenesis, since the Pvl phenotype can be caused by the defect at any stage during vulval development; 2)The spinning-disc microscopy provides high-resolution imaging, which allows us to separate the defects of vulval morphogenesis in more precise groups.

Some of our candidate genes show a conserved function in morphogenesis. For example, the *wve-1* controls actin filament polymerization and *septin* modulates membrane structure, both of which are important for the tissue morphogenesis through the animal kingdom (Table 3.1.) (Beise and Trimble, 2012; Sullivan-Brown et al., 2016).

We have studied the selected candidate genes, and the other genes in the Pvl list are also worth further investigating. This is because the genes that are crucial for embryonic development or reproductivity might be missed in our screen due to their lethal or sterile RNAi phenotypes. For example, the adherens junction proteins that are important for morphogenesis were not in our candidate list. To further identify the contribution of our 227 candidate genes whose RNAi knockdown caused lethal or sterile phenotype, a tissue specific knock-down or analysis of the P0 generations should be performed. It would be

very interesting to look at the gastrulation of these embryonic lethal genes for their general function in morphogenesis.

Apart from the morphogenetic events during vulval tube formation till the “Christmas tree” stage, the vulval system has further potential for the study of organogenesis. The last step of vulval morphogenesis is the vulval eversion, during which the inner face of vulval lumen is turned towards outside of the worm body. Such a fierce morphologic event involving the collaboration of the neighboring muscle cells. The underlying mechanism of vulval eversion is largely unknown. The RNAi clones that lead to a normal vulval lumen at L4 stage might have caused a Pvl phenotype by the failure of the vulval eversion. The description of the wild-type vulval eversion by 4D recording and the proper readout approach are required to study the vulval eversion.

3.4.2. The candidates that could not be analyze with mutants

The phenotypes we found in the screen could not always be verified by mutants since the available mutant allele is not null allele, knock-down efficiency is unknown, or the knock-out of the protein by the mutant triggers some redundant pathways (Table 3.3.).

In addition, there are no mutant strains for five interesting candidate genes. The RNAi of the *uba-2* gene that encodes one of the Ubiquitin ligase constantly, reproductively shows dorsal expansion defect from different screens. Yet the UBA-2 function in AC invasion or basal laminae breaching has not been described (Matus et al., 2010), possibly due to lack of appropriate mutant. *C18E9.4* and *pad-1* are two conserved genes that show strong and unique phenotype of toroid matching defect upon RNAi knockdown. The *C. elegans* PAD-1 has been reported with strong Pvl phenotype upon knockdown and its human homolog is the Down-syndrome related protein (Guipponi et al., 2000). The animals treated with *aco-2* RNAi showed strong and multiple defects. In addition, the *aco-2* has been implicated in regulating vulval morphogenesis. Knockdown of *kbp-1* by RNAi demonstrated a strong and

unique phenotype in toroid matching. The KBP-1 protein has been reported to be involved in body morphogenesis (Sönnichsen et al., 2005).

Thanks to the advancement in biotechnology, we can use the CRISPR/Cas9 technique to create appropriate knockout mutants to validate the interesting RNAi phenotypes, where no mutants exist so far.

3.4.3 A reporter of microtubule dynamics

The RNAi phenotypes of the three tubulin chaperone genes motivated us to analyze the regulation and dynamics of microtubules in toroid formation. For the visualization of microtubules using high-resolution microscopy, we constructed a reporter for microtubule dynamics. *ebp-2* encodes the microtubule plus end binding protein in *C. elegans* and was chosen for this purpose (Kozlowski et al., 2007). We used the *dlg-1* promoter to drive *ebp-2* expression in epithelial cells, and fused it to a bright monomeric green fluorescent protein (mNeonGreen) at the N-terminus. Since the plus end of growing microtubule is highly dynamic at the front edge of migrating cells, this reporter allows us to look at microtubules during toroid formation. Moreover, we expect to observe two dots at the migrating front from two sides, moving towards the vulval midline. Such an approach will be more direct observing the “matching” of vulval cells during toroid formation and monitor the behavior of microtubules. Several ex-chromosomal arrays of the mNeonGreen::EBP-2 showed a variable expression pattern. We have not yet established an appropriate MOSSCI line. In future, it would be worth constructing an endogenous reporter using CRISPR/Cas9 technique.

3.5 Reference

Beise, N., and Trimble, W. (2012). Septins at a glance. Journal of Cell Science *124*, 4141–4146.

Brenner, S. (1974). The genetics of Caenorhabditis elegans. Genetics *77*, 71–94.

Dickinson, D.J., Ward, J.D., Reiner, D.J., and Goldstein, B. Engineering the Caenorhabditis elegans genome using Cas9-triggered homologous recombination. Nature Methods *10*, 1028–1034.

Diogon, M., Wissler, F., Quintin, S., Nagamatsu, Y., Sookhareea, S., Landmann, F., Hutter, H., Vitale, N., and Labouesse, M. (2007). The RhoGAP RGA-2 and LET-502/ROCK achieve a balance of actomyosin-dependent forces in *C. elegans* epidermis to control morphogenesis. Development *134*, 2469–2479.

Farooqui, S., Pellegrino, M.W., Rimann, I., Morf, M.K., Muller, L., Frohli, E., and Hajnal, A. (2012). Coordinated lumen contraction and expansion during vulval tube morphogenesis in Caenorhabditis elegans. Developmental Cell *23*, 494–506.

Fernandes, J.S., and Sternberg, P.W. (2007). The tailless Ortholog nhr-67 Regulates Patterning of Gene Expression and Morphogenesis in the *C. elegans* Vulva. PLoS Genet *3*, e69.

Guipponi, M., Brunschwig, K., Chamoun, Z., Scott, H.S., Shibuya, K., Kudoh, J., Delezoide, A.-L., Samadi, El, S., Chettouh, Z., Rossier, C., et al. (2000). C21orf5, a Novel Human Chromosome 21 Gene, Has a Caenorhabditis elegans Ortholog (pad-1) Required for Embryonic Patterning. Genomics *68*, 30–40.

Haag, A., Gutierrez, P., Bühler, A., Walser, M., Yang, Q., Langouët, M., Kradolfer, D., Frohli, E., Herrmann, C.J., Hajnal, A., Escobar-Restrepo, J.M., 2014. An In Vivo EGF

Receptor Localization Screen in *C. elegans* Identifies the Ezrin Homolog ERM-1 as a Temporal Regulator of Signaling. PLoS Genet 10, e1004341. doi:10.1371/journal.pgen.1004341.s007

Herman, T., Hartwieg, E., and Horvitz, H.R. (1999). sqv mutants of Caenorhabditis elegans are defective in vulval epithelial invagination. Proc Natl Acad Sci U S A *96*, 968–973.

Inoue, T., Oz, H.S., Wiland, D., Gharib, S., Deshpande, R., Hill, R.J., Katz, W.S., and Sternberg, P.W. (2004). *C. elegans* LIN-18 is a Ryk ortholog and functions in parallel to LIN-17/Frizzled in WNT signaling. Cell *118*, 795–806.

Kamath, R.S., Martinez-Campos, M., Zipperlen, P., Fraser, A.G., and Ahringer, J. (2001). Effectiveness of specific RNA-mediated interference through ingested double-stranded RNA in Caenorhabditis elegans. Genome Biol *2*, RESEARCH0002.

Koppen, M., Simske, J.S., Sims, P.A., Firestein, B.L., Hall, D.H., Radice, A.D., Rongo, C., and Hardin, J.D. (2001). Cooperative regulation of AJM-1 controls junctional integrity in Caenorhabditis elegans epithelia. Nat Cell Biol *3*, 983–991.

Kozlowski, C., Srayko, M., and Nedelec, F. (2007). Cortical microtubule contacts position the spindle in *C. elegans* embryos. Cell *129*, 499–510.

Lesa, G.M. (2003). Long chain polyunsaturated fatty acids are required for efficient neurotransmission in *C. elegan*s. Journal of Cell Science *116*, 4965–4975.

Lundin, V.F., Srayko, M., Hyman, A.A., and Leroux, M.R. (2008). Efficient chaperone-mediated tubulin biogenesis is essential for cell division and cell migration in *C. elegans*. Developmental Biology *313*, 320–334.

Matus, D.Q., Li, X.Y., Durbin, S., Agarwal, D., Chi, Q., Weiss, S.J., and Sherwood, D.R. (2010). In Vivo Identification of Regulators of Cell Invasion Across Basement Membranes. Science Signaling *3*, ra35–ra35.

Rimann, I., and Hajnal, A. (2007). Regulation of anchor cell invasion and uterine cell fates by the egl-43 Evi-1 proto-oncogene in Caenorhabditis elegans. Developmental Biology *308*, 187–195.

Schmid, T., Hajnal, A., 2015. ScienceDirectSignal transduction during C. elegans vulval development: a NeverEnding story. Current Opinion in Genetics & Development 32, 1–9. doi:10.1016/j.gde.2015.01.006

Sharma-Kishore, R., White, J.G., Southgate, E., and Podbilewicz, B. (1999). Formation of the vulva in Caenorhabditis elegans: a paradigm for organogenesis. Development *126*, 691–699.

Sherwood, D.R., Butler, J.A., Kramer, J.M., and Sternberg, P.W. (2005). FOS-1 promotes basement-membrane removal during anchor-cell invasion in *C. elegans*. Cell *121*, 951–962.

Sönnichsen, B., Koski, L.B., Walsh, A., Marschall, P., Neumann, B., Brehm, M., Alleaume, A.-M., Artelt, J., Bettencourt, P., Cassin, E., et al. (2005). Full-genome RNAi profiling of early embryogenesis in Caenorhabditis elegans. Nature *434*, 462–469.

Sternberg, P.W. (2005). Vulval development. WormBook 1–28.

Sullivan-Brown, J.L., Tandon, P., Bird, K.E., Dickinson, D.J., Tintori, S.C., Heppert, J.K., Meserve, J.H., Trogden, K.P., Orlowski, S.K., Conlon, F.L., et al. (2016). Identifying Regulators of Morphogenesis Common to Vertebrate Neural Tube Closure and Caenorhabditis elegans Gastrulation. Genetics *202*, 123–139.

Weinstein, N., Mendoza, L., 2013. A network model for the specification of vulval precursor cells and cell fusion control in *Caenorhabditis elegans*. Front. Genet. 4, 1–24. doi:10.3389/fgene.2013.00112

Ziel, J.W., Hagedorn, E.J., Audhya, A., and Sherwood, D.R. (2009). UNC-6 (netrin) orients the invasive membrane of the anchor cell in *C. elegan*s. Nat Cell Biol *11*, 183–189.

Figure 3.1.

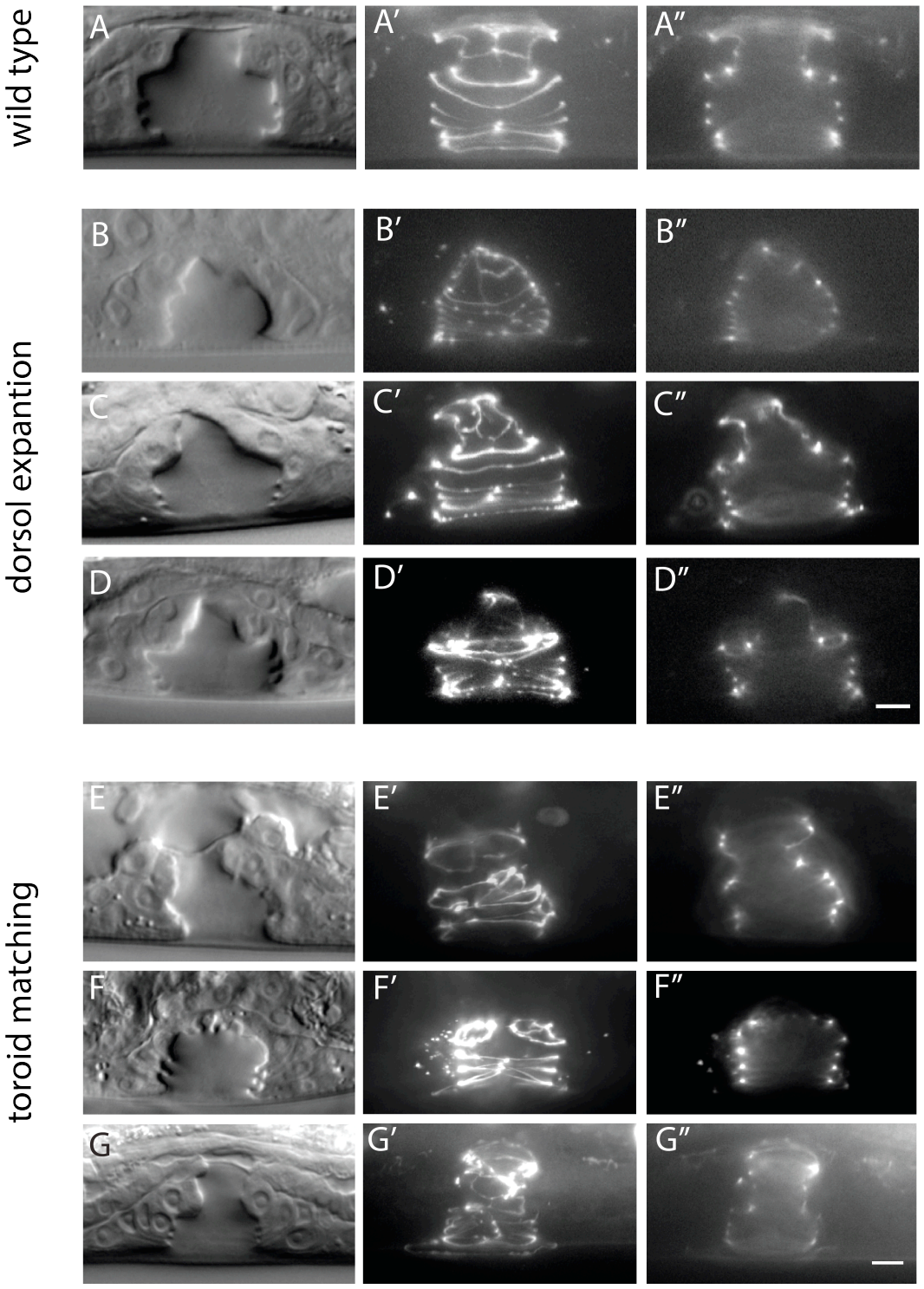
wild type
dorsol expantion
toroid matching
A
A′
A″
B
B′
B″
C
C′
C″
D
D′
D″
E
E′
E″
F
F′
F″
G
G′
G″

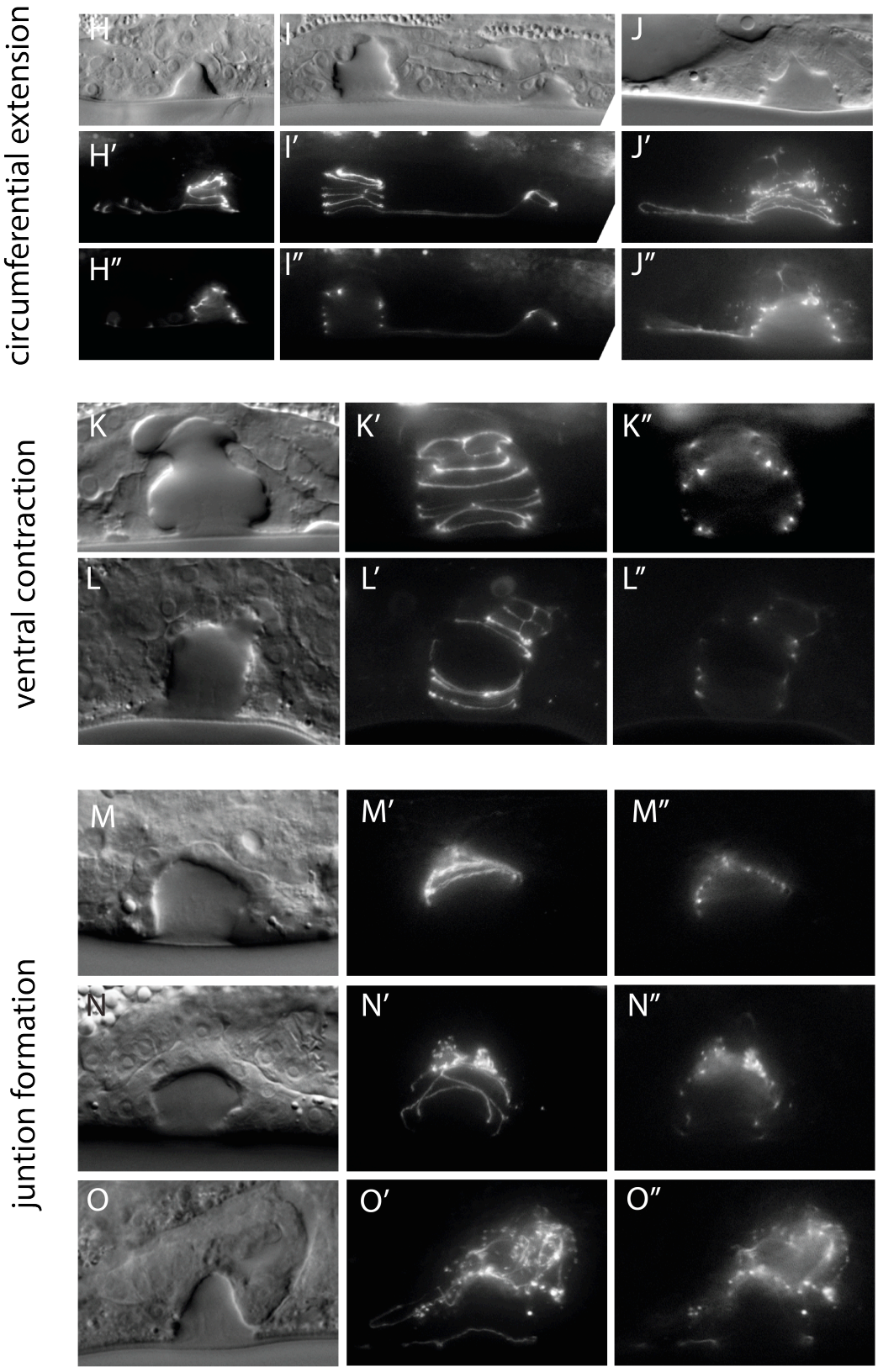

Figure 3.1. Five groups of the morphogenetic defects at the "Christmas tree" stage. The scale bar indicates 5 μm.

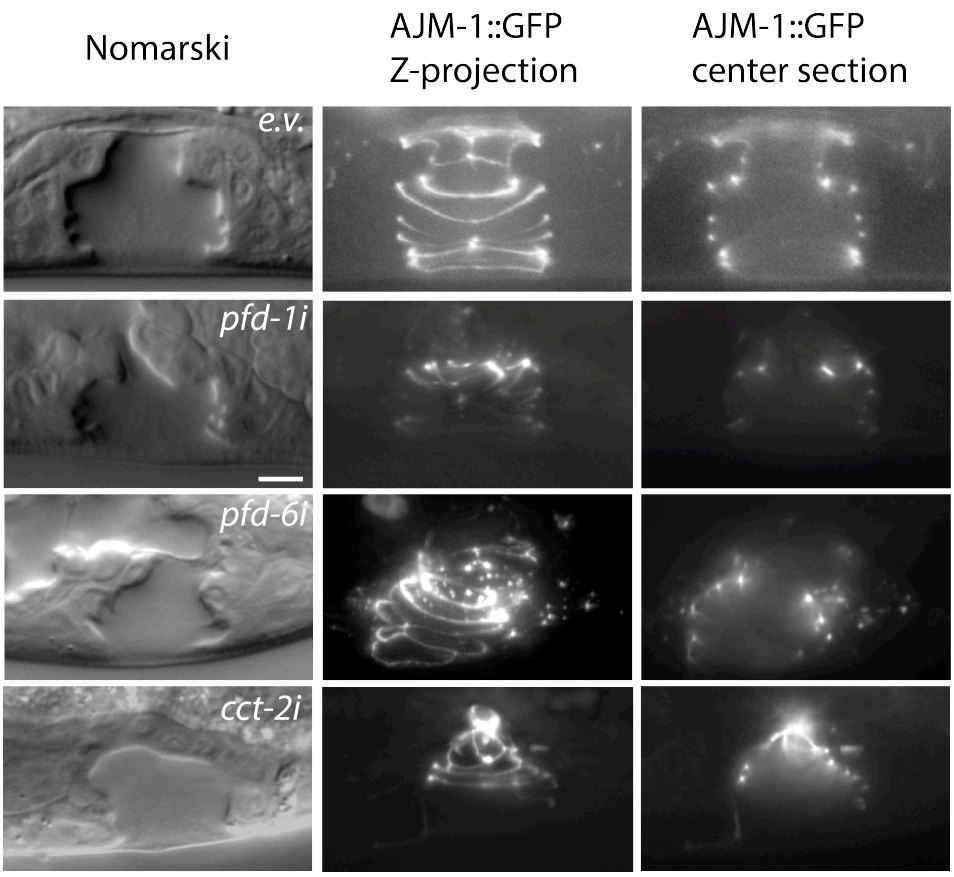

Figure 3.2. The RNAi phenotypes of the chaperone genes *pfd-1, pfd-6* and *cct-2.*

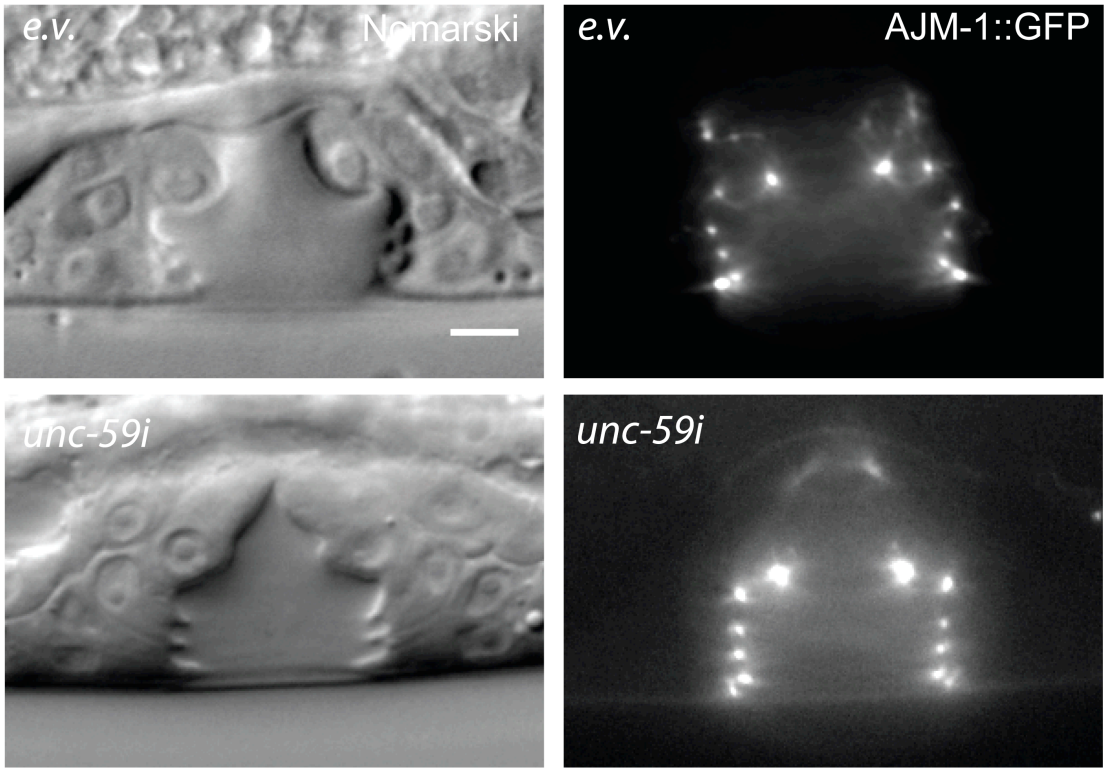

Figure 3.3. The RNAi phenotypes of the *septin* gene *unc-59.* The scale bar indicates 5 µm.

Table 3.1. List of candidate genes found from the Pvl RNAi screen.

Gene	Brief Description	Phenotypes	Known function in vulva
aakg-5	AMP kinase (AMPK)	toroid matching, dorsal expansion, ventral contraction	
aco-2	aconitase	toroid matching, circumferential extension	morphogenesis
arf-3	ADP-ribosylation factor; regulated by MEC-3.	circumferential extension	
bicd-1	dynein regulator	ventral contraction	
cam-1	receptor tyrosine kinase	toroid matching	part of WNT pathway during vulval development
cap-2	actin capping protein	circumferential extension	
ccf-1	Transcription complex	junction formation	
ccnk-1	cyclin K	dorsal expansion, ventral contraction, junction formation	
cct-2	eukaryotic cytosolic chaperonin	toroid matching, dorsal expansion, ventral contraction	general development
cdc-42	RHO GTPase	junction formation	
cdc-6	CDC-6	junction formation	
cdt-2	denticleless E3 ubiquitin protein ligase	dorsal expansion, ventral contraction	negative and positive regulation of vulval development
chn-1	E4 ubiquitin-chain elongation factor	junction formation	
cogc-2	the conserved oligomeric Golgi complex (COGC)	toroid matching	
csnk-1	CaSeiN kinase	toroid matching, circumferential extension	
dcp-66	NuRD component p66	junction formation	vulval development
ddx-23		junction formation	
dmd-5	DM(Doublesex/MAB) domain protein	toroid matching, ventral contraction	
dpl-1	the E2F-heterodimerization partne; class B synMuv gene	toroid matching, ventral contraction	class B synMuv gene
eff-1	transmembrane and secreted glycoproteins; fusogen	dorsal expansion, ventral contraction	AC fusion
egl-18	the GATA-family of transcription factors	dorsal expansion, ventral contraction	vulval cell fate specification
gex-2	ligand of the small GTPase Rac1	junction formation	
grdn-1		junction formation	
guk-1	guanylate kinase	dorsal expansion, ventral contraction	
his-10	H4 histone	dorsal expansion, ventral contraction	
his-37	H4 histone	dorsal expansion, ventral contraction	
his-38	H4 histone	toroid matching	
his-60	H4 histone	toroid matching, circumferential extension	
his-67	H4 histone	circumferential extension	
hsp-110	heat shock protein	toroid matching, circumferential extension	

kbp-1	KNL(kinetochore null) Binding protein	toroid matching	
let-49	transcriptional coactivator	dorsal expansion, ventral contraction	
lin-29	zinc finger transcription factor	circumferential extension	expressed in vulval muscle cells and vulval cells
lin-31	helix (WH)-like transcription factor that is a member of the HNF3/ Forkhead family of DNA-binding proteins	circumferential extension	vulval cell fate induction
lin-9	negative regulator of the RTK/Ras pathway	circumferential extension	Class A synMuv gene
mdt-10	predicted to have RNA polymerase II transcription cofactor activity	ventral contraction	
mdt-22	predicted to have RNA polymerase II transcription cofactor activity	dorsal expansion, ventral contraction	
mpk-1	MAP kinase	circumferential extension	Ras signaling pathway during vulval development
mrg-1	transcriptional regulator	toroid matching	
mrpl-37	Mitochondrial Ribosomal Protein	circumferential extension	
nhr-67	nuclear receptor	toroid matching	vulval gene expression
npp-17	RAE(Ribonucleic Acid Export factor) homolog	toroid matching	
npr-3	G-protein-coupled receptor	toroid matching	
nsh-1		toroid matching	
ntl-2	transcription complex	toroid matching	
orc-5	origin recognition complex, subunit 5	dorsal expansion, ventral contraction	
pab-1	poly(A)-binding protein	toroid matching, dorsal expansion, ventral contraction	
pad-1	highly conserved but unfamiliar protein	toroid matching, circumferential extension	
pbrm-1	chromatin remodeling and transcriptional regulation	junction formation	Ras signaling pathway during vulval development
pdcd-2	PROGRAMMED CELL DEATH 2	junction formation	
pfd-1	prefoldin subunit 1	toroid matching, dorsal expansion,	
pfd-6	prefoldin subunit 6	toroid matching	vulval development
pigv-1	PhosphatidylInositol Glycan anchor biosynthesis, class V protein	dorsal expansion	
pitr-1	phosphate permease	toroid matching, dorsal expansion, ventral contraction	negative regulation of vulval development
pmk-2	mitogen-activated protein kinase (MAPK)	ventral contraction	
pole-2	POLE(DNA POLymerase Epsilon) homolog	toroid matching, circumferential extension	
pry-1	containing RGS and DIX domains that related to members of the Axin protein family	junction formation	negative regulation WNT signaling pathway during vulval development
ref-2	transcription factor	circumferential extension	
rfp-1	ubiquitin-protein ligase	toroid matching	vulval development
rpa-2	the medium subunit of replication protein A (RPA)	junction formation	

rsa-2	Regulator of Spindle Assembly	toroid matching, dorsal expansion, ventral contraction,	
rsp-6	RNA binding protein	dorsal expansion, ventral contraction	suppresses the SynMuv phenotype of *lin-15(n765)*
sams-4	methionine adenosyltransferase	dorsal expansion, ventral contraction	
ser-3	octopamine receptor	junction formation	
sds-22	protein phosphatase 1,regulatory subunit 7	dorsal expansion, ventral contraction	
sdz-30		toroid matching	
sel-8	nuclear protein required for GLP-1 and LIN-12 signalling	toroid matching, ventral contraction	
sem-5	Src homology (SH) domain 2 and 3-containing protein	toroid matching	vulval induction
skr-2	ubiquitin-ligase complex	junction formation	
snpc-1.1	small nuclear RNA activating complex, polypeptide 1	dorsal expansion, ventral contraction	
sox-2	HMG-box transcription factor	circumferential extension	
src-2	non-receptor protein tyrosine kinase	toroid matching, circumferential extension	
taf-1	TATA-binding protein associated factor	toroid matching, circumferential extension	
taf-12	transcription initiation factor	junction formation	
tag-267		junction formation	
trr-1	atypical protein kinase	toroid matching	class C synMuv gene
uba-2	ubiquitin-like 2 activating enzyme	circumferential extension, dorsal expansion, ventral contraction	AC invasion
ubc-12	ubiquitin-conjugating enzyme	toroid matching, dorsal expansion, ventral contraction	vulva eversion
unc-59	septin isoform	toroid matching, ventral contraction	strong pvl in adult
usp-48	ubiquitin carboxylterminal hydrolase	dorsal expansion, ventral contraction	negative regulation of vulval development
vab-23	coiled-coil containing a C-terminal C4H2 zinc finger domain	toroid matching	toroid matching
vgln-1	high density lipoprotein binding protein	circumferential extension	
wve-1	WAVE protein	ventral contraction	
C03D6.1		toroid matching	
C18E9.4	mitochondrial NADH dehydrogenase complex	toroid matching	
F54C9.9		circumferential extension	
F56B3.4		dorsal expansion, ventral contraction, junction formation	
T11G6.8		junction formation	
T21B10.3		circumferential extension	
T28D6.5		dorsal expansion, ventral contraction	
Y44F5A.1		toroid matching	
Y48B6A.1	phosphoprotein in mitotic spindles	junction formation	
ZC404.7		dorsal expansion, ventral contraction	

Table 3.2. The GO clusters of the candidate genes.

Level	Developmental biology							
Annotation Cluster 1	**Enrichment Score: 86.96318427321809**							
Category	Term	Count	%	PValue	List Total	Pop Hits	Pop Total	Fold Enrichment
GOTERM_BP_FAT	GO:0003006~reproductive developmental process	86	99	2.07E-83	87	831	7838	9.323595723
Annotation Cluster 2	**Enrichment Score: 24.058482140853375**							
Category	Term	Count	%	PValue	List Total	Pop Hits	Pop Total	Fold Enrichment
GOTERM_BP_FAT	GO:0048729~tissue morphogenesis	35	40	1.86E-24	87	345	7838	9.139763452
Annotation Cluster 3	**Enrichment Score: 17.3519482290947**							
Category	Term	Count	%	PValue	List Total	Pop Hits	Pop Total	Fold Enrichment
GOTERM_BP_FAT	GO:0009791~post-embryonic development	59	68	6.50E-19	87	1779	7838	2.987872562
Annotation Cluster 4	**Enrichment Score: 15.119733379602769**							
Category	Term	Count	%	PValue	List Total	Pop Hits	Pop Total	Fold Enrichment
GOTERM_BP_FAT	GO:0045927~positive regulation of growth	57	66	8.79E-16	87	1904	7838	2.697080556
Annotation Cluster 5	**Enrichment Score: 7.0437325120874865**							
Category	Term	Count	%	PValue	List Total	Pop Hits	Pop Total	Fold Enrichment
GOTERM_BP_FAT	GO:0018991~oviposition	17	20	6.58E-08	87	287	7838	5.336457207
Annotation Cluster 6	**Enrichment Score: 5.847269666607764**							
Category	Term	Count	%	PValue	List Total	Pop Hits	Pop Total	Fold Enrichment
GOTERM_BP_FAT	GO:0040027~negative regulation of vulval development	10	11	2.84E-06	87	110	7838	8.190177638
Annotation Cluster 9	**Enrichment Score: 2.9693308863110612**							
Category	Term	Count	%	PValue	List Total	Pop Hits	Pop Total	Fold Enrichment
GOTERM_BP_FAT	GO:0051240~positive regulation of multicellular organismal process	11	13	0.003142342	87	330	7838	3.003065134
Annotation Cluster 10	**Enrichment Score: 1.8783901571181763**							
Category	Term	Count	%	PValue	List Total	Pop Hits	Pop Total	Fold Enrichment
GOTERM_BP_FAT	GO:0008406~gonad development	5	6	0.02090998	87	96	7838	4.692289272

Level	Cell biology							
Annotation Cluster 7	**Enrichment Score: 3.61251181854164**							
Category	Term	Count	%	PValue	List Total	Pop Hits	Pop Total	Fold Enrichment
GOTERM_CC_FAT	GO:0005654~nucleoplasm	8	9	2.20E-09	30	64	7912	32.96666667
GOTERM_CC_FAT	GO:0031974~membrane-enclosed lumen	8	9	7.69E-07	30	148	7912	14.25585586
SP_PIR_KEYWORDS	nucleus	15	17	3.56E-05	85	928	19674	3.741252535
SP_PIR_KEYWORDS	transcription regulation	9	10	0.00108957	85	485	19674	4.295112189
GOTERM_CC_FAT	GO:0005667~transcription factor complex	3	3	0.004301971	30	27	7912	29.3037037
Annotation Cluster 8	**Enrichment Score: 3.044102146382626**							
Category	Term	Count	%	PValue	List Total	Pop Hits	Pop Total	Fold Enrichment
GOTERM_BP_FAT	GO:0016477~cell migration	7	8	1.38E-04	87	73	7838	8.638954495
Annotation Cluster 12	**Enrichment Score: 1.4866058099259039**							
Category	Term	Count	%	PValue	List Total	Pop Hits	Pop Total	Fold Enrichment
GOTERM_BP_FAT	GO:0060184~cell cycle switching	3	3	0.032613258	87	26	7838	10.39522546
Level	Molecular Biology							
Annotation Cluster 11	**Enrichment Score: 1.6046837341527869**							
Category	Term	Count	%	PValue	List Total	Pop Hits	Pop Total	Fold Enrichment
SP_PIR_KEYWORDS	Chaperone	3	3	0.014522544	85	43	19674	16.14829001
Annotation Cluster 13	**Enrichment Score: 1.4551813058531753**							
Category	Term	Count	%	PValue	List Total	Pop Hits	Pop Total	Fold Enrichment
SP_PIR_KEYWORDS	chromosomal protein	3	3	0.014522544	85	43	19674	16.14829001
Annotation Cluster 14	**Enrichment Score: 1.4259695043701137**							
Category	Term	Count	%	PValue	List Total	Pop Hits	Pop Total	Fold Enrichment
SP_PIR_KEYWORDS	alternative splicing	8	9	0.00395396	85	470	19674	3.939724656
Annotation Cluster 15	**Enrichment Score: 1.211672020525296**							
Category	Term	Count	%	PValue	List Total	Pop Hits	Pop Total	Fold Enrichment
GOTERM_BP_FAT	GO:0000226~microtubule cytoskeleton organization	5	6	0.02795413	87	105	7838	4.290093049

Table 3.3. The mutant validation for selected candidates.

candidate gene	alleles	reason chosen	mutant phenotype
aco-2	none	briefly reported to function in vulval morphogenesis	-
arf-3	*tm1877*	unique phenotype in circumferential extension and not reported in acto-myosin regulation	wild type
bicd-1	*ok2371*	dynein regulator	wild type
cam-1	*gm122*	Wnt pathway	cell induction
cap-2	*ok1929*	its known function as actin capping protein matches the phenotype of circumferential extension	sterile
cct-2	ok3438	strong phenotypes	cell induction
cogc-2	*tm3457*	known function as Golgi complex and unique phenotype in toroid matching	wild type
csnk-1	*tm1762*	strong phenotypes	wild type
C18E9.4	none	strong and unique phenotype on toroid matching	-
dmd-5	*ok1394*	strong phenotypes	wild type
dpl-1	*n2994*	strong phenotypes	cell induction
kbp-1	none	strong and unique phenotype on toroid matching	-
npr-3	*tm1583*	known as membrane receptor, matches the unique phenotype of toroid matching	wild type
nhr-67	*ok631*	strong phenotypes	toroid matching and cell induction
ntl-2	*ok974*	strong and unique phenotype in toroid matching	wild type
pad-1	none	strong phenotypes	-
pfd-1	*gk526*	regulation of tubulin and strong phenotypes	sterile
pfd-6	*ok2785*	regulation of tubulin and unique phenotype in toroid matching	sterile
rfp-1	*ok572*	regulation of vulval development and unique phenotype in toroid matching	cell induction
rsa-2	*tm3051*	strong phenotypes	embryonic lethal
sel-8	*sa54*	strong phenotypes	sterile
sem-5	*cs15*	strong phenotypes	sterile
src-2	*ok819*	function in morphogenesis and strong phenotypes	wild type
trr-1	*n3630*	unique phenotype in toroid matching and has potential function in morphogenesis as an atypical protein kinase	wild type
uba-2	none	strong phenotypes	-
unc-59	*e261&e1005*	strong phenotypes	primary toroid matching

CHAPTER IV. The role of Septins in the vulval toroid matching.

4.1. Introduction

4.1.1. The tissue matching mechanisms in morphogenesis

A key feature of tissue morphogenesis is the fusion of multiple tissues which is required for many development and regenerative processes such as neural tube closure and wound healing respectively (Millard and Martin, 2008). For a proper tissue fusion event to happen, patterned cells have to be aligned precisely in a process that is called tissue matching.

The tissue matching mechanisms have been suggested from studies of dorsal closure in *Drosophila* and ventral enclosure in *C. elegans*. The original positions of cells within the tissue is the basis for tissue matching, while the filopodia sent from the leading edge of the cells are required to initiate the cell attachment (Millard and Martin, 2008). The actomyosin network and the microtubule dynamics provide the mechanical force and the structural support that drive cell shape change and cell migration. Several signaling pathways have been reported in controlling tissue matching through different means. The small GTPases Rho, Rac, CDC-42 regulate actomyosin activities, the planar cell polarity (PCP) pathways control tissue polarity and collative cell movement, and the Ephrin/Eph pathway determines the position of the matching cells (Martin and Parkhurst, 2004; Muñoz-Soriano et al., 2012). While cell adhesion proteins are implicated in mediating tissue fusion and are expressed throughout the epithelium, whether adhesion proteins involve in the patterned tissue matching remains to be elucidated (Millard and Martin, 2008).

4.1.2. *C. elegans* vulval toroids formation as a seminal system for the study of tissue matching

In order to resolve the molecular details of tissue matching during morphogenesis, it is required to study this process on the level of single cells. Researchers have developed various reporters to visualize molecular events in single cells. An advanced reporter system for the study of tissue matching is based on *engrailed* and *patched* promoter driven RFP-Moesin and GFP-Moesin expression in the epithelium of *Drosophila* embryo. This allows to distinguish differential patterning of para-segments. Yet this system does not permit to discriminate or genetically manipulate individual cells within one para-segment (Millard and Martin, 2008).

C. elegans vulval toroid formation provides a handy model to overcome the shortages of the current systems by enables the study of tissue matching at single-cell resolution. The vulval lumen is formed by 22 cells with seven sub-cell fates termed VulA, VulB1, VulB2, VulC, VulD, VulE and VulF. Vulval cells migrate from both sides, meet their counterpart partner cells accurately, make cell junctions in the middle of the vulva, undergo a sub-sequential intra-toriod fusion and form the seven donut-like toroids stacked one on top of another, eventually building the mirror-imaged vulval tube. The fate specification of vulval cells that is regulated by RTK-RAS-MAPK, NOTCH and WNT pathways have been extensively studied, which facilitates the genetical marking and manipulation in different toroids. By using the vulval toroid system, the SMP-1/PLX-1 pathway has been found to mediate the contact-dependent stop signal and the stepwise toroid matching that triggers the individual toroid formation one after another at the different time windows (Liu et al., 2005). One question we would like to address is whether the cell fate within the vulval tissue is required for the accurate toroid matching additional to the SMP-1/PLX-1 signal model.

4.1.3. Septins as a tool to study toroid formation.

Septin proteins have originally been found in budding yeast, where they seem to be essential for cytokinesis. Septins form a double ring structure flanking the actomyosin ring at the leading edge of the cleavage furrows in telophase (Beise and Trimble, 2012). F-actin is negatively regulated by Septins. In the asymmetric cell division, the PAR proteins maintain proper accumulation of F-actin on the contractile ring via keeping Septins and ANI-1 away from division plane (Jordan et al., 2016).

In addition to cytokinesis and asymmetric cell division, Septin proteins are important for tissue morphogenesis. For example, during cell migration, Septins promote F-actin-mediated focal adhesion dynamics (Cassani et al., 2014). During collective cell movement, the PCP and Septin proteins collaboratively restrict the localization of the actomyosin network, guiding the polarized cell membrane shortening (Shindo and Wallingford, 2014). Finally, Septins have also been shown to maintain the epithelial cell polarity by regulating microtubule organization (Spiliotis et al., 2008).

The absence of an embryonic phenotype makes the *septin* mutants very useful for establishing phenotypes in organogenesis (Nguyen and Sawa, 2000). In *C. elegans*, UNC-59 and UNC-61 are the only two Septin family members, which form the non-polar filaments in the sequence of UNC-59/UNC-61/UNC-61/UNC-59 (John et al., 2007). The assembly of Septin chains involves the cycles of GTP loading and hydrolysis that are mediated by Cdc-42 (Gladfelter, 2002). Importantly, UNC-59 and UNC-61 are required for the post-embryonic cytokinesis and the morphogenesis in neuronal cells but not essential for embryogenesis (Nguyen and Sawa, 2000). In a previous screen looking for regulators of morphogenesis in *C. elegans,* we found that *unc-59* and *unc-61* RNAi cause defects in primary toroid matching of the vulva (Chapter III). We aim to characterize in detail of the primary vulval toroid matching defect in the *septin* mutants. We found that the cytoskeletons, the vulval cell polarity and the AC invasion did not have significant defects except the change associated with the primary toroid junction defect. The first discernible

defect induced by lack of Septins was found to be in the determination of the VulE cell division axis, which changed from the T division to O division. At later stages during vulval development, other vulval cells displayed normal divisions. The specific questions we want to answer in this project are why and how Septins define the division angle of the VulE cells and what are the implications of this effect on cell positions within the tissue and the consequence on tissue matching. In addition, our data suggested that the VulD cell participates in the primary toroid formation but does not affect the formation of the other secondary toroids in the *septin* mutant. Based on this phenotype, we would like to also use the *septin* mutant as a tool to address whether the cell fate is required in the toroid matching.

4.2. Materials and methods

4.2.1. General methods and strains

C. elegans strains were maintained at 20°C on standard nematode growth plates as described (Brenner, 1974). The wild-type strain was *C. elegans* Bristol, variety N2.

Strains used were as follows: LGI: *unc-59(e261), unc-59(e1005),* LGIII: i*tIs174[par-3::PAR-3::GFP, unc-119(+)]; par-3(it71) unc-32(e189)*, LGV: *unc-61(e228)*, Extrachromosomal and integrated arrays: *zhIs396[P_{dlg-1}>lifeact::mNeonGreen::unc-54 3'utr, P_{lin-48}>gfp], swIs79[ajm-1::gfp, P_{scm-1}::gfp, unc-119(+)]* (Diogon et al., 2007). *TH65[unc-119(ed3); ddIs15(yfp::tubulin alpha, unc-119(+))], ayIs4[egl-17::GFP] mcIs46[dlg-1::rfp; unc119(+)].*

4.2.2. Microscopy and image analysis

Fluorescent images recording were obtained using an Olympus BX61 wide-field microscope equipped with a X-light spinning disc confocal system using a 60x Plan Apo

lens and a Hamamatsu Orca CCD camera. The animals were mounted on 5% agarose pads containing 0.5 mM tetramisole. Images were recorded with an an X-light spinning disc system at 10 minute time intervals taking 30 to 40 z-stacks with a step size of 0.3 µm per time point. Spinning disc images were processed using the Huygens Deconvolution platform (SVI) to increase the signal to noise ratio and analyzed using Fiji (ImageJ (NIH)) or Imaris (Bit-plane) software.

4.2.3. Ablation experiments

Laser ablation experiments were performed with amicropoint dye laser (Photonics Instruments) attenuated to around 70% maximal intensity at a pulse rate of 10 Hz aimed at the nucleoli for cell ablations. Animals at the 4-cell stage were mounted on 5% agarose pads containing 0.5 mM tetramisole for ablation and were incubated at 20°C to recover and grown for 7 h after ablation.

4.2.4. MitoTracker staining

The MitoTracker staining protocol was adapted from Sherwood et al. (2005). worms were incubated for 2 h at RT in a 10 µM solution of MitoTracker Red CMXRos (Molecular probes) in M9 buffer. The initial volume was diluted 5 times by addition of M9 and pipetted on agar plates with *E.coli.* Animals were incubated at 20°C to recover for 1 h. For observation under Nomarski optics, animals of the indicated stages were mounted on 5% agarose pads. Fluorescent images were acquired on Olympus BX61 wide-field microscope equipped with a X-light spinning disc confocal system using a 60x Plan Apo lens and a Hamamatsu Orca CCD camera controlled by the Visview software package. Bleaching of the redundant MitoTracker for 2 min was applied to obtain a better defined signal on the basement membrane.

4.3. Results

4.3.1 The *septin* mutants display defect in primary lumen formation.

We characterized the *septin* mutant phenotype in vulval morphogenesis by using the adherens junction marker AJM-1::GFP. The null mutants *unc-59(e261)*, *unc-59(e1005)* and *unc-61(e228)* confirmed the previously observed primary lumen defects by RNAi (data not shown). The penetrance of the phenotype was 100% in the three cases (*unc-59(e261)* n=85, *unc-59(e1005)* n=42 and *unc-61(e228)* n=62). Since *unc-59* and *unc-61* showed very similar phenotypes, currently in this work we focused on the *unc-59(e261)* mutant, which in the rest of the text is referred as the *septin* mutant. The 3D reconstruction of AJM-1::GFP in *septin* mutant displayed a normal vulval epithelium at 4-cell stage but abnormal cell positions of VulD and VulE cells during the last round of vulval cell division (Fig.4.1. A,B,E and F). At the “Christmas tree” stage, a fraction of AJM-1::GFP was mis-localized next to the VulF toroid (Fig.4.1. C,D,G and H). Concomitantly, all the primary junctions were miss-matched. An abnormal secondary lumen was also observed with low penetrance <10% , which might be caused by the severe failure of primary lumen formation.

4.3.2. F-actin is mis-localized in the primary lumen but well organized in the secondary lumen.

Since Septin restricts F-actin localization, we hypothesize that the loss of *septin* might cause the mis-localization of F-actin during vulval morphogenesis. By analysing the distribution of the F-actin reporter LifeAct::mNeonGreen in the *unc-59(e261)* mutant, we observed a normal F-actin pattern prior to vulval invagination (Fig.4.2. A and F). During vulval morphogenesis, F-actin localized at the apical junction of the secondary lumen was not significantly changed compared to the wild type (Fig. 4.2.). On the other hand, the F-actin on the apical membrane of the primary vulval lumen was abnormal during vulval

morphogenesis and eventually did not connect with utse at the “Christmas tree” stage, leaving a closed dorsal lumen (Fig.4.2 E’ and J’). However, since the actomyosin network interacts with the cell junctions, it is not clear whether the defect of F-actin in the primary lumen is a cause or consequence of the mismatched vulval junctions.

4.3.3. AC invasion is normal in *septin* mutants.

The failure of AC invasion have been reported as the main reason for the closed primary lumen at the “Christmas tree” stage (Sherwood et al., 2005). We therefore check whether Septin is involved in the regulation of AC invasion by using Mitotracker, a dye that stains basal laminal membranes. The gaps generated by AC invasion were in the basal laminal membranes of both the wild type and *unc-59(e261)* animals, indicating that AC invasion was not affected by loss of *septin* (Fig.4.3.).

4.3.4. Cell polarity is not significantly affected in *septin* loss-of-function animals

Septins have been reported to control cell polarity through the regulation of vesicle trafficking (Bowen et al., 2011). We asked whether the mismatched toroid junction was caused by the loss of polarity in the vulval cells. We crossed the apical membrane marker PAR-3::GFP to the *septin* mutant to monitor vulval cell polarity during vulval morphogenesis. Notably, despite the mis-formed primary lumen, the apical identify of the membrane facing the lumen was retained as judged by the expression of PAR-3::GFP (Fig.4.4 B-E’,G-J’). At the 4 cell stage before vulval invagination, the apical membrane of the vulval precursor cells were normal at the ventral side similar to the wild type (Fig.4.4. A-A’, F-F’). Thus, we conclude that the vulval cell polarity is not significantly affected in *unc-59(e261)* mutants.

4.3.5. Loss of Septin causes the abnormal VulE cell divison

One important function of Septin is controlling cytokinesis during cell division. We asked whether the aberrant primary lumen resulted from the defects in vulval cell division. A time lapse recording of vulval invagination in *unc-59(e261)* null mutant animals showed that VulE cell was still the first vulval cell diviide from the 4 to the 8 cell stage. However, the position of the VulE cell nucleus was abnormal compared to wild type (Fig.4.5. A-B'''). This phenotype was also demonstrated with mispositioned AJM-1::GFP, which demonstrated the abnormal positions of one VulE cell and the VulD cell at one side of vulva (Fig.4.1. F and Fig.4.5. A-B'''). To check whether the cell division axis of the VulE cells is properly oriented, we crossed an endogenous translational YFP::alpha-Tubulin reporter that marks the mitotic spindle with the *septin* mutants. In *unc-59(e261)* mutant, the VulE cell did not undergo the wild-type T division but an abnormal O division, in which the cell division axis is neither perpendicular nor parallel to the vulval midline. One possibility is that the O division was caused by cytokinesis failure, in which the cell cytoplasm are not able to be separated entirely. Further dissection with time lapse recording of the VulE division and primary toroid formation are required to be performed to validate this hypothesis.

4.4. Additional experiment

Another question we addressed was whether the cell sub-fate contributes to the precise cell matching during toroid formation. To answer this question, we used the cell fate reporter EGL-17::GFP that marks the VulC and VulD cell fates at the "Christmas tree" stage and the apical junction marker DLG-1::RFP that visualizes the toroid shape. By ablating the different cells on each side of the vulval epithelium, for example one VulD and one VulE cell on different side, we generated the asymmetric cell meeting with different cell fates. A group of the symmetric VulE cell ablation was performed as control, in which the ablation was performed but not in the purpose of generating asymmetric cell meeting. At the "Christmas tree" stage when toroids had been formed, the different combinations of

asymmetric ablation showed the self-toroids instead of forming one continued vulval lumen that is in the wild-type animals (Fig 4.6. A-C'', G-N). Thus, the cell fate specific matching might be required during toroid formation. However, in our control experiment with the symmetric ablation of two VulE cells, in which the following VulD to VulA cells should stay in the symmetric position, the self-toroids were still formed (Fig 4.6. D-F''). Further experiments are needed to address the role of cell fate specificity on toroid matching.

4.5. Discussion and Outlook

4.5.1. Septins regulate primary toroid formation.

We found that both *septin* mutants, *unc-59(e261)* and *unc-61(e228)*, cause similar toroids matching defect during morphogenesis of the *C. elegans* vulva.This is consistent with the fact that UNC-61 and UNC-59 interact with each other *in vivo*, forming filamentous structures. Previous studies have reported the *unc-59* and *unc-61* mutant share similar defects and do not enhance the phenotypes of each other during worm embryonic development. However, to validate the proposed common function in vulval morphogenesis, phenotypic analysis of the double mutants of *unc-59(e261)* and *unc-61(e228)* should be performed.

We also found that most of the *septin* mutant animals showed the mismatching of primary toroid while secondary toroids formed properly. The first discernible event that might alter later morphogenetic events was the abnormal toroid junctions in VulD and VulE cells after VulE division. VulE division and its consequent cell shape change are highly dynamic. To reveal the detail of the primary toroid formation in s*eptin* mutants, 4D time-lapse recordings with AJM-1::GFP should be performed to monitor the process of the last round of cell division.

4.5.2 The regulation of VulE division by Septin.

The manner of cell division in vulval development is normally thought to be determined by the cell fate. We observed a change of VulE division plane orientated from the T division to an O division. How does Septin influence the orientation of division plane will be an interesting question to address. One possibility could be that the failure of cytokinesis blocks the separation of the VulE cytoplasm and affects the proper localization of the VulE nucleus. The endogenous GFP reporter of NMY-2 is able to visualize the process of cytokinesis (data not shown). Therefore, it would be interesting to check if the NMY-2::GFP pattern is changed in the *septin* mutant.

In cells, mitotic microtubules establish the spindle orientation and the plane of cell division. The YFP::alpha-tubulin reporter in the *septin* mutant revealed a change in spindle orientation. Thus, a second possibility could be that Septins control the cell division plane through the regulation of microtubule dynamics before cytokinesis.

Another different question raised in the context of the VulE division defect in the *septin* mutant is how does the position of the vulval cell affects tissue matching and toroid formation. We could speculate that this process might involve the behavior of filopodia that searches for guidance cues and suitable sites for cell attachment during tissue matching. Time-lapse recording with the LifeAct::mNeonGreen reporter that visualizes the behavior of filopodia during VulE toroid formation will give interesting insights to this process.

4.5.3. The role of Septin in morphogenesis.

In the telophase of cell division, loss of Septins leads to the increase of F-actin at the contractile ring during cytokinesis. Our data showed no significant change of F-actin and lumen shape in the secondary lumen , suggesting that Septins might not function in the secondary vulval lumen morphogenesis. In *Drosophila* epithelia, Septins enable the closure of the cytokinetic furrow by strengthening the cytokinetic actomyosin ring, which must overcome the tensile forces exerted by the apical adherens junctions (Founounou et

al., 2013; Guillot and Lecuit, 2013). We expect that F-actin localizes in proximity to Septins similar to its localization in cytokinesis, a scenario that the F-actin might be restricted to a confined region through Septins. Thus, the expression patterns of UNC-59 and UNC-61 in the primary vulval cells will help understanding the mis-localization of F-actin change in *septin* mutants. It has been reported that Ani-1 functions together with Septins to limit the F-actin localization to the actomyosin ring in cytokinesis. Septins require Ani-1 to be enriched at the contracting ring but do not contribute to the localization of Ani-1 (Jordan et al., 2016). If the septin mutant phenotype is caused by the loss of regulation on F-actin localization, loss of Ani-1 should be able to phenocopy the toroid matching defect in *septin* mutant.

4.5.4. Septin can be used as a tool to study toroid matching mechanisms during vulval morphogenesis.

The primary toroid is mis-matched in *septin* mutants. The vulval cell fate is likely unchanged due to the fact that the epithelial junction marker AJM-1::GFP is expressed in all the vulval cells in *unc-59(e261)* mutant animals. However, the VulD and VulE cell positions are altered in *septin* mutant. The phenotype provided by the *septin* mutant can be used as a tool to study tissue matching mechanism. The fact that the VulD cell can substitute a VulE cell to form the primary lumen and not affect the secondary lumen in *septin* mutants suggests that the cell sub-fate might be not required for the SMP/PLX guided top-down homotypic cell matching. This answer will be easy to find out by simply checking the toroid junctional marker DLG-1::RFP together with the VulC/D cell fate marker EGL-17::GFP in *septin* mutants.

4.6. Reference

Beise, N., and Trimble, W. (2012). Septins at a glance. Journal of Cell Science *124*, 4141–4146.

Bowen, J.R., Hwang, D., Bai, X., Roy, D., Spiliotis, E.T., 2011. Septin GTPases spatially guide microtubule organization and plus end dynamics in polarizing epithelia. The Journal of Cell Biology 194, 187–197. doi:10.1083/jcb.201102076

Brenner, S. (1974). The genetics of Caenorhabditis elegans. Genetics *77*, 71–94.

Cassani, C., Raspelli, E., Chiroli, E., and Fraschini, R. (2014). Vhs2 is a novel regulator of septin dynamics in budding yeast. Cell Cycle *13*, 1590–1601.

Dickinson, D.J., Ward, J.D., Reiner, D.J., and Goldstein, B. Engineering the Caenorhabditis elegans genome using Cas9-triggered homologous recombination. Nature Methods *10*, 1028–1034.

Diogon, M., Wissler, F., Quintin, S., Nagamatsu, Y., Sookhareea, S., Landmann, F., Hutter, H., Vitale, N., and Labouesse, M. (2007). The RhoGAP RGA-2 and LET-502/ROCK achieve a balance of actomyosin-dependent forces in *C. elegans* epidermis to control morphogenesis. Development *134*, 2469–2479.

Farooqui, S., Pellegrino, M.W., Rimann, I., Morf, M.K., Muller, L., Frohli, E., and Hajnal, A. (2012). Coordinated lumen contraction and expansion during vulval tube morphogenesis in Caenorhabditis elegans. Developmental Cell *23*, 494–506.

Gladfelter, A.S. (2002). Septin ring assembly involves cycles of GTP loading and hydrolysis by Cdc42p. The Journal of Cell Biology *156*, 315–326.

John, C.M., Hite, R.K., Weirich, C.S., Fitzgerald, D.J., Jawhari, H., Faty, M., Schläpfer, D., Kroschewski, R., Winkler, F.K., Walz, T., et al. (2007). The Caenorhabditis elegans septin complex is nonpolar. Embo J *26*, 3296–3307.

Jordan, S.N., Davies, T., Zhuravlev, Y., Dumont, J., Shirasu-Hiza, M., and Canman, J.C. (2016). Cortical PAR polarity proteins promote robust cytokinesis during asymmetric cell division. The Journal of Cell Biology *212*, 39–49.

Liu, Z., Fujii, T., Nukazuka, A., Kurokawa, R., Suzuki, M., Fujisawa, H., and Takagi, S. (2005). *C. elegans* PlexinA PLX-1 mediates a cell contact-dependent stop signal in vulval precursor cells. Developmental Biology *282*, 138–151.

Martin, P., and Parkhurst, S.M. (2004). Parallels between tissue repair and embryo morphogenesis. Development *131*, 3021–3034.

Millard, T.H., and Martin, P. (2008). Dynamic analysis of filopodial interactions during the zippering phase of *Drosophila* dorsal closure. Development *135*, 621–626.

Muñoz-Soriano, V., Belacortu, Y., and Paricio, N. (2012). Planar cell polarity signaling in collective cell movements during morphogenesis and disease. Curr. Genomics *13*, 609–622.

Nguyen, T.Q., and Sawa, H. (2000). The C-elegans septin genes, unc-59 and unc-61, are required for normal postembryonic cytokineses and morphogenesis but have no essential function in embryogenesis. Journal of Cell Science *113*, 3825–3837.

Sherwood, D.R., Butler, J.A., Kramer, J.M., Sternberg, P.W., 2005. FOS-1 promotes basement-membrane removal during anchor-cell invasion in C. elegans. Cell 121, 951–962. doi:10.1016/j.cell.2005.03.031

Shindo, A., and Wallingford, J.B. (2014). PCP and septins compartmentalize cortical actomyosin to direct collective cell movement. Science *343*, 649–652.

Spiliotis, E.T., Hunt, S.J., Hu, Q., Kinoshita, M., and Nelson, W.J. (2008). Epithelial polarity requires septin coupling of vesicle transport to polyglutamylated microtubules. The Journal of Cell Biology *180*, 295–303.

Ziel, J.W., Hagedorn, E.J., Audhya, A., and Sherwood, D.R. (2009). UNC-6 (netrin) orients the invasive membrane of the anchor cell in *C. elegans.* Nat Cell Biol *11*, 183–189.

Figure 4.1.

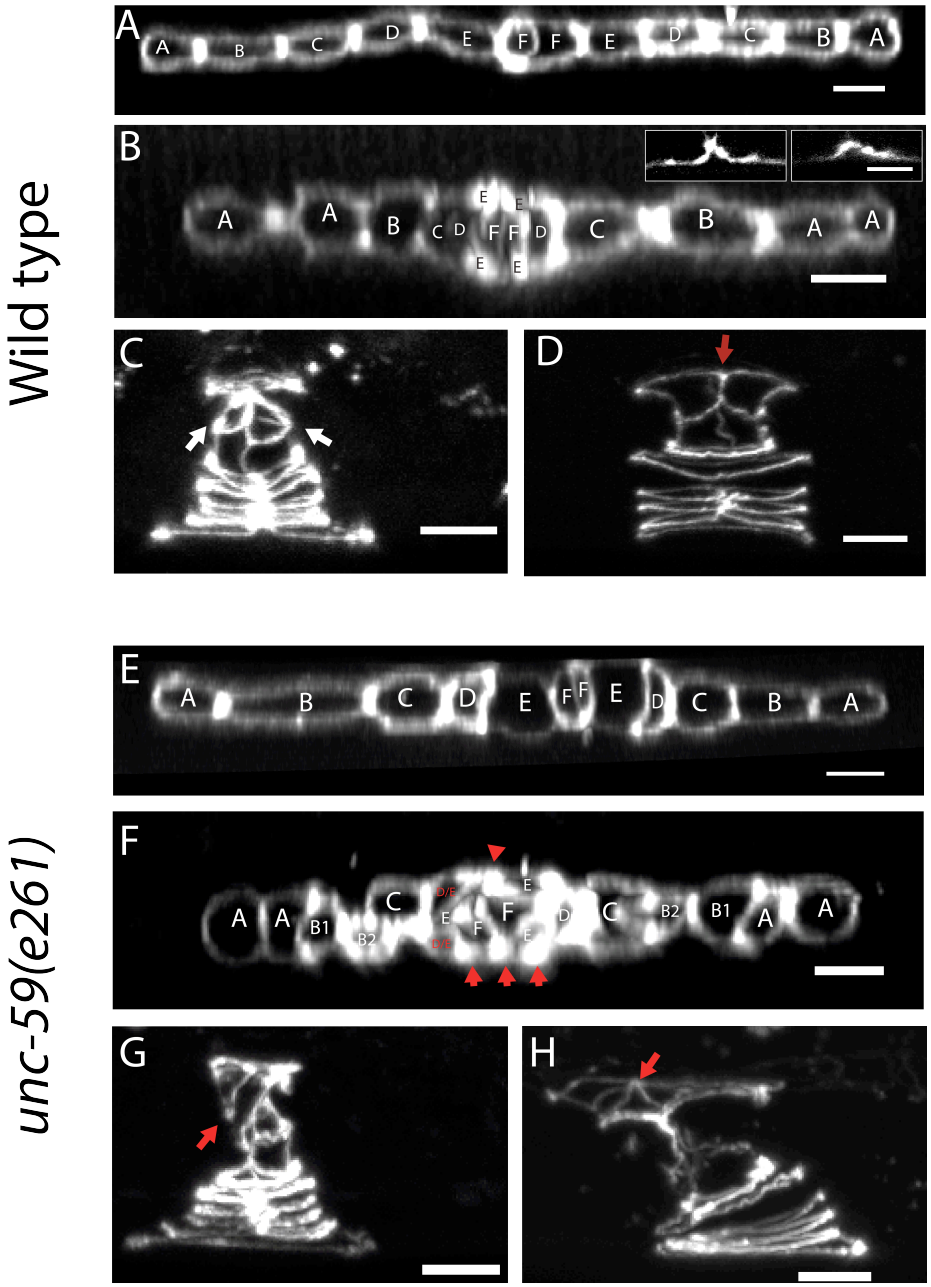

Figure 4.1. The defect of the primary toroid junction in *unc-59(e261)* mutant animals. The adherens junctions of vulva marked by AJM-1::GFP at different stages are demonstrated after the 3D reconstruction in the wild type (A-D) and the *unc-59(e261*) (E-H) mutant animal. The *unc-59(e261)* adherens junctions are similar to wild type at 4-cell stage (A and E). At 4 to 8 cell stage, in wild type the VulE junctions contact at the vulval middle line (B, the upper right windows show the lateral view at the layer of VulE contact at two sides). One side of the VulE junctions in *unc-59(e261)* mutant contact with each other (F, the red arrow head), while the junctions at another side are still quite far away(three red arrows in F). At the triangle stage, toroids in wild-type are mirror-imaged (C, white arrows) and asymmetric *unc-59(e261)* mutant (G, red arrow). At Christmas stage, the junction between the utse and two VulF cells are in the middle of the vulva(D, red arrow) and in unc-59(e261) is mis-localized (H, red arrow). The dorsal view of vulval junctions (A,B,E and F); the lateral view of vulval junctions (C,D,G and H). The vulval cell fates are marked in capital A to F in side of the GFP pattens (A,B,E, and F). The positions of one VulD cell and one VulE cell are indistinguishable and marked in red capitals (F). Scale bars represent 5μm.

Figure 4.2.

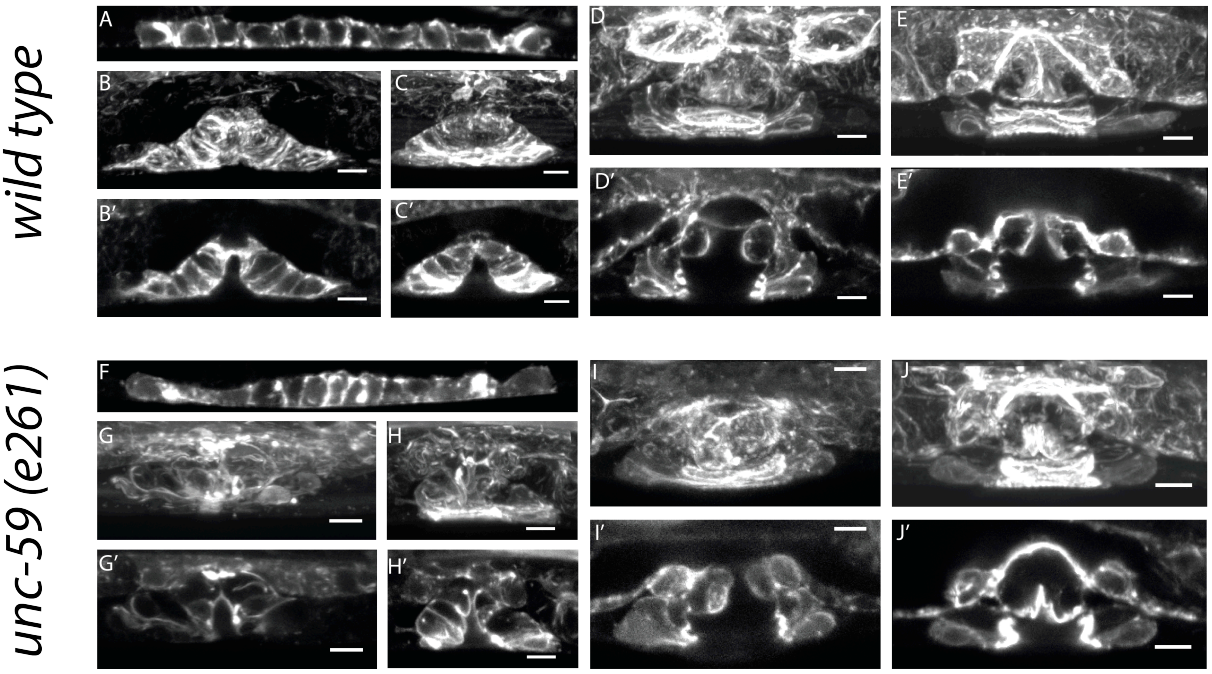

Figure 4.2 The F-actin is dis-organized in *unc-59(e261)* mutants. The expression pattern of LifeAct::mNeonGreen in the vulva of wild-type (A-E') and *unc-59(e261)* (F-J') animals at 4-cell stage(A,F), 8-cell stage (B,B',G, G'), triangle stage(C,C'H,H'), early Christmas stage(D,D',I,I') and late Christmas stage (E,E'J,J'). (A,B',C',D',F, G', H', I', J') demonstrate the mid-sagittal section of vulva. (B,C,D,E,G,H,I,J) indicate the z-projection of vulva. Scale bars represent 5µm.

Figure 4.3.

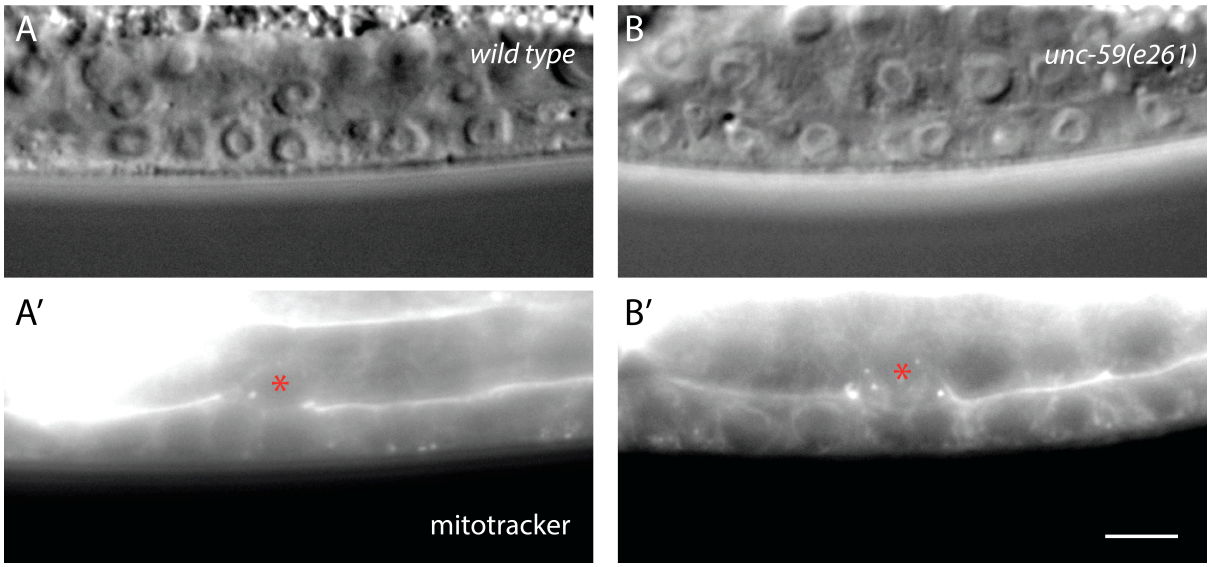

Figure 4.3. AC is able to breach basal lamina in *unc-59(e261).* The Nomarski pictures of wild type (A) and *unc-59(e261)* (B) and the mitotracker staining of basal lamina in wild type (A') and *unc-59(e261)* (B'). The red stars indicates the position of AC(A' and B'). Scale bar represents 5μm.

Figure 4.4.

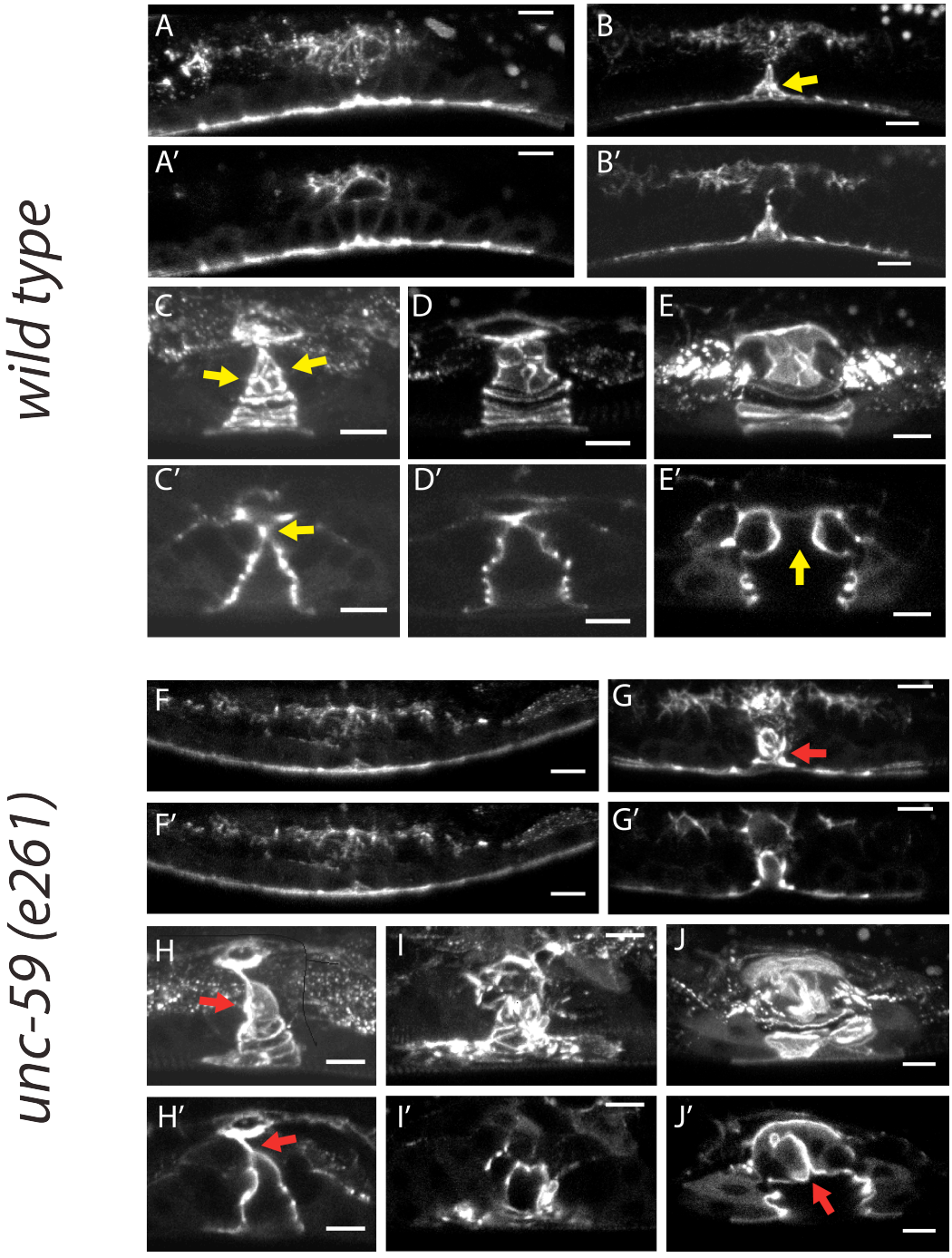

Figure 4.4. The *unc-59(e261)* mutant displays normal cell polarity in vulva. The expression pattern of Par-3::GFP in wild type (A-E') and the *unc-59(e261)* mutants (F,J') at different stages. In each group of pictures, the upper panel indicates the z-projection of z-stacks (A,B,C,D,E,F,G,H,I and J) , the lower panel indicates the mid-sagittal section (A',B',C',D',E',F',G',H',I' and J'). At 8-cell stage and triangle stage, the GFP patterns are symmetric in wild type (B, C,C', yellow arrows) and asymmetric in *unc-59(e261*) mutant(G,H,H' , red arrows). At "Christmas tree" stage, the wild type vulval lumen is connected to the utse membrane(E' yellow arrow) while the unc-59(e261) vulval lumen is closed (J' red arrow). Scale bars represent 5μm.

Figure 4.5.

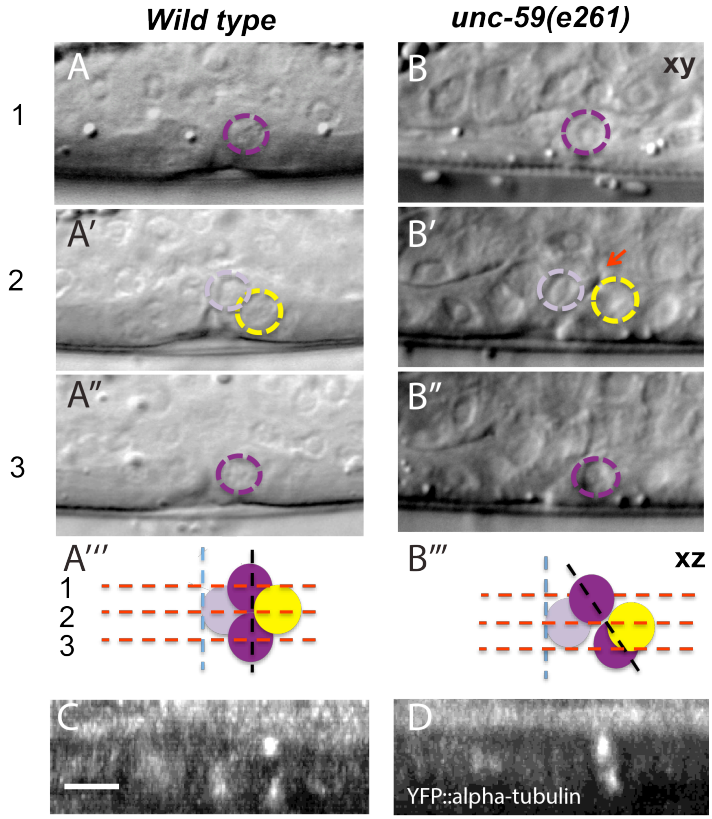

Figure 4.5. O division of VulE cell in *unc-59(e261)* mutant animals. The Nomarski pictures of the different layers of wild-type(A-A'') and *unc-59(e261)* (B-B'') vulva after VulE cell division.The numbers of 1,2,3 show the position demonstrated in the diagram(A''' and B'''). The dark purple dished cycles or rounds indicate the VulE nucleus, yellow cycles or round indicate the VulD nucleus and the light purple dished cycles or rounds indicate the VulF nucleus. The red arrow indicates the gap formed between two cells(B'). The expression of YFP::alpha-tubulin during VulE division in wild type (C) and *unc-59(e261)* mutant (D). Scale bar represents 5μm.

Figure 4.6.

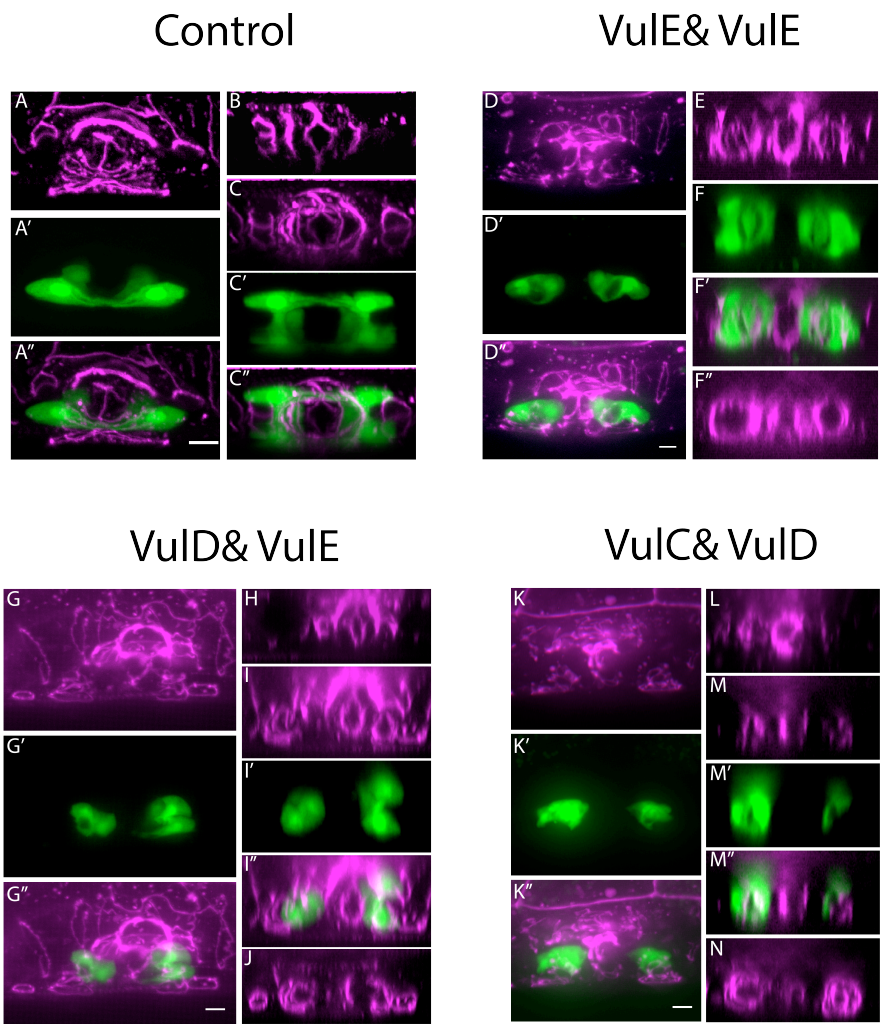

Figure 4.6. The vulval asymmetric-ablation experiment is inconclusive. Wild-type vulva at L4 stage demonstrates a continue lumen(A-C''), which is represented as the EGL-17::GFP marked VulC and VulD cells form the circulars of toroids (A' and C') with the DLG-1::mCherry marked adherens junctions around it (A'' and C''). The L4 stage vulva after symmetric ablation of VulE cells (D-F''), or asymmetric ablation of one VulD and one VulE, or asymmetric ablation of one VulC and one VulD, all display the self-toroids on both sides of the vulval center. (A,D,G and K) show the DLG-1::mCherry z-projections from the lateral side; (A',D',G' and K') show the EGL-17::GFP z-projections from the lateral side; (A'',G'',K'' and K'') show the merged pictures. (C,F,I and M) display the DLG-1::mCherry mid-sagittal section from the dorsal side; (C',F',I' and M') display the EGL-17::GFP mid-sagittal section from the dorsal side; (C'',F'',I'' and M'') display the merged pictures. (E,H and L) show the DLG-1::mcherry marked signal lumen of the VulF toroid. (J) shows the DLG-1::mcherry marked self-toroids located at the ventral side of the ablated vulval cells. Scale bars represent 5μm.

CHAPTER V. General discussion

5.1. Conclusion and perspective

5.1.1. A novel fashion of membrane constriction that initiates lumen formation

The apical constriction has been indicated as one classic way for the initiation of biological tube. It is driven by the tension, which is generated from the F-actin that links to apical junctions and the non-muscle myosin II that moves along the parallel aligned F-actin. Through the study of the AC invasion induced vulval epithelial invagination I found a new type of membrane constriction on the lateral membranes of the epithelial cells. It is interesting that the actomyosin network on the lateral membranes displayed a similar pattern as it on the apical membranes, suggesting the lateral constriction might use the actomyosin force-generating machinery that drives the apical constriction. The laser cutting experiment and the mutant analysis of the genes that involves in force generation validate this hypothesis. However, our data showed that the F-actin located at the basal side of vulval cells was not anchored by any junctional proteins like the case of F-actin linked with apical junctions. We found the AC may provide functions that substitutes the role of cell junctions, which is the anchoring of F-actin, recruiting NMY-2 and fixing membrane size after each contraction. In conclusion, the physic contact between the invading AC and the vulval epithelial cells guides an actomyosin-driven lateral membrane constriction during epithelial invagination.

Naturally there are some open questions in this model. For example, what is the exact role of the AC protrusions that form contacts with the VulF basal lateral membranes and how do they function together with the apical junctions? The shrinkage of the VulF lateral membrane was towards the AC, which associated with the moving up lumen space. How is the force balanced in this directional membrane constriction? In the future, more

precise cutting on the AC protrusions and the different areas of the constricting VulF lateral membranes might help with the answers. The mathematical modeling that calculates the force distribution based on the shape of the cells might also provide new aspects for our understanding.

5.1.2. The force generation pathway in VulF cells.

The dogma for the regulation of the actomyosin network is composed of the activators of actin polymerization, the proteins that regulate F-actin localization and the regulators of the myosin activity. We preformed an RNAi screen searching for the three types of candidate genes that are involved in the acto-myosin force generation pathway in VulF cells. The genes encoding the membrane-curvature sensing protein TOCA-1, TOCA-2 and the small GTPase CDC-42 were found in the screen. TOCA-1 and TOCA-2 trigger the NMY-2 accumulation at the AC/VulF-contact site, where the VulF is under the AC-invasion-caused mechanical deformation. In addition, TOCA-1 and TOCA-2 have been shown to activate CDC-42 and its downstream WAVE and WSP-dependent actin regulating pathway during *C. elegans* epidermal morphogenesis (Weinstein et al., 2015). Together, our data explains how the AC function in the regulation of the F-actin polymerization and localization through the recruitment of TOCA-1 and TOCA-2 at the AC/VulF contact sites and the activation of CDC-42.

In our screen, the small GTPase Rho-1 and MRCK-1 were found to promote the recruitment of NMY-2 at the AC/VulF contact sites as well. It has been reported that Rho-1 activates the myosin light chain 4 (MLC-4) through the positive regulation on the Rho kinase LET-502, and the MRCK-1 activates MLC-4 via the negative regulation of the MLC-4 inactivator MEL-11 (Fig.1.7.A) (Lundquist, 2006). We have found that the LET-502 is not required for the force generation in VulF lateral membrane contraction. Thus, although Rho-1 and MRCK-1 both have been indicated in controlling MLC-4 activity, the

mechanism of how does Rho-1 contribute to the force generation in VulF cells was not completely discovered. Unknown factors that active MLC-4 under the control of Rho-1 are missing in this model. One candidate could be the PAK-1 kinase protein, which has been shown to function redundantly with LET-502 during *C. elegans* embryonic elongation (Gally et al., 2009). The epistasis analysis of *pak-1* and other force regulating genes would be performed for the answer.

5.1.3. Tissue-specific regulation in vulval morphogenesis.

The primary and the secondary vulval cell fate are induced by the RAS and the NOTCH pathway respectively (Berset et al., 2001; Schmid and Hajnal, 2015). During vulval morphogenesis, the secondary lumen formation is also under the control of the NOTCH pathway through the activation of LET-502 (Farooqui et al., 2012). In our vulval morphogenesis screen, upon RNAi knockdown three chaperone genes that regulate the maturation of tubulin, the *pfd-1*, *pfd-6* and *cct-2*, displayed tissue-specific defects in the primary and/or the secondary lumen. We also found that *unc-59* and *unc-61,* which encode Septin proteins, are important for the primary lumen formation. In addition, it is unknown why the F-actin aligned differently in the primary and the secondary lumen (Farooqui et al., 2012). Putting together, these data suggest that there is the tissue-specific signal that regulate the different morphogenetic processes in the primary and the secondary vulval lumen. The study of the Septin proteins in the regulation of the primary lumen formation may be the path that leads to an answer.

5.2. Implications from the current study

5.2.1. AC-dependent vulval invagination: a model for the cancer cell-induced angiogenesis?

During metastasis, cancer cell induces angiogenesis to promote its growth and dissemination (Lopes-Bastos et al., 2016). Cancer cell can induce angiogenesis through direct interaction with endothelia cell. Such a process have been found to involve EGF, FGF2 and Interleukin-8 that are secreted by the cancer cell and the activation of VEGF pathway in endothelia cells (Cascone et al., 2011). However, due to the complexity of tissue in mammals, the details of the communications between cancer cell and endothelial cell in the *in vivo* environment remain to be studied. AC invasion has served as an excellent model to study of metastasis due to its invasive features that are similar to cancer cells (Sherwood and Sternberg, 2003). The homolog of the mammalian oncogene *fos* in *C. elegans* encodes a transcriptional factor that controls the AC invasion, a process breaches the basement membranes on top of the vulval epithelium (Sherwood et al., 2005). The system of AC-invasion induced tube formation in *C. elegans* vulval development has advantages to perform the time-lapse recording with high-resolution imaging, as well as genetically and physically manipulate in the single cell. These advantages make the AC invasion a user-friendly model for understanding the basis of the similar biological events such as the cancer cell induced angiogenesis.

5.2.2. Common regulators of tissue matching in vulval toroids formation and neural tube closure

Neural tube closure is an important morphogenetic process during vertebrate embryonic development. As one of the most common birth defect in human, the failure of neural tube closure causes neural tube defect in approximate 0.1% live birth children (Massarwa et al., 2013). The morphogenesis of neural tube closure in vertebrate and vulval toroids formation in *C. elegans* both involve the process of the tissue matching that requires the junction formation and the actomyosin generated force (Dalpe et al., 2004; Farooqui et al., 2012; Haigo et al., 2003; Sokol, 2016; Sullivan-Brown et al., 2016). Several studies

indicate the *C. elegans* gastrulation shares common molecular pathways with the *C. elegans* vulval toroids formation and vertebrate neural tube closure (Sullivan-Brown et al., 2016). For example, the SMP-1/PLX-1 pathway regulates cell matching in *C. elegans* gastrulation and vulval toroids formation (Liu et al., 2005), and the WAVE complex has been indicated in the regulation of cell shape change during the embyonic gastrulation in *C. elegans* and the neural tube formation in *Xenopus* (Sullivan-Brown et al., 2016). Thus, the vertebrate homologs of the candidate genes found in our vulval morphogenesis screen might also function in neural tube closure and worth further study.

5.3 Reference

Berset, T., Hoier, E.F., Battu, G., Canevascini, S., and Hajnal, A. (2001). NOTCH inhibition of RAS signaling through MAP kinase phosphatase LIP-1 during *C. elegans* vulval development. Science *291*, 1055–1058.

Cascone, T., Herynk, M.H., Xu, L., Du, Z., Kadara, H., Nilsson, M.B., Oborn, C.J., Park, Y.-Y., Erez, B., Jacoby, J.J., et al. (2011). Upregulated stromal EGFR and vascular remodeling in mouse xenograft models of angiogenesis inhibitor-resistant human lung adenocarcinoma. J. Clin. Invest. *121*, 1313–1328.

Dalpe, G., Brown, L., and Culotti, J.G. (2005). Vulva morphogenesis involves attraction of plexin 1-expressing primordial vulva cells to semaphorin 1a sequentially expressed at the vulva midline. Development *132*, 1387–1400.

Farooqui, S., Pellegrino, M.W., Rimann, I., Morf, M.K., Muller, L., Frohli, E., and Hajnal, A. (2012). Coordinated lumen contraction and expansion during vulval tube morphogenesis in Caenorhabditis elegans. Developmental Cell *23*, 494–506.

Gally, C., Wissler, F., Zahreddine, H., Quintin, S., Landmann, F., and Labouesse, M. (2009). Myosin II regulation during *C. elegans* embryonic elongation: LET-502/ROCK, MRCK-1 and PAK-1, three kinases with different roles. Development *136*, 3109–3119.

Haigo, S.L., Hildebrand, J.D., Harland, R.M., and Wallingford, J.B. (2003). Shroom Induces Apical Constriction and Is Required for Hingepoint Formation during Neural Tube Closure. Current Biology *13*, 2125–2137.

Massarwa, R., Ray, H.J., and Niswander, L. (2013). Morphogenetic movements in the neural plate and neural tube: mouse. Wiley Interdiscip Rev Dev Biol *3*, 59–68.

Liu, Z., Fujii, T., Nukazuka, A., Kurokawa, R., Suzuki, M., Fujisawa, H., and Takagi, S. (2005). *C. elegans* PlexinA PLX-1 mediates a cell contact-dependent stop signal in vulval precursor cells. Developmental Biology *282*, 138–151.

Lopes-Bastos, B.M., Jiang, W.G., and Cai, J. (2016). Tumour-Endothelial Cell Communications: Important and Indispensable Mediators of Tumour Angiogenesis. Anticancer Res. *36*, 1119–1126.

Lundquist, E. (2006). Small GTPases. WormBook.

Schmid, T., and Hajnal, A. (2015). ScienceDirectSignal transduction during *C. elegans* vulval development: a NeverEnding story. Current Opinion in Genetics & Development *32*, 1–9.

Sherwood, D.R., and Sternberg, P.W. (2003). Anchor Cell Invasion into the Vulval Epithelium in *C. elegans*. Developmental Cell *5*, 21–31.

Sherwood, D.R., Butler, J.A., Kramer, J.M., and Sternberg, P.W. (2005). FOS-1 promotes basement-membrane removal during anchor-cell invasion in *C. elegans*. Cell *121*, 951–962.

Sokol, S.Y. (2016). Chapter Twenty-One - Mechanotransduction During Vertebrate Neurulation. In Essays on Developmental Biology, Part B, P.M. Wassarman, ed. (Academic Press), pp. 359–376.

Sullivan-Brown, J.L., Tandon, P., Bird, K.E., Dickinson, D.J., Tintori, S.C., Heppert, J.K., Meserve, J.H., Trogden, K.P., Orlowski, S.K., Conlon, F.L., et al. (2016). Identifying Regulators of Morphogenesis Common to Vertebrate Neural Tube Closure and Caenorhabditis elegans Gastrulation. Genetics *202*, 123–139.

Weinstein, N., Ortiz-Gutiérrez, E., Muñoz, S., Rosenblueth, D.A., Álvarez-Buylla, E.R., and Mendoza, L. (2015). A model of the regulatory network involved in the control of the cell cycle and cell differentiation in the Caenorhabditis elegans vulva. BMC Bioinformatics *16*, 81.

CHAPTER VI Appendix

6.1. Curriculum Vitae

Personal information

Qiutan YANG

Origin: China, Sichuan province,

Birthday: 09 August 1987

Email: qiutan.yang@imls.uzh.ch

Tel: +41 78 722 0859

Address: Winterthurstr. 190, CH-8057 Zurich

Education

11.2011- 04. 2016(expected)
Ph. D. student on Developmental Biology, University of Zurich, Switzerland

09.2008-06.2011
M.S. Genetics, West China Hospital, Sichuan University, China

09.2004-06.2008
B.S. Biotechnology, Sichuan Normal University, China

09.2001-06.2004
High school, No. 2 high school of Lu County, Sichuan Province, China

Research Experience

11.2011 – 04.2016 (present), **Study vulval morphogenesis in *C. elegans***.
Ph.D. thesis advisor: Prof. Dr. Alex Hajnal, University of Zurich

10.2010 – 08.2011, **Dissect the WNT signalling in *Drosophila* midgut and *mouse intestine*** for the "Sino-Swiss Science and Technology Cooperation (SSSTC)" Program.
Host advisor: Prof. Dr. Konard Basler, University of Zurich

06.2009 – 09.2010, **Study on the regulation of cell polarity in the protonephron and neuron system of *Xenopus*.**
Master thesis co-advisor: Prof. Dr. Mao Bingyu, Chinese Academy of Science.

11.2007 – 06.2009, **Investigate the molecular mechanism of Polycystic Kidney Disease in mice, and study on the improvement of murine trans-genetic and knockout techniques.**
Bachelor and Master thesis advisor: Prof. Dr. Zhou Qin, West China Hospital.

Received Grants
2010. The SSSTC Grant, China and Switzerland.
2014. Travel Grant, MLS, UZH.
2015. Travel award, SDB, U.S.A.

Attended conference
2012
C. elegans Development, Cell Biology& Gene Expression Meeting

2013
19th International *C. elegans* meeting

2014
C. elegans Development Topic Meeting; Asia-Pacific *C. elegans* Meeting 2014

2015
The 2015 Gordon Conference on Developmental Biology
SDB (the Society for Developmental Biology) 74th Annual Meeting

Publications during Ph.D.
1.**Yang Q**, Escobar J, Hajnal A. Sequential apical and lateral cell constrictions initiate vulval lumen formation in C. elegans. ***Developmental Cell,*** in preparation

2. Haag A, Gutierrez P, Bühler A, Walser M, **Yang Q**, Langouët M, Kradolfer D, Frohli E, Herrmann CJ, Hajnal A, et al. An in vivo EGF receptor localization screen in *C. elegans* identifies the Ezrin homolog ERM-1 as a temporal regulator of signaling. ***PLoS Genet*** 10, e1004341.

6.2 Collaborating publication

(Contribution: providing data and analysis of LifeAct::GFP in wild type and *erm-1(tm677)* mutants)

OPEN ACCESS Freely available online

PLOS | GENETICS

An In Vivo EGF Receptor Localization Screen in *C. elegans* Identifies the Ezrin Homolog ERM-1 as a Temporal Regulator of Signaling

Andrea Haag[1,2☽], Peter Gutierrez[1,2☽], Alessandra Bühler[1☽], Michael Walser[1], Qiutan Yang[1,2], Maeva Langouët[1¤a], David Kradolfer[1¤b], Erika Fröhli[1], Christina J. Herrmann[1], Alex Hajnal[1]*, Juan M. Escobar-Restrepo[1]

1 University of Zurich, Institute of Molecular Life Sciences, Zurich, Switzerland, **2** PhD program in Molecular Life Sciences, Uni ETH Zürich, Switzerland

Abstract

The subcellular localization of the epidermal growth factor receptor (EGFR) in polarized epithelial cells profoundly affects the activity of the intracellular signaling pathways activated after EGF ligand binding. Therefore, changes in EGFR localization and signaling are implicated in various human diseases, including different types of cancer. We have performed the first *in vivo* EGFR localization screen in an animal model by observing the expression of the EGFR ortholog LET-23 in the vulval epithelium of live *C. elegans* larvae. After systematically testing all genes known to produce an aberrant vulval phenotype, we have identified 81 genes regulating various aspects of EGFR localization and expression. In particular, we have found that ERM-1, the sole *C. elegans* Ezrin/Radixin/Moesin homolog, regulates EGFR localization and signaling in the vulval cells. ERM-1 interacts with the EGFR at the basolateral plasma membrane in a complex distinct from the previously identified LIN-2/LIN-7/LIN-10 receptor localization complex. We propose that ERM-1 binds to and sequesters basolateral LET-23 EGFR in an actin-rich inactive membrane compartment to restrict receptor mobility and signaling. In this manner, ERM-1 prevents the immediate activation of the entire pool of LET-23 EGFR and permits the generation of a long-lasting inductive signal. The regulation of receptor localization thus serves to fine-tune the temporal activation of intracellular signaling pathways.

Citation: Haag A, Gutierrez P, Bühler A, Walser M, Yang Q, et al. (2014) An In Vivo EGF Receptor Localization Screen in *C. elegans* Identifies the Ezrin Homolog ERM-1 as a Temporal Regulator of Signaling. PLoS Genet 10(5): e1004341. doi:10.1371/journal.pgen.1004341

Editor: Andrew D. Chisholm, University of California San Diego, United States of America

Received November 26, 2013; **Accepted** March 16, 2014; **Published** May 1, 2014

Funding: This work was supported by a grant from the Swiss National Science Foundation (no. 31003A-146131) to AHaj and by the Kanton of Zürich. The funders had no role in study design, data collection and analysis, decision to publish, or preparation of the manuscript.

Competing Interests: The authors have declared that no competing interests exist.

* E-mail: alex.hajnal@imls.uzh.ch

☽ These authors contributed equally to this work.

¤a Current address: INSERM U781 and Department of Genetics, Foundation IMAGINE, Paris Descartes University, Necker-Enfants Malades Hospital, Paris, France
¤b Current address: ETH Zurich, Institute of Agricultural Sciences, Zurich, Switzerland

Introduction

The formation of epithelial tissues involves the polarized distribution of growth factor receptors that determine cell proliferation and differentiation. Notably, changes in EGFR localization have a major impact on signaling and organogenesis [1–3].

In *C. elegans*, the *let-23* gene encodes the sole member of the EGFR/ErbB family of receptor tyrosine kinases. *let-23* is involved in a variety of developmental processes including the induction of the hermaphrodite vulva [4]. In early second stage (L2) larvae, LET-23 is expressed at equal levels in the six equivalent vulval precursor cells (VPCs) (P3.p through P8.p) (**Figure 1A**) [5,6]. Beginning in the L2 stage, the gonadal anchor cell (AC) secretes the EGF ortholog LIN-3, which binds to LET-23 on the basolateral plasma membrane of the VPCs to activate the LET-60 RAS/MPK-1 MAPK signaling pathway [4] (**Figure 1B**). In order to reach high levels of receptor activity, LET-23 must be retained on the basolateral membrane of the VPCs by a ternary protein complex consisting of the PDZ-domain proteins LIN-2 CASK, LIN-10 MINT and LIN-7 VELIS. LIN-7 directly binds to the C-terminal PDZ binding motif of LET-23 [5]. The VPC that is nearest to the AC, P6.p, receives most of the inductive LIN-3 signal and hence adopts the primary (1°) cell fate. P6.p then produces several DELTA ligands, which induce via the NOTCH pathway the secondary (2°) cell fate in the neighboring VPCs P5.p and P7.p [7,8] (**Figure 1B**). NOTCH signaling blocks RAS/MAPK signaling and results in the endocytosis and degradation of LET-23 in the 2° VPCs [9–11]. The distal VPCs P3.p, P4.p and P8.p, which receive only little inductive signal, down-regulate LET-23 expression and adopt the tertiary (3°), uninduced cell fate. As the pathway components are conserved, the study of vulval induction of the worm can be used to find new core components or those required for fine-tune the signaling output. For this purpose, we performed the first systematic *in vivo* screen for regulators of LET-23 EGFR localization and expression in live *C. elegans* larvae.

Through this approach, we have identified 81 genes causing a variety of LET-23::GFP mislocalization phenotypes upon RNAi

Author Summary

Abnormal signaling by the epidermal growth factor receptor (EGFR) contributes to the development of various human diseases, including different cancer types. One important mechanism that controls intracellular signal transduction is by regulation of the subcellular receptor localization in the signal-receiving cell. We are investigating the regulation of the EGFR homolog LET-23 in the Nematode *C. elegans* by observing the localization of the EGFR in the epithelial cells of live animals. This approach has allowed us to study the dynamics of receptor trafficking in cells embedded in their natural environment and receiving physiological concentrations of various extracellular signals. In a systematic RNA interference screen, we have identified 81 genes controlling EGFR localization and signaling in different subcellular compartments. One new regulator of EGFR signaling identified in this screen encodes the Ezrin Homolog ERM-1. We show genetic and biochemical evidence indicating that ERM-1 is part of a buffering mechanism to maintain a pool of immobile EGFR in the basolateral membrane compartment of the epithelial cells. This mechanism permits the generation of a long-lasting EGFR signal during multiple rounds of cell divisions. The control of receptor localization is thus necessary for the precise temporal regulation of signal transduction during animal development.

knock-down. A subset of these genes also controls the strength of the LET-23 EGFR signal produced in the VPCs. We have identified ERM-1, the homologue of mammalian Ezrin, Radixin and Moesin proteins, as a temporal regulator of LET-23 EGFR signaling. Based on our genetic and biochemical data, we propose that ERM-1 binds to and sequesters the LET-23 EGFR in an inactive compartment at or close to the basolateral membrane of the VPCs. In this manner, ERM-1 competes with the activating LET-23/LIN-2/LIN-7/LIN-10 complex [5]. ERM-1 may act as a buffer that prevents the immediate activation of the entire pool of basolateral LET-23 EGFR at vulval induction and thus allows the generation of a prolonged signal.

Results

An In Vivo Screen Identifies Novel Regulators of LET-23 EGFR Localization and Expression

We performed RNAi knock-down of all genes (705 clones) reported to exhibit a protruding vulva (Pvl) phenotype, which is indicative of a defect in vulval fate specification or execution (**Table S1**) and examined LET-23 localization and expression in the vulval epithelium of live L3 larvae expressing a functional LET-23::GFP reporter (**Figure 1C–E**). The LET-23::GFP reporter used showed the same vulval expression pattern as endogenous LET-23 detected by antibody staining [5], and LET-23::GFP protein levels in total extracts were comparable to endogenous LET-23 levels (**Figure S1A**). Moreover, *let-23::gfp* efficiently rescued the *let-23(sy1)* vulvaless (Vul) phenotype (**Figure S1B**), and RNAi against *lin-7* or a mutation in *lin-2* caused an apical mislocalization of LET-23::GFP, as shown previously for endogenous LET-23 by antibody staining [5] (**Figure 1I**, and **Figure S1D**). In total, we identified 81 candidates that change different aspects of LET-23::GFP expression or localization (**Table 1**). We further classified these genes according to the specific mislocalization phenotypes observed (**Figure 1F**): Apical enrichment (24 genes, **Figure 1I,J**), accumulation in intracellular punctae or uniform cytoplasmic distribution (23 genes, **Figure 1M** and **Figure S2,C,D**), persisting expression in the 2° cells (31 genes, **Figure 1K and Figure S2E**), enrichment on the lateral membrane (2 genes, **Figure S2F**) and complex mislocalization phenotypes (10 genes, **Figure 1L**). Grouping the 81 genes into Clusters of Orthologous Groups (KOGs) indicated that a variety of processes are involved in regulating LET-23 localization (**Figure 1G**) [12]. In particular, genes involved in transcription, intracellular trafficking, signal transduction and protein stability and posttranslational modification were slightly overrepresented, while genes involved in chromatin modification, DNA replication and repair were underrepresented when compared to the distribution of the KOGs among the genes causing a Pvl phenotype that were screened.

Changes in LET-23 EGFR Localization Alter RAS-Mediated Signaling

For a subset of the candidates with predicted roles in signaling or trafficking, we examined whether inhibition of these genes altered the activity of the RAS/MAPK pathway. This was tested by performing RNAi in the sensitized *let-60 ras(n1046)* gain-of-function background in which more than 3 VPCs are induced [13] and scoring the average number of induced VPCs per animal (**Figure 1Q**). It should be noted that the VPCs in the *let-60 ras(n1046)* gain-of-function background are still sensitive to the AC signal [13]. In those cases where RNAi caused a penetrant embryonic or larval lethal phenotype, we performed Pn.p cell-specific RNAi using an *rde-1(ne219lf); let-60(n1046gf)* RNAi resistant background expressing *rde-1(wt)* from the Pn.p cell-specific *lin-31* promoter [14]. For example, RNAi against *sft-4* or against the small GTPase *aex-6* caused persistent LET-23::GFP expression in 2° VPCs (**Figure 1K** and **Table 1**). Moreover, Pn.p cell-specific *sft-4* RNAi significantly enhanced vulval induction in the *let-60(gf)* background (**Figure 1Q**). The yeast *sft-4* homolog ERV29 encodes a SURF protein with a putative di-lysine endoplasmic reticulum (ER) localization signal that sorts secretory cargo proteins in the ER into COPII vesicles [15]. An *sft-4::gfp* translational reporter showed expression in the VPCs in perinuclear structures that resemble the ER (**Figure 1N**). Thus, ER to Golgi transport might be involved in controlling LET-23 turnover in the VPCs.

RNAi of *C11H1.3* caused a complex mislocalization phenotype with a moderate apical enrichment, punctate LET-23::GFP accumulation at or close to the apical membrane (**Figure 1L**) and an increase in vulval induction in the *let-60(n1046gf)* background (**Figure 1Q**). C11H1.3 encodes a predicted E3 ubiquitin ligase that is expressed in the VPCs in intracellular vesicles (**Figure 1O**). Therefore, C11H1.3 may control LET-23 localization and stability through ubiquitination of the receptor itself or of an associated factor. A penetrant mislocalization phenotype with punctate cytoplasmic accumulation of LET-23::GFP was observed in *ego-2* RNAi treated animals (**Figure 1M**), and a translational *ego-2::gfp* reporter was expressed in the cytoplasm and nuclei of all the VPCs (**Figure 1P**). *ego-2* encodes a BRO1 domain protein that is related to mammalian PTPN23, which regulates the transport of ubiquitinated EGFR through the ESCRT III complex to the intralumenal vesicles of multivesicular bodies [16]. Interestingly, *ego-2* has also been reported to regulate GLP-1 NOTCH signaling during germ cell development and embryogenesis as well as LIN-12 NOTCH signaling during somatic gonad development [17]. Therefore, *ego-2* might be a general regulator of LET-23 EGFR and LIN-12/GLP-1 NOTCH via control of their endocytic transport.

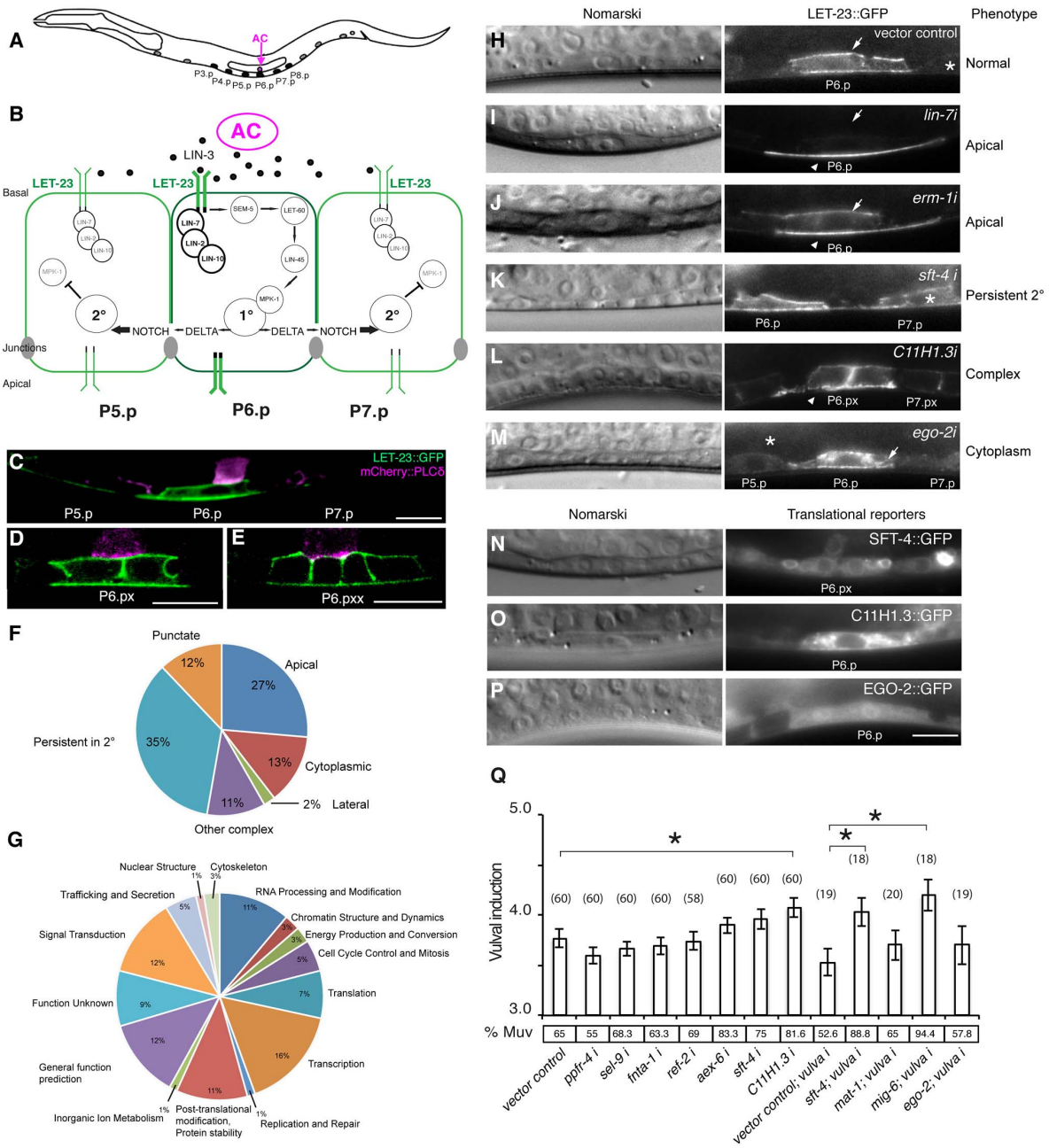

Figure 1. Identification of genes regulating LET-23 EGFR localization and signaling. (A) Schematic drawing of an L2 larva with the location of the VPCs and AC. P5.p, P6.p and P7.p get induced to form the mature vulva. P3.p, P4.p and P8.p divide once and fuse to the hypodermis. (B) Overview of the LET-23 EGFR and NOTCH signaling network controlling 1° and 2° vulval fate specification. (C) LET-23::GFP expression (green) in P6.p of a late L2 larva during vulval induction. The AC is labeled with an *mCherry::plcδ^{PH}* reporter (magenta) [35]. Note the low LET-23::GFP levels in the 2° P5.p and P7.p. (D) Expression of the LET-23::GFP reporter in the 1° lineage at the Pn.px and (E) Pn.pxx stage. (F) Pie charts indicating the frequencies of the different classes of mislocalization phenotypes observed after RNAi and (G) the Clusters of Orthologous Groups (KOGs) of the 81 genes identified in the screen (H–M). Examples of different genes identified in the LET-23 localization screen. Left panels show the corresponding Nomarski images and right panels LET-23::GFP expression in the 1° cells and their neighbors (asterisks). (H) The negative empty vector control and (I) *lin-7* RNAi as positive control. (J) *erm-1* RNAi as an example for reduced basolateral (arrow) and increased apical localization (arrow head), (K) *sft-4* RNAi with normal localization in P6.p but persistent expression in P7.p (asterisk), and (L) *C11H1.3* RNAi (Pn.px stage) with punctate apical accumulation (arrow head). (M) *ego-2* RNAi with cytoplasmic accumulation of LET-23::GFP in P6.p (arrow head) and P5.p (asterisk). (N) perinuclear localization of SFT-4::GFP in the vulval cells and the AC and (O) intracellular punctate expression of C11H1.3::GFP in P6.p. (P) Cytoplasmic and nuclear expression of EGO-2::GFP in P6.p. (Q) Vulval induction in *let-60(n1046gf)* larvae treated with different RNAi clones. Vulval induction (VI) indicates the average number of induced

VPCs per animal. "vulva i" indicates Pn.p cell-specific RNAi in the *rde-1(lf);let-60(n1046gf); [P_{lin-31}::rde-1]* background. %Muv (Multivulva) indicates the fraction of animals with VI>3. The numbers of animals scored are indicated in brackets. * Indicates $p<0.05$ as determined in a two tailed student's t-test - two-sample unequal variance. *t-test* values in *RNAi: C11H1.3* (0.003), *sft-4* (0.013), *mig-6* (0.002). Error bars represent the standard error of the mean. The scale bars are 10 μm.
doi:10.1371/journal.pgen.1004341.g001

ERM-1 Controls LET-23 EGFR Trafficking

One of the strongest apical enrichment mislocalization phenotypes was observed in *erm-1* RNAi treated animals (**Figure 1J**), prompting us to analyze the role of ERM-1 in LET-23 localization and signaling in more detail. *erm-1* encodes the sole *C. elegans* member of the Ezrin, Radixin and Moesin (ERM) protein family. ERM proteins link the cortical actin cytoskeleton and the plasma membrane and recruit transmembrane proteins to specific membrane compartment [18]. In addition, *C. elegans* ERM-1 is required for apical lumen morphogenesis in the intestine [19] [20]. In contrast to the apical localization observed in the intestine, an ERM-1::mCherry reporter showed basolateral and junctional localization and a partial overlap with LET-23::GFP in the VPCs and their descendants (**Figure 2A-A″**). Only after vulval invagination (at the Pn.pxxx stage), ERM-1 relocalized to the apical, luminal plasma membrane of the vulval toroids (data not shown). To confirm the RNAi phenotype, we examined LET-23::GFP expression in *erm-1(tm677)* null mutants. Homozygous *erm-1(tm677)* larvae showed decreased basolateral and increased apical membrane localization of LET-23::GFP in the VPCs and their descendants, resulting in a significantly increased ratio of apical to basolateral LET-23::GFP signal intensity when compared to heterozygous *erm-1(tm677)*/+ controls (**Figure 2B–D**). The localization of the apical junction marker DLG-1::RFP [21] or the plasma membrane marker CED-10::GFP [22] were not changed, indicating that overall polarity of the VPCs was not altered in *erm-1(tm677)* mutants (data not shown and **Figure S3**). However, we detected a reduced basolateral staining of the F-actin reporter lifeAct::GFP [23] in the VPCs of *erm-1(tm677)* mutants, which is consistent with the role of ERM proteins as membrane linkers for cortical F-actin (**Figure 2D–F′**).

To test whether the reduced basolateral expression of LET-23::GFP is due to decreased basolateral secretion or to an increased membrane mobility and recycling rate of LET-23, we performed Fluorescence Recovery After Photobleaching (FRAP) experiments on the basal and lateral membranes of the vulval cells at the Pn.pxx stage and calculated the mobile fraction and half time of recovery ($t_{1/2}$) of LET-23::GFP (**Figure 2G–L**) (see materials and methods). In *erm-1(tm677)* larvae, the total mobile fraction of LET-23::GFP was significantly higher than in heterozygous controls in both the basal and lateral compartments, while the $t_{1/2}$ was not significantly changed (**Figure 2L**, $t_{1/2} = 76$ sec in heterozygous *erm-1(tm677)*/+ vs. 81 sec in homozygous *erm-1(tm677)* mutants). Thus, *erm-1(tm677)* mutants exhibit an increased mobility of LET-23::GFP on the basolateral plasma membrane, rather than a decreased rate of basolateral secretion or retention.

ERM-1 Inhibits Ligand-Dependent Internalization of LET-23 EGFR

Changes in the ligand concentrations could alter the steady-state levels of LET-23 EGFR on the basolateral membrane. For example, reducing the dose of LIN-3 EGF may decrease receptor endocytosis and thus diminish the ratio of apical to basal EGFR, while increasing the dose of LIN-3 may promote receptor endocytosis on the basolateral membrane and therefore increase the apical to basal ratio. On the other hand, mutations in components of the LIN-2/LIN-7/LIN-10 complex that is necessary to retain the EGFR on the basolateral membrane also cause a strong reduction in basolateral EGFR localization, yet they result in reduced receptor activation [5]. To distinguish between these different scenarios, we tested if the increased apical LET-23::GFP localization in *erm-1(tm677)* mutants could be due to a higher rate of LET-23 endocytosis after binding to LIN-3 EGF secreted from the AC. In *lin-3(e1417)* mutants, in which LIN-3 activity in the AC is strongly reduced [24], apical LET-23::GFP localization was nearly two-fold reduced (**Figure 3A,C**). However, in *erm-1(tm677)*; *lin-3(e1417)* double mutants the apical to basal LET-23::GFP ratio was lower than in *erm-1(tm677)* but higher than in *lin-3(e1417)* single mutants (**Figure 3B,C**). Since the viable *lin-3(e1417)* allele used does not eliminate all LIN-3 activity, we conclude that the apical accumulation of LET-23::GFP in the absence of ERM-1 is at least in part ligand-dependent. On the other hand, a pulse of ectopic LIN-3 ubiquitously expressed under control of the heat-shock promoter *hs*::*lin-3* [25] caused the almost complete disappearance of LET-23::GFP from the basolateral membrane and accumulation on the apical membrane within 230 minutes (**Figure 3D,F**). In homozygous *erm-1(tm677)* mutants, however, a LIN-3 pulse caused a smaller increase in the apical LET-23::GFP pool and persisting receptor expression on the basolateral membrane (**Figure 3E,F**). Thus, not only LET-23 endocytosis but also basolateral recycling are increased in *erm-1(tm677)* mutants, which is consistent with the increased mobile fraction of LET-23::GFP observed in the FRAP experiments (**Figure 2L**). By contrast, activation of the EGFR signaling pathway downstream of the receptor using for example the *let-60(gf)* mutation did not change LET-23::GFP localization (data not shown). Thus, the LIN-3 ligand stimulates and ERM-1 inhibits internalization and recycling of LET-23 on the basolateral membrane.

ERM-1 Acts as a Negative Regulator of the EGFR/RAS/MAPK Pathway

Enhanced receptor endocytosis could result in the attenuation of LET-23 signaling, while faster recycling to the plasma membrane could promote signaling [1]. To determine how the altered LET-23 dynamics in *erm-1* mutants affects signaling, we performed epistasis analysis by combining *erm-1(tm677)* with mutations in different components of the EGFR/RAS/MAPK pathway [4] and quantifying vulval induction. In *erm-1(tm677)* single mutants, the three proximal VPCs were always induced as in the wild-type (**Figure 4A**). However, in *let-60(gf); erm-1(tm677)* double mutants, the average number of induced VPCs was significantly increased compared to *let-60(gf); erm-1(tm677)*/+ controls, resulting in an enhanced Multivulva (Muv) phenotype (**Figure 4A**). Thus, ERM-1 negatively regulates RAS/MAPK signaling during vulval induction. Mutations in the *lin-2/lin-7/lin-10* receptor localization complex or in the PDZ binding motif in *let-23(sy1)* cause a penetrant Vulvaless (Vul) phenotype because LET-23 mislocalized to the apical membrane cannot bind to LIN-3 [5]. Interestingly, *erm-1(tm677)* partially suppressed the *lin-2(n397)*, *lin-7(e1413)*, *lin-10(e1439)* and *let-23(sy1)* Vul phenotypes (**Figure 4A**), indicating that ERM-1 inhibits vulval induction independently of the LIN-2/LIN-7/LIN-10 receptor localization complex. However, the suppression of the *lin-2(n397)* Vul phenotype was not accompanied by a visible re-localization of LET-23::GFP to the basolateral

Table 1. Genes that control the localization or expression of LET-23::GFP.

Gene	KOG Information	LET-23 localization	Known functions in vulval development
	RNA processing and modification		
C18A3.3	Nucleolar protein-like/EBNA1-binding protein	Punctate	
rsp-6	Alternative splicing factor SRp20/9G8 (RRM superfamily)	Persistent in 2°	
prp-4	U4/U6 small nuclear ribonucleoprotein Prp4 (WD40 repeats)	Other complex	
ddx-23	U5 snRNP-like RNA helicase subunit	Persistent in 2°	
npp-17	mRNA export protein (contains WD40 repeats)	Persistent in 2°	
prpf-4	U4/U6-associated splicing factor PRP4	Other complex	
aly-2	RRM motif-containing protein	Apical	
ccf-1	mRNA deadenylase subunit	Persistent in 2°	
larp-1	La RNA-binding motif	Persistent in 2°	Likely affects oogenesis via regulation of Ras-MAPK signaling
	Chromatin Structure and dynamics		
lin-9	Retinoblastoma pathway protein LIN-9/chromatin-associated protein Aly	Other complex	Negative regulation of the RTK/Ras-mediated signal transduction pathway that controls vulval development
met-2	Histone methyltransferase	Apical	Negatively regulates lin-3 transcription to restrict vulval development to three of the six VPCs
	Energy production and conversion		
nduf-7	NADH-ubiquinone oxidoreductase, NUFS7/PSST	Apical	
aco-2	Aconitase/homoaconitase (aconitase superfamily)	Persistent in 2°	
	Cell cycle control and mitosis		
air-2	Serine/threonine protein kinase	Punctate	
ned-8	Ubiquitin-like protein	Cytoplasmic	
cdc-37	Cell division cycle 37 protein, CDC37	Cytoplasmic/Persistent in 2°	
mat-1	DNA-binding cell division cycle control protein	Lateral	
	Translation		
eif-3.E	Translation initiation factor 3, subunit e (eIF-3e)	Punctate	
C30C11.1	Mitochondrial ribosomal protein L32	Apical	
fbf-2	Translational repressor Pumilio/PUF3 and related RNA-binding proteins	Persistent in 2°	Inhibits primary vulval cell fate specification
iftb-1	Translation initiation factor 2, beta subunit (eIF-2beta)	Punctate	
alg-2	Translation initiation factor 2C (eIF-2C) and related proteins	Apical/Cytoplasmic	
T13H5.5	Mitochondrial ribosomal protein S18b	Apical	
	Transcription		
pbrm-1	Chromatin remodeling complex RSC, subunit RSC1/Polybromo and related	Punctate	Interacts with two or more components of the EGF/RAS signaling pathway during vulval development
lin-1	Predicted transcription factor	Other complex	General effector of MAP kinase-mediated signaling required for vulval induction
rpc-1	RNA polymerase III, large subunit	Persistent in 2°/Apical	
C55A6.9	Putative RNA polymerase II regulator	Apical	
let-381	Transcription factor of the Forkhead/HNF3 family	Punctate	
pax-3	Homeodomain like	Persistent in 2°/Apical	
lin-31	Forkhead/HNF-3-related transcription factor	Persistent in 2°/complex	Tissue-specific effector of MAP kinase-mediated signaling in the vulva
kin-10	Casein kinase II, beta subunit	Persistent in 2°	

Table 1. Cont.

Gene	KOG Information	LET-23 localization	Known functions in vulval development
T02C12.2	Small nuclear RNA activating protein complex - 50kD subunit (SNAP50)	Persistent in 2°	
rpb-11	RNA polymerase, subunit L	Persistent in 2°	
let-49	Transcriptional coactivator	Other complex	
tag-246	SWI/SNF transcription activation complex subunit	Persistent in 2°	Required for full levels of LIN-3/EGF signaling during vulval development
sptf-3	Zn finger protein	Other complex	
	Replication and repair		
hsr-9	DNA damage checkpoint protein RHP9/CRB2/53BP1	Apical/Cytoplasmic	
	Post-translational modification, protein turnover, chaperones		
tag-170	Thioredoxin domain-containing	Apical	
C11H1.3	Predicted E3 ubiquitin ligase	Other complex	
gsto-1	Glutathione S-transferase	Apical	
mig-6	Serine proteinase inhibitor (KU family) with thrombospondin repeats	Cytoplasmic	
usp-48	Ubiquitin carboxyl-terminal hydrolase	Punctate	
sig-7	Predicted peptidyl prolyl cis-trans isomerase	Persistent in 2°/Apical	
let-70	Ubiquitin-protein ligase	Persistent in 2°	
fnta-1	Farnesyltransferase, alpha subunit/protein geranylgeranyltransferase type I	Punctate	
rfp-1	E3 ubiquitin ligase involved in syntaxin degradation	Apical	
	Inorganic ion transport and metabolism		
tat-5	P-type ATPase	Persistent in 2°	
	General Functional Prediction only		
C06E4.6	Reductases with broad range of substrate specificities	Persistent in 2°/Apical	
ref-2	Zn-finger	Apical	
gex-3	Membrane-associated hematopoietic protein	Persistent in 2°	
F39B2.1	Zn finger protein	Other complex	
hrp-1	RRM domain	Punctate/Persistent in 2°	
hmg-1.2	HMG box-containing protein	Apical	
cdc-42	Ras-related small GTPase, Rho type	Persistent in 2°	
ngp-1	Nucleolar GTPase	Apical	
chp-1	CHORD domain Co-chaperone	Cytoplasmic	
ego-2	Predicted signal transduction protein	Cytoplasmic	Positively regulates LIN-12/Notch signaling in the anchor cell-ventral uterine (AC/VU) cell fate decision
	Function Unknown		
B0495.6	Uncharacterized conserved protein	Cytoplasmic	
F27C1.6	Uncharacterized conserved protein	Cytoplasmic	
ZK265.6	Uncharacterized conserved protein	Apical	
nsh-1	Conserved nuclear protein	Cytoplasmic	Strawberry notch homolog, positively regulates *lin-3/egf* expression during RAS-dependent vulval induction
F43D2.1	G1/S-specific cyclin C like	Other complex	
cdt-2	WD domain g-beta repeat	Persistent in 2°	
K12H4.5	Unknown	Apical	
	Signal Transduction		
abi-1	Abl interactor ABI-1, contains SH3 domain	Persistent in 2°	

Table 1. Cont.

Gene	KOG Information	LET-23 localization	Known functions in vulval development
sel-8	Nuclear protein glutamine/asparagine (Q/N)-rich ('prion') domain	Persistent in 2°	Required for GLP-1 and LIN-12 signaling
mpk-1	Mitogen-activated protein kinase	Apical	Mitogen-activated protein (MAP) kinase ERK ortholog required for vulval cell fate specification
nud-1	Nuclear distribution protein NUDC	Apical	
par-3	PDZ protein	Persistent in 2°	
par-2	RING finger	Persistent in 2°	
cki-1	Cyclin-dependent kinase inhibitor	Cytoplasmic	
sys-1	Armadillo Repeats	Persistent in 2°	Functions in a Wnt/MAPK signaling pathway as a beta-catenin-like transcriptional coactivator
ppfr-4	Protein phosphatase 2A-associated protein	Lateral	
pry-1	Member of the Axin family of proteins	Persistent in 2°	Negative regulator of Wnt signaling pathways
	Intracellular trafficking and secretion		
sft-4	Putative cargo transport protein ERV29	Persistent in 2°	
arf-3	GTP-binding ADP-ribosylation factor Arf1	Cytoplasmic	
sel-9	Transmembrane emp24 domain protein	Apical	Likely functions to negatively regulate the transport of LIN-12 and GLP-1 to the cell surface
aex-6	GTPase Rab27, small G protein superfamily	Persistent in 2°	
	Nuclear structure		
npp-11	Nuclear pore complex, Nup98 component (sc Nup145/Nup100/Nup116)	Punctate	
	Cytoskeleton		
erm-1	Radixin, moesin and related proteins of the ERM family	Apical	
wve-1	Wiskott Aldrich syndrome proteins	Punctate	

doi:10.1371/journal.pgen.1004341.t001

membrane (data not shown). In contrast, *erm-1(tm677)* did not suppress the *lin-3(e1417)* Vul phenotype, suggesting that vulval induction in *erm-1(tm677)* mutants still depends on the AC signal (**Figure 4A**).

ERM-1 Forms a Complex with LET-23 EGFR Independently of the LIN-2/LIN-7/LIN-10 Complex

ERM proteins are composed of an N-terminal FERM domain and a C-terminal actin-binding domain [26]. They can switch from a closed, inactive conformation in the cytoplasm to an open, active conformation at the plasma membrane [27]. The FERM domain in the open conformation interacts with plasma membrane proteins either directly or indirectly through adaptor proteins [26], while binding of the actin cytoskeleton to the C-terminus of ERM proteins regulates the activity of the entire complex [28]. Since our genetic analysis indicated that ERM-1 controls LET-23 signaling independently of the LIN-2/LIN-7/LIN-10 complex, we tested if ERM-1 and LET-23 might exist in an alternate complex. For this purpose, different portions of purified recombinant ERM-1 tagged at the N-terminus with glutathione S-transferase (GST) were incubated with total worm lysates, and bound LET-23 was detected on Western-blots. LET-23 from wild-type worm extracts bound to N-terminal fragments containing the entire FERM domain (GST::ERM-1_{1-240} and GST::ERM-1_{1-311}), while a C-terminal fragment (GST::ERM-$1_{312-564}$) or truncated FERM domains (GST::ERM-1_{1-100} or GST::ERM-1_{1-167}) did not bind LET-23 (**Figure 4B,C**). Moreover, LET-23 extracted from *sy1* mutants, in which LET-23 lacks the PDZ binding motif, or from *lin-7(e1413)* mutants still bound to the ERM-1 FERM domain (**Figure 4D,E**). Thus, LET-23 and ERM-1 exist in a complex that is distinct from the LIN-2/LIN-7/LIN-10 localization complex.

ERM-1 Is a Temporal Regulator of EGFR Signaling

The increased basolateral LET-23 mobility in *erm-1(tm677)* mutants may result in an overall elevated activity of the RAS/MAPK pathway, as more LET-23 molecules are available to interact with LIN-3. The co-localization of LET-23 and ERM-1 together with the *in vitro* protein interaction experiments suggested that both proteins form a complex at the basolateral membrane of the VPCs. We thus hypothesized that ERM-1 may prevent the instant activation of the entire basolateral pool of LET-23 once the AC begins to secrete LIN-3 at the mid L2 stage, allowing the cells to maintain a high LET-23 activity after vulval induction. To test this model, we quantified the expression levels of the RAS/MAPK target EGL-17::CFP [29] in the descendants of the VPCs. In wild-type mid L3 larvae, we observed a peak of EGL-17::CFP expression after vulval induction in the 1° descendants of P6.p (**Figure 5A–C′,G**). By contrast, *erm-1(tm677)* mutants showed a gradual decrease rather than an increase in EGL-17::CFP

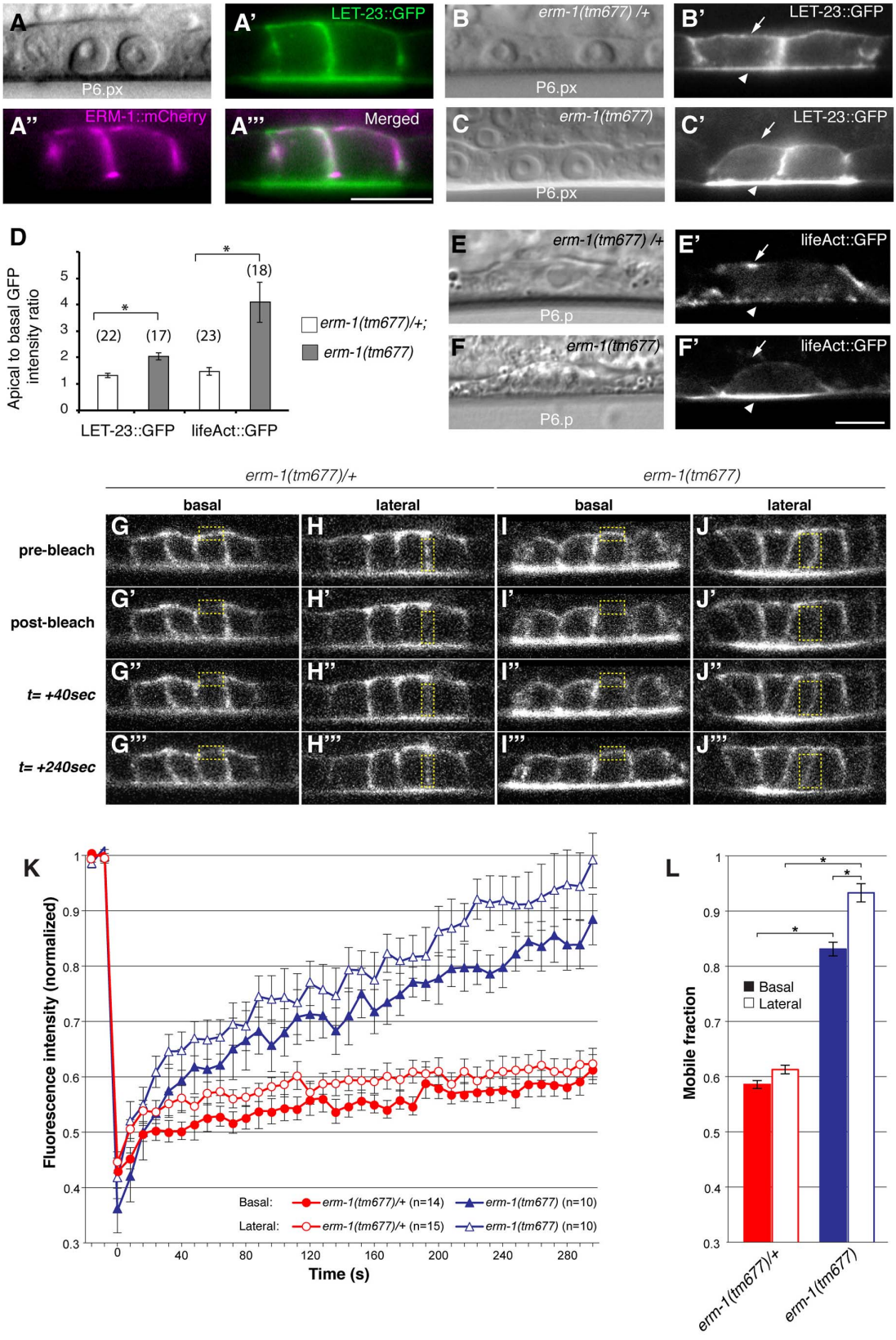
A
P6.px
A'
LET-23::GFP
A''
ERM-1::mCherry
A'''
Merged
B
erm-1(tm677) /+
P6.px
B'
LET-23::GFP
C
erm-1(tm677)
P6.px
C'
LET-23::GFP
D
Apical to basal GFP intensity ratio
(22)
(17)
(23)
(18)
LET-23::GFP
lifeAct::GFP
erm-1(tm677)/+;
erm-1(tm677)
E
erm-1(tm677) /+
P6.p
E'
lifeAct::GFP
F
erm-1(tm677)
P6.p
F'
lifeAct::GFP
erm-1(tm677)/+
erm-1(tm677)
basal
lateral
basal
lateral
pre-bleach
post-bleach
t= +40sec
t= +240sec
K
Fluorescence intensity (normalized)
Time (s)
Basal: erm-1(tm677)/+ (n=14) erm-1(tm677) (n=10)
Lateral: erm-1(tm677)/+ (n=15) erm-1(tm677) (n=10)
L
Mobile fraction
Basal
Lateral
erm-1(tm677)/+
erm-1(tm677)

Figure 2. ERM-1 controls LET-23::GFP localization at the basolateral membrane of the vulval cells. (A) Nomarski image, (A′) LET-23::GFP (green) and (A″) ERM-1::mCherry (magenta) expression at the Pn.px stage. (A‴) shows a merged image of (A′) and (A″) indicating partial co-localization at the basolateral membrane. (B) Nomarski and (B′) LET-23::GFP expression in a heterozygous *erm-1(tm677)/+* and (C, C′) a homozygous *erm-1(tm677)* larva at the Pn.px stage. Arrows indicate the basal and arrowheads the apical membrane domains. (D) Apical to basal LET-23::GFP and lifeAct::GFP intensity ratios in P6.p in *erm-1(tm677)/+* versus *erm-1(tm677)*. The numbers of animals analyzed are indicated in brackets. Error bars represent the standard error of the mean. (E) Nomarski and (E′) lifeAct::GFP expression in P6.p of a heterozygous *erm-1(tm677)/+* and (F, F′) a homozygous *erm-1(tm677)* larva. (G–J‴) Example images of the FRAP experiment at the time points indicated to the left of panels G-G‴. (G-G‴ and I-I‴) Basal and (H-H‴ and J-J‴) lateral membrane regions outlined with the dotted yellow boxes were photobleached in heterozygous *erm-1(tm677)/+* and homozygous *erm-1(tm677)* larvae, respectively, at the Pn.pxxx stage. (K) Quantification of the FRAP experiments. The y axis indicates LET-23::GFP intensity normalized to the signal intensity measured before bleaching inside the bleached areas and to the total signal intensity in the cell, and the x-axis the time after photo-bleaching. The numbers of animals analyzed are shown in brackets. (L) Quantification of the mobile fraction from the FRAP curves. *Indicates $p<0.05$, as determined in a two tailed student's t-test - two-sample unequal variance. The scale bars are 10 μm.
doi:10.1371/journal.pgen.1004341.g002

expression after vulval induction (**Figure 5D–G**). Thus, ERM-1 is required for the generation of a long-lasting RAS/MAPK signal in the 1° vulval cells after fate specification has occurred.

Discussion

Regulation of EGFR Localization Allows Pattern Formation

In order to systematically search for regulators of LET-23 EGFR trafficking and signaling, we performed an *in vivo* receptor localization screen in *C. elegans* larvae. There do exist certain limitations of this system, such as the inability to isolate individual cell for biochemical studies. However, an important advantage of our approach over previous studies performed with cultured epithelial cells [1] is the ability to observe the dynamics of receptor trafficking under normal conditions, in epithelial cells embedded in their natural environment and receiving physiological concentrations of various extracellular signals. The different regulators of LET-23 EGFR localization and signaling identified in our screen point at a complex network controlling LET-23 EGFR trafficking and signaling in different sub-cellular compartments. In a system, such as the VPCs, where ligand availability is limiting [8,30], these additional control mechanisms at the level of the receptor are necessary to prevent too many cells from engaging in signaling at the same time and to focus the inductive signal on a single cell (P6.p). A perturbation of LET-23 EGFR trafficking can lead to a multivulva phenotype because decreased ligand sequestering by the 1° VPC P6.p results in increased LET-23 EGFR activation in the distal VPCs [30]. The down regulation of the LET-23 EGFR in all but the 1° VPC is therefore an important mechanism to break the symmetry of the initially equivalent VPCs and select a single cell for the 1° fate. The most frequent phenotype we observed in our screen (31 genes) was persisting LET-23 EGFR expression in 2° VPCs, and for those genes that had a significant effect on signaling we found increased rather than decreased vulval induction in the *let-60* background. This suggests that a relatively large number of negative regulators of EGFR signaling is required to generate the invariant pattern of vulval cell fates with a single 1° cell flanked by two 2° cells.

Genes Regulating LET-23 EGFR Trafficking Are Conserved

A recent study has indicated that around 38% of all predicted protein coding genes in *C. elegans* possess at least one human homolog [31]. However, we found for 91% of the genes identified in our screen (74 of 81) at least one human homolog in the

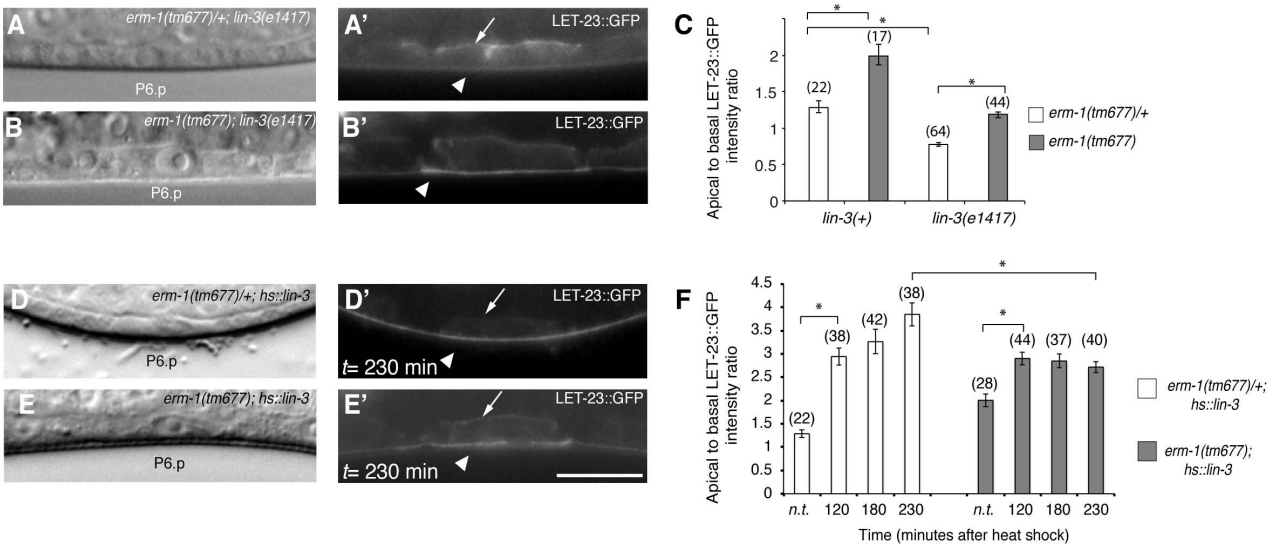

Figure 3. The LIN-3 EGF ligand stimulates and ERM-1 inhibits internalization and recycling of LET-23 on the basolateral membrane. (A) Nomarski image and (A′) LET-23::GFP expression in *erm-1(tm677)/+; lin-3(e1417)* and (B, B′) *erm-1(tm677); lin-3(e1417)* double mutants at the Pn.p stage. Arrows indicate the basal and arrowheads the apical membrane domains. (C) Apical to basal LET-23::GFP intensity ratios in P6.p in *erm-1(tm677)/+* versus *erm-1(tm677)* single and in *erm-1(tm677)/+; lin-3(e1417)* versus *erm-1(tm677); lin-3(e1417)* double mutants. (D) Nomarski image and (D′) LET-23::GFP expression in a heterozygous *erm-1(tm677)/+* and (E,E′) a homozygous *erm-1(tm677)* mutant 230 minutes after heat-shock induction of LIN-3. (F) Apical to basal LET-23::GFP intensity ratios at different time points after heat-shock. n.t. indicates animals of the same genotype that were not subjected to a heat-shock. *Indicates $p<0.001$ as determined in a two tailed student's t-test - two-sample unequal variance. The scale bars are 10 μm.
doi:10.1371/journal.pgen.1004341.g003

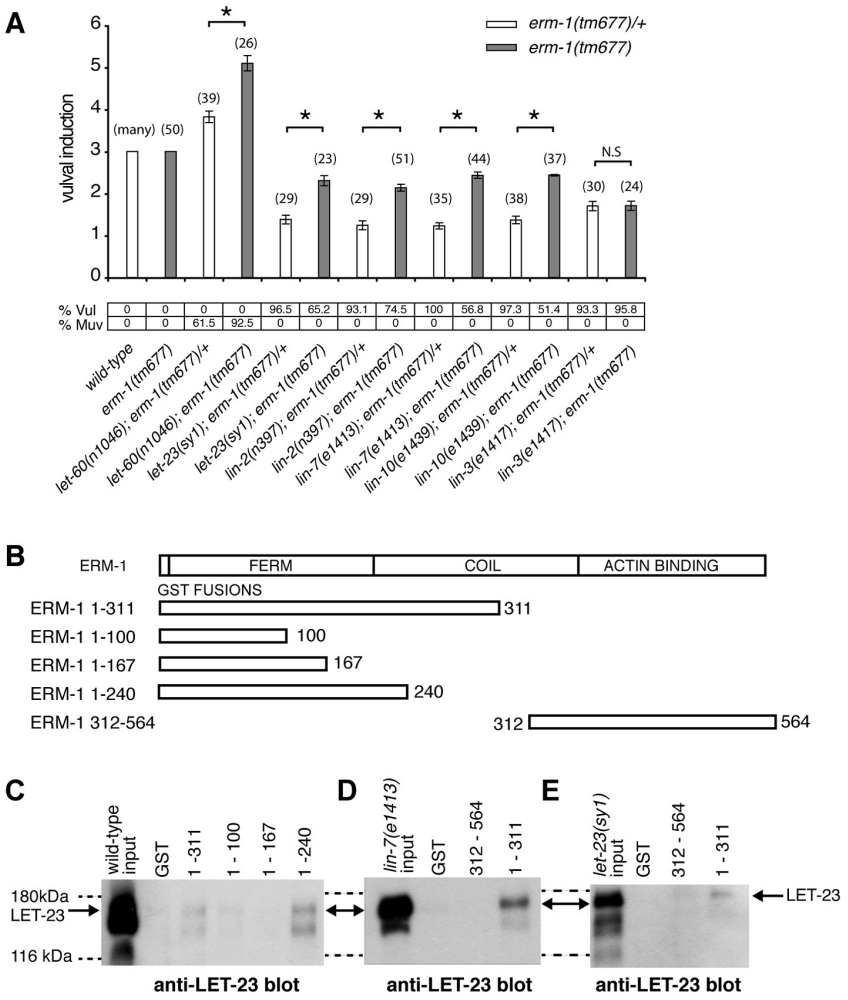

Figure 4. ERM-1 negatively regulates vulval induction and binds to LET-23. (A) Genetic epistasis analysis between *erm-1* and components of the *egfr/ras/mapk* pathway. Vulval induction (VI) indicates the average numbers of induced VPCs in different double mutant combinations scored in *erm-1(tm677)* heterozygous (white bars) versus homozygous (gray bars) animals. %Vul indicates the fraction of animals with VI<3 and % Muv the fraction of animals with VI>3. The numbers of animals scored for each genotype are indicated in brackets. N.S: no significant change. *Indicates $p<0.05$ as determined in a two tailed student's t-test - two-sample unequal variance. (B) Structures of the GST::ERM-1 fusion proteins tested for LET-23 binding. (C) Interaction of LET-23 from wild-type extracts with different GST::ERM-1 fusion proteins detected on an anti-LET-23 Western blot. (D) Binding of LET-23 extracted from *lin-7(e1413)* and (E) from *let-23(sy1)* mutants to GST::ERM-1 proteins. The dashed lines indicate the approximate positions of the 180 kDa and 116 kDA protein standards.
doi:10.1371/journal.pgen.1004341.g004

OrthoList, suggesting that the mechanisms regulating EGFR trafficking are strongly conserved. Further studies of these mammalian homologs may provide new means of interfering with deregulated EGFR signaling in human cells.

ERM-1 Is a Temporal Regulator of EGFR Signaling

We describe a new function of the *C. elegans* Ezrin homolog ERM-1 in regulating EGFR signaling on the basolateral membrane of the vulval cells. Based on the subcellular localization and dynamics and on genetic and biochemical data, we propose that ERM-1 forms a complex with the LET-23 EGFR at the basolateral plasma membrane to recruit the receptor into an actin-rich inactive membrane compartment and limit receptor activation (**Figure 5H,I**). A similar function has been proposed for mammalian NF2 Merlin, which shares similarity to Ezrin/Radixin/Moesin proteins. In confluent cultured epithelial cells, Merlin coordinates adherens junction stabilization with EGFR signaling by recruiting the EGFR into an apical membrane compartment, where the receptor cannot be activated [32]. In analogy, ERM-1 may link a fraction of the LET-23 EGFR pool at the basolateral membrane to cortical F-actin and restrict the access of the receptor to the activating LIN-2/LIN-7/LIN-10 complex [5]. In the absence of the tripartite LIN-2/LIN-7/LIN-10 complex, most of the residual basolateral LET-23 EGFR is probably bound and inactivated by ERM-1. The inhibitory ERM-1 complex thus antagonizes the activating LIN-2/LIN-7/LIN-10 complex to prevent the instant activation and subsequent degradation of the entire basolateral pool of LET-23 EGFR once the AC begins to secrete LIN-3 in the mid-L2 stage. This mechanism allows the vulval cells to maintain high LET-23 EGFR

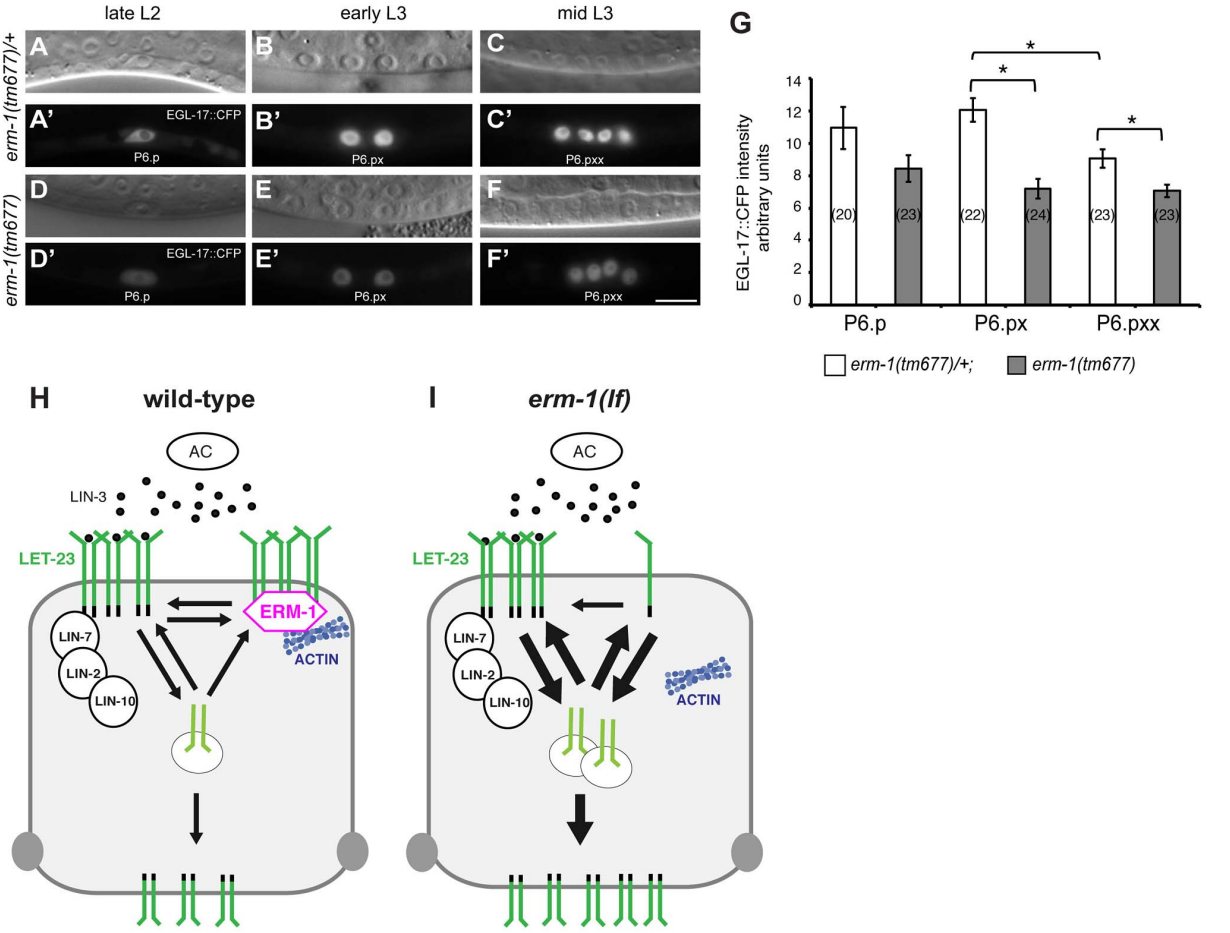

Figure 5. Temporal regulation of LET-23 EGFR signaling by ERM-1. (A, B, C) Nomarski images and (A′, B′, C′) EGL-17::CFP expression in *erm-1(tm677)/+* controls versus (D through F′) homozygous *erm-1(tm677)* mutants at the Pn.p (A′, D′), Pn.px (B′, E′) and Pn.pxx (C′, F′) stages. The scale bar is 10 μm. (G) Quantification of nuclear EGL-17::CFP intensities in P6.p and its descendants. The numbers of animals analyzed are indicated in brackets. *Indicates $p<0.01$ as determined in a two tailed student's t-test - two-sample unequal variance. Error bars represent the standard error of the mean. (H) Two antagonistic complexes control LET-23 localization at the basolateral membrane of the VPCs. The ternary LIN-2/LIN-7/LIN-10 complex promotes receptor activation, while the ERM-1 complex (magenta) prevents LET-23 endocytosis and signaling from basolateral membrane. ERM-1 may sequester LET-23 in an actin-rich membrane compartment to prevent receptor activation. (I) In the absence of ERM-1, more LET-23 can be activated via the LIN-2/LIN-7/LIN-10 complex, resulting in enhanced receptor endocytosis and recycling, and ultimately an increased accumulation of LET-23 on the apical plasma membrane.
doi:10.1371/journal.pgen.1004341.g005

activity at later time points after vulval induction. LET-23 EGFR may be released from the ERM-1 complex when the vulval lumen is formed and ERM-1 relocalizes to the apical plasma membrane of the toroids. Such a buffering mechanism may be important, as sustained RAS/MAPK signaling is required during the subsequent phase of vulval morphogenesis when RAS/MAPK activity induces the expression of genes required for the execution of the vulval fates [4,33]. Thus, the strength and duration of EGFR activation during development must be precisely controlled to achieve the correct levels of RAS/MAPK activity required for organogenesis.

Materials and Methods

Strains and General Methods

C. elegans strains were maintained at 20°C on standard nematode growth media [34] and the reference wild-type strain of *C. elegans* used was Bristol N2. Mutant strains used: LGI: *erm-1(tm677)/hT2[bli-4(e937) let(q782) qIs48] (I;III)*, *rde-1(ne219)*, *lin-10(e1339)*. LGII: *let-23(sy1)*, *lin-7(e1413)*, *syIs12[hs::lin-3EGF]*[25]. LGIII: *unc-119(ed3)*, *unc-119(e2498)*. *LGIV: lin-3(e1417)*, *let-60(n1046)*. LGX: *lin-2(n397)*. Integrated and extra-chromosomal arrays: *qyIs23[Pcdh-3::mCherry::plcδ^{PH}; unc-119(+)] II* [35], *zhIs038[let-23::gfp, unc-119(+)] IV*, *zhEx484[C11H1.3::gfp; Pmyo-2::mCherry]*, *zhIs396[Pdlg-1::lifeact::gfp::unc-54 3′utr, Plin-48::gfp]* [23], *zhEx486[sft-4::gfp; Pmyo-2::mCherry]*, *zhEx487[ego-2::gfp; Pmyo-2::mCherry]*, *zhEx519 [erm-1::mCherry; unc-119(+);Pmyo-2::mCherry]; zhEx418[Plin-31::rde-1; Pmyo-2::mcherry]*.

The construction of the translational reporter constructs used in this study is described in the **Text S1** and **Table S2** (see also **Figure S4**).

Extra-chromosomal arrays were obtained by microinjection of plasmids at 20 to 50 ng/μl along with the coinjection marker *Pmyo2::mCherry or unc-119(+)* at 2 to 10 ng/μl and pBluescript to a final concentration of 150 to 200 ng/μl as described [36]. *zhIs038*

was obtained by bombardment of *unc-119* mutants with plasmid coated gold particles as described [37]. Primers used and details on the construction of plasmids can be found in the Supplementary Material.

GST Pull-down and Western Blots

GST fusion proteins were purified from *E. coli* BL-21 with glutathione-sepharose beads, incubated with 500 µg total protein worm extracts, and bound LET-23 was detected on Western blots with affinity-purified rabbit anti-LET-23 antibodies (1:1000 dilution) raised against the C-terminal 196 amino acids [5].

RNAi Screen and Microscopy

RNAi was performed by bacterial feeding as described [38]. LET-23::GFP localization was scored in L3 larvae of the F1 generation mounted on 3% agarose pads supplemented with 5 mM tetramisol. For each RNAi clone, the vulval cells in 30 to 50 animals were observed at 40 to 63-fold magnification with a Leica DMRA wide-field microscope. Positive RNAi clones from the rescreen were verified by DNA sequencing. Images were recorded with a Hamamatsu ORCA-ER CCD camera controlled by the Openlab 5 software package (Improvision). Confocal images were recorded with a Olympus FV-1000 or a Zeiss LSM710 confocal microscope and analyzed with ImageJ [39]. Apical to basolateral intensity ratios were determined in mid-sagittal frames taken with the same illumination and same exposure settings by manually selecting the basal and apical membrane compartments and measuring total fluorescence intensities.

Fluorescence Recovery after Photobleaching

Larvae at the Pn.pxx stage were imaged at 20°C using a 63×/1.4 NA oil lens on an Zeiss LSM710 confocal microscope equipped with 458/488/514 nm argon and 405 nm diode lasers. A selected area of the basal or lateral membrane was bleached using the 488 nm argon laser at 85% power setting for 886.6 µsec to bleach around 70% of the signal, and fluorescence recovery was monitored over the following 296 seconds taking a frame every 8 seconds with a 488 nm laser excitation at 20% power intensity, a pinhole equivalent to 2.12 Airey units, a frame size of 256×256 dpi, and a pixel size of 0.53 µm. Data were analyzed in ImageJ by first registering the images with the StackReg plugin and then using the FRAP Norm plugin by Joris Meys [40] to measure recovery. Normalized curves were fitted to the formula $I(t) = A \cdot (1\text{-}e^{-kt}) + C$ using the solver function in MS Excel to calculate the total mobile fraction A and half time as $t_{1/2} = 1/k$.

Heat Shock Treatment

Synchronized L3 larvae were heat-treated at 33°C for 30 minutes in a water bath, transferred to 20°C, and imaged at 120, 180, 230 minute after induction under the same illumination and exposure conditions. Quantification of the apical to basal LET-23::GFP intensity ratio with and without heat-shock treatment as described in the results.

Supporting Information

Figure S1 Characterization of the LET-23::GFP reporter. (**A**) Expression of endogenous LET-23 (aprox. 150 kDa) and LET-23::GFP (aprox. 177 kD) in total worm lysates of L4 larvae and young adults detected on Western blots probed with anti-LET-23(left) and anti-GFP(right) antibodies. The upper band is LET-23::GFP and the lower band is endogenous LET-23. Integrated LET-23::GFP is expressed at similar levels as endogenous LET-23. (**B**) Complete rescue of the *let-23(sy1)* Vulvaless phenotype with an extra-chromosomal *let-23::gfp* array obtained by microinjection. The percentages of animals with a Vul phenotype in the presence an absence of the extra-chromosomal array are shown. The numbers of animals scored are indicated in brackets. (**C**) LET-23::GFP expressed from the integrated array used for the screen (*zhIs038*) is localized at basolateral and apical plasma membrane of the vulval cells in wild-type larvae, but (**D**) mislocalized to the apical compartment in *lin-2(n397)* mutants. (**D′**) shows the LET-23::GFP channel of (**D**) merged with the corresponding Nomarski picture. The scale bar is 10 µm.
(JPG)

Figure S2 Additional examples of genes identified in the receptor localization screen. In each row, the left panels show the Nomarski images and right panels the fluorescent images. (**A**) Normal LET-23::GFP expression in vector controls, (**B**) apical enrichment (arrow) in *ngp-1* RNAi, (**C**) punctate localization (arrow) in E04F6.4 RNAi, (**D**) cytoplasmic enrichment in *arf-3* RNAi, (**E**) persistent expression in 2° cells (asterisk) in *rab-27* RNAi, and (**F**) enrichment at the lateral membrane separating the two P6.p descendants in *ppfr-4* RNAi animals. The scale bars are 10 µm.
(JPG)

Figure S3 Polarity of the vulval cells in erm-1(tm677) mutants. (**A**) Nomarski image and (**A′**) Normal basolateral localization of the CED-10::GFP reporter in heterozygous *erm-1(tm677)*/+ and (**B**) Nomarski image and (**B′**) localization of the CED-10::GFP reporter in homozygous *erm-1(tm677)* mutants. The scale bar is 10 µm.
(JPG)

Figure S4 Structure of (A) the LET-23::GFP and (B) ERM-1::mCherry reporter constructs.
(JPG)

Table S1 List of 705 Pvl genes used for the mislocalization/missexpression screen.
(DOCX)

Table S2 Sequences of primers used.
(DOCX)

Text S1 Details on the construction of the translational reporter constructs used in this study. A schematic drawing of the LET-23::GFP and ERM-1::mCherry constructs is shown in **Figure S4A**, and the sequences of primers used are listed in **Table S2**.
(DOC)

Acknowledgments

We thank Matthias Morf for comments on the manuscript, Jonas Hartmann for helpful discussion about FRAP and curve fitting and the whole Hajnal lab for fruitful discussions. We are also thankful to S. Mitani (National Bioresource Project for the Nematode, Japan) for providing the *erm-1(tm677)* deletion allele and the *C. elegans* Genetics Center for providing strains.

Author Contributions

Conceived and designed the experiments: AHaa PG AB MW QY DK AHaj JMER. Performed the experiments: AHaa PG AB MW QY ML DK EF JMER. Analyzed the data: AHaa PG AB MW QY AHaj JMER. Contributed reagents/materials/analysis tools: CJH. Wrote the paper: AHaa AHaj JMER.

References

1. Sorkin A, Goh LK (2009) Endocytosis and intracellular trafficking of ErbBs. Experimental Cell Research 315: 683–696.
2. Shtiegman K, Kochupurakkal BS, Zwang Y, Pines G, Starr A, et al. (2007) Defective ubiquitinylation of EGFR mutants of lung cancer confers prolonged signaling. Oncogene 26: 6968–6978. doi:10.1038/sj.onc.1210503.
3. Sweeney WE, Chen Y, Nakanishi K, Frost P, Avner ED (2000) Treatment of polycystic kidney disease with a novel tyrosine kinase inhibitor. Kidney Int 57: 33–40. doi:10.1046/j.1523-1755.2000.00829.x.
4. Sternberg PW (2005) Vulval development. Wormbook: 1–28. doi:10.1895/wormbook.1.6.1.
5. Kaech SM, Whitfield CW, Kim SK (1998) The LIN-2/LIN-7/LIN-10 complex mediates basolateral membrane localization of the *C. elegans* EGF receptor LET-23 in vulval epithelial cells. Cell 94: 761–771.
6. Whitfield CW, Bénard C, Barnes T, Hekimi S, Kim SK (1999) Basolateral localization of the *Caenorhabditis elegans* epidermal growth factor receptor in epithelial cells by the PDZ protein LIN-10. Mol Biol Cell 10: 2087–2100.
7. Chen N, Greenwald I (2004) The lateral signal for LIN-12/Notch in *C. elegans* vulval development comprises redundant secreted and transmembrane DSL proteins. Dev Cell 6: 183–192.
8. Simske JS, Kim SK (1995) Sequential signalling during *Caenorhabditis elegans* vulval induction. Nature 375: 142–146. doi:10.1038/375142a0.
9. Berset T, Hoier EF, Battu G, Canevascini S, Hajnal A (2001) Notch inhibition of RAS signaling through MAP kinase phosphatase LIP-1 during *C. elegans* vulval development. Science 291: 5. doi:10.1126/science.1055642.
10. Stetak A, Hoier EF, Croce A, Cassata G, Di Fiore PP, et al. (2006) Cell fate-specific regulation of EGF receptor trafficking during *Caenorhabditis elegans* vulval development. EMBO J 25: 11. doi:10.1038/sj.emboj.7601137.
11. Yoo AS, Bais C, Greenwald I (2004) crosstalk between the egfr and *lin-12*/notch pathways in *C. elegans* vulval development. Science 303: 5. doi:10.1126/science.1091639.
12. Tatusov RL, Fedorova ND, Jackson JD, Jacobs AR, Kiryutin B, et al. (2003) The COG database: an updated version includes eukaryotes. BMC Bioinformatics 4: 41. doi:10.1186/1471-2105-4-41.
13. Beitel GJ, Clark SG, Horvitz HR (1990) *Caenorhabditis elegans* ras gene *let-60* acts as a switch in the pathway of vulval induction. Nature 348: 503–509. doi:10.1038/348503a0.
14. Qadota H, Inoue M, Hikita T, Köppen M, Hardin JD, et al. (2007) Establishment of a tissue-specific RNAi system in *C. elegans*. Gene 400: 8. doi:10.1016/j.gene.2007.06.020.
15. Foley DA, Sharpe HJ, Otte S (2007) Membrane topology of the endoplasmic reticulum to Golgi transport factor Erv29p. Mol Membr Biol 24: 259–268. doi:10.1080/09687860601178518.
16. Ali N, Zhang L, Taylor S, Mironov A, Urbé S, et al. (2013) Recruitment of UBPY and ESCRT exchange drive HD-PTP-dependent sorting of EGFR to the MVB. Curr Biol 23: 453–461. doi:10.1016/j.cub.2013.02.033.
17. Liu Y, Maine EM (2007) The Bro1-domain protein, EGO-2, promotes Notch signaling in *Caenorhabditis elegans*. Genetics 176: 2265–2277. doi:10.1534/genetics.107.071225.
18. Algrain M, Turunen O, Vaheri A, Louvard D, Arpin M (1993) Ezrin contains cytoskeleton and membrane binding domains accounting for its proposed role as a membrane-cytoskeletal linker. The Journal of Cell Biology 120: 129–139.
19. Van Fürden D, Johnson K, Segbert C, Bossinger O (2004) The *C. elegans* ezrin-radixin-moesin protein ERM-1 is necessary for apical junction remodelling and tubulogenesis in the intestine. Developmental Biology 272: 262–276. doi:10.1016/j.ydbio.2004.05.012.
20. Göbel V, Barrett PL, Hall DH, Fleming JT (2004) Lumen morphogenesis in *C. elegans* requires the membrane-cytoskeleton linker *erm-1*. Dev Cell 6: 865–873. doi:10.1016/j.devcel.2004.05.018.
21. Diogon M, Wissler F, Quintin S, Nagamatsu Y, Sookhareea S, et al. (2007) The RhoGAP RGA-2 and LET-502/ROCK achieve a balance of actomyosin-dependent forces in *C. elegans* epidermis to control morphogenesis. Development 134: 2469–2479. doi:10.1242/dev.005074.
22. Lundquist E, Reddien P, Hartwieg E, Horvitz HR, Bargmann C (2001) Three *C. elegans* Rac proteins and several alternative Rac regulators control axon guidance, cell migration and apoptotic cell phagocytosis. Development 128: 14.
23. Farooqui S, Pellegrino MW, Rimann I, Morf MK, Müller L, et al. (2012) Coordinated lumen contraction and expansion during vulval tube morphogenesis in *Caenorhabditis elegans*. Dev Cell 23: 494–506. doi:10.1016/j.devcel.2012.06.019.
24. Hwang BJ (2004) A cell-specific enhancer that specifies *lin-3* expression in the *C. elegans* anchor cell for vulval development. Development 131: 143–151. doi:10.1242/dev.00924.
25. Katz WS, Hill RJ, Clandinin TR, Sternberg PW (1995) Different levels of the *C. elegans* growth factor LIN-3 promote distinct vulval precursor fates. Cell 82: 11.
26. Hughes SC, Fehon RG (2007) Understanding ERM proteins–the awesome power of genetics finally brought to bear. Current Opinion in Cell Biology 19: 6. doi:10.1016/j.ceb.2006.12.004.
27. Nakamura F, Amieva MR, Furthmayr H (1995) Phosphorylation of threonine 558 in the carboxyl-terminal actin-binding domain of moesin by thrombin activation of human platelets. J Biol Chem 270: 31377–31385.
28. Turunen O, Wahlström T, Vaheri A (1994) Ezrin has a COOH-terminal actin-binding site that is conserved in the ezrin protein family. The Journal of Cell Biology 126: 1445–1453.
29. Burdine RD, Branda CS, Stern MJ (1998) EGL-17(FGF) expression coordinates the attraction of the migrating sex myoblasts with vulval induction in C. elegans. Development 125: 1083–1093.
30. Hajnal A, Whitfield CW, Kim SK (1997) Inhibition of *Caenorhabditis elegans* vulval induction by *gap-1* and by *let-23* receptor tyrosine kinase. Gene 11: 2715–2728. doi:10.1101/gad.11.20.2715.
31. Shaye DD, Greenwald I (2011) OrthoList: a compendium of *C. elegans* genes with human orthologs. PLoS ONE 6: e20085. doi:10.1371/journal.pone.0020085.
32. Curto M, Cole BK, Lallemand D, Liu C-H, McClatchey AI (2007) Contact-dependent inhibition of EGFR signaling by Nf2/Merlin. The Journal of Cell Biology 177: 893–903. doi:10.1083/jcb.200703010.
33. Pellegrino MW, Farooqui S, Fröhli E, Rehrauer H, Kaeser-Pebernard S, et al. (2011) LIN-39 and the EGFR/RAS/MAPK pathway regulate *C. elegans* vulval morphogenesis via the VAB-23 zinc finger protein. Development 138: 4649–4660. doi:10.1242/dev.071951.
34. Brenner S (1974) The genetics of *Caenorhabditis elegans*. Genetics 77: 24.
35. Ziel JW, Hagedorn EJ, Audhya A, Sherwood DR (2009) UNC-6 (netrin) orients the invasive membrane of the anchor cell in *C. elegans*. Nature Cell Biology 11: 183–189. doi:10.1038/ncb1825.
36. Mello CC, Kramer JM, Stinchcomb D (1991) Efficient gene transfer in *C.elegans*: extrachromosomal maintenance and integration of transforming sequences. EMBO J 10: 3959–3970.
37. Praitis V, Casey E, Collar D, Austin J (2001) Creation of low-copy integrated transgenic lines in *Caenorhabditis elegans*. Genetics 157: 1217–1226.
38. Kamath RS, Fraser AG, Dong Y, Poulin G, Gotta M, et al. (2003) Systematic functional analysis of the *Caenorhabditis elegans* genome using RNAi. Nature 421: 231–237
39. Schneider CA, Rasband WS, Eliceiri KW (2012) NIH Image to ImageJ: 25 years of image analysis. Nat Methods 9: 671–675.
40. Phair RD, Scaffidi P, Elbi C, Vecerová J, Dey A, et al. (2004) Global nature of dynamic protein-chromatin interactions in vivo: three-dimensional genome scanning and dynamic interaction networks of chromatin proteins. Molecular and Cellular Biology 24: 6393–6402. doi:10.1128/MCB.24.14.6393-6402.2004.

6.3. Acknowledgments

I would first like to thank my mentor and supervisor Prof. Dr. Alex Hajnal, who has largely supported me to work on my favorite Ph.D. projects and guided me to overcome difficulties during study. I am very grateful to his patience and all the discussions of our projects. I remember the day I started to pick worm, Alex told me, “It is normal if you kill them at the beginning...”, “Twenty years ago the dissecting microscope was not so good and we manage to pick worms, so will you, just need more practices”. Although, I think I was doing fine. But I heard this kind encouragements from time to time throughout my Ph.D. training specially when things are not looking so great. I am very glad that I am influenced by his passion in science and have learned his positive attitude.

A Big thank you to the members of my thesis committee, Prof. Dr. Anne Spang, Prof. Dr. Yves Barral and Prof. Dr. Stefan Luschnig, who give invaluable inputs to stimulate our scientific thinking and help us shaping the projects.

It is a pleasure to get to know and supervise two groups of students for small projects in block courses. I appreciate that I learn a lot from the teaching experiences with the motivated students: Silvan Spiri, Rea Müller, Claudia Caprez, Sabrina Maxeiner and Anita Meier.

Many thanks to the former and current members in Hajnal & Hengartner lab and Zuoyen Lee, with whom I share the enjoyable lab life and the thursday brainstorming joint worm meeting. Specially I would like to thank Matthias Morf and Juan Escobar for the teaching and nice discussion in the first year of my Ph.D., Evelyn Lattmann for discussion or debating during each coffee break, Michael Walser and Sabrina Maxeiner for talking and suggesting on scientific writing, Daniel Rorz and Louisa Müller for collaborating in the AC invasion project. I appreciate Irene Hoffman, Michael Daube, Giusepp Ianiri and Erika Fröhli for their daily aids and supports in the lab.

I would like to thank Jana Doehner and Ursula Luethi from Microscopy center in University

of Zurich for assistance with multi-photo and STED microscopies, and Werner Boll for assistance with confocal microscopy. I wish to thank Susanna Bachmann for her nice support in MLS Ph.D. program.

I acknowledge the Sino-Swiss Science and Technology Cooperation Program for funding me one year of master study in Switzerland, the Zurich Molecular Life science Ph.D. program for travel grants, the Society of Developmental Biology for conference travel award, and the Swiss National Science Foundation (to Alex).

Finally, to Mom, Dad, grandma, Yingxue, Nellcia, Shaoyang and Yanuo, thank you for supporting all my decisions during Ph.D., and thank you for always being with me. It is the happiest thing being a daughter, granddaughter and true friend during the study of this degree and the rest of life.